united nations
educational, scientific
and cultural
organization

international atomic
energy agency

the
abdus salam
international centre for theoretical physics

SMR: 1133/26

WINTER COLLEGE ON
SPECTROSCOPY AND APPLICATIONS

(8 - 26 February 1999)

"THz-Spectroscopy"

3. Literature

presented by:

Rene BEIGANG
Fachbereich Physik
Universität Kaiserslautern
Erwin-Schrodinger Strasse
67663 Kaiserslautern
Germany

---

3. Literature

1. List of publications connected with THz generation and applications

2. Copies of some publications (first page only)

3. List of groups working in the field of THz generation and applications

4. "Characterization of on optoelectronic Terahertz beam system"
Martin van Exter et al.

5. "Time domain spectroscopy of molecular vapors with subpicosecond pulses of THz radiation"
Hermann Harde et al.

6. "T-Ray Imaging"
Dan Mittleman et al.

L. Allen and J. H. Eberly. *Optical Resonance and Two-Level Atoms.* John Wiley & Sons, New York, 1975.

Robert J. Anderson and Peter R. Griffiths. Errors in absorbance measurements in infrared fourier transform spectrometry because of limited instrument resolution. *Analytical Chemistry*, 47(14):2339–2347, 1975.

P. W. Anderson. *Phys. Rev. Lett.*, 76, 1949.

D. H. Auston. Ultrafast optoelectronics. In W. Kaiser, editor, *Ultrashort Laser Pulses:Generation and Applications in Topics in Applied Physics: Volume 60*, pages 183–232, 1992.

J. Ballard and W. B. Johnston. Experimental spectral line parameters in the 1–0 band of nitric oxide. *J. Molec. Spec.*, 127:70–82, 1988.

S. L. Chuang and S. Schmitt-Rink et al. Optical Rectification at Semiconductor Surfaces. *Physical Review Letters*, 68(1):102–105, 1992.

G. W. Chantry. *Submillimetre Spectroscopy.* Academic Press, London, 1971.

F. E. Doany D. Grischkowsky and C. C. Chi. Carrier lifetime versus ion-implantation dose in silicon on sapphire. *App. Phys. Lett.*, 50(8):460–462, 1987.

D. Grischkowsky, S. R. Keiding, M. van Exter, and Ch. Fattinger. Far-infrared time–domain spectroscopy with terahertz beams of dielectrics and semiconductors. *Optical Society of America B*, 7:2006–2015, 1990.

P. R. Griffiths and J. A. de Haseth. *Fourier Transform Infrared Spectrometry.* John Wiley & Sons, New York, 1986.

H. Harde, R. A. Cheville, and D. Grischkowsky. Terahertz studies of collision–broadened rotational lines. *J. Phys. Chem. A*, 101:3646–3660, 1997.

B. B. Hu and A. S. Weling et al. dc-eletric-field dependence of THz radiation induced by femtosecond optical excitation of bulk GaAs. *Physical Review B*, 49(3):2234–2237, 1994.

G. Herzberg. *Molecular Spectra and Molecular Structure; Volume One: Spectra of Diatomic Molecules.* Van Nostrand Reinhold Company, Cincinnati, 1950. Second Edition.

H. Harde and D. Grischkowsky. Coherent transients excited by subpicosecond pulses of terahertz radiation. *Opt. Soc. Am. B*, 8(8):1642–1651, 1991.

Frank Hilbk-Kortenbruck. Raum– und Zeitanalyse der Abstrahlung neuartiger Höchstfrequenzemitter im GHz– und THz–Bereich. Diplomarbeit, Rheinisch–Westfälisch Technische Hochschule Aachen, 1998.

H. Harde, N. Katzenellenbogen, and D. Grischkowsky. Line-Shape Transition of Collision Broadened Lines. *Physical Review Letters*, 74(8):1307–1310, 1995.

Robert H. Hunt, Robert A. Toth, and Earle K. Plyler. High-resolution determination of the width of self-broadened lines of carbon monoxide. *J. Chem. Phys.*, 49(9):3909–3912, 1968.

Jean-Claude M. Diels and Joel J. Fontaine et al. Control and measurement of ultrashort pulse shapes (in amplitude and phase) with femtosecond accuracy. *Applied Optics*, 24(9):1270–1282, 1985.

P. Uhd Jepsen and S. R. Keiding. Radiation patterns from lens-coupled terahertz antennas. *Optics Letters*, 20(8):807–809, 1995.

Brian H. Kolner and David M. Bloom. Electrooptic Sampling in GaAs Integrated Circuits. *IEEE J. Quantum Electron.*, 22(1):79–93, 1986.

N. Katzenellenbogen and D. Grischkowsky. Efficient generation of 380 fs pulses of THz radiation by ultrafast laser pulse excitation of a biased metal-semiconductor interface. *Applied Physics Letters*, 58(21):222–224, 1991.

K. Kopitzki. *Einführung in die Festkörperphysik.* Teubner Studienbücher, Stuttgart, 1989. 2. Auflage.

F. K. Kneubühl and M. W. Sigrist. *Laser.* Teubner Studienbücher, Stuttgart, 1991. 3.Auflage.

A. V. Kuznetsov and C. J. Stanton. Ultrafast optical generation of carriers in a DC electric field: Transient localization and photocurrent. *Phylical Review B*, 48:10828–10845, 1993.

J. C. G. Lesurf. *Millimetre-wave Optics, Devices and Systems.* Adam Hilger, New York and Bristol, 1990.

M. Li and F. G. Sun et al. Measurement and analysis of terahertz radiation from bulk semiconductors. *Appl. Phys. Lett.*, 67(1):25–27, 1995.

Ajay Nahata and David H. Auston. Generation of terahertz radiation from a poled polymer. *Applied Physics Letters*, 67(10):1358–1360, 1995.

Ajay Nahata and Tony F. Heinz. Generation of subpicosecond electrical pulses by optical rectification. *Optics Letters*, 23(11):867–869, 1998.

T. Nakazawa and M. Tanaka. Measurements of intensities and self- and foreign-gas-broadened half-widths of spectral lines in the co fundamental band. *J. Quant. Spectrosc. Radiat. Transfer*, 28(5):409–416, 1982.

G. Otter and R. Honecker. *Atome-Moleküle-Kerne: Band 2 Molekül- und Kernphysik.* B. G. Teubner, Stuttgart, 1996.

B. M. Oliver. Thermal and quantum noise. *Proceedings of the IEEE*, 53:436–454, 1965.

J. G. Proakis and D. G. Manolakis. *Digital Signal Processing.* Macmillan, New York, 1992. 2. Edition.

H. M. Pickett, R. L. Poynter, E. A. Cohen, M. L. Delitsky, J. C. Pearson, and H. S. P. Müller. *Submillimeter, Millimeter, and Microwave Spectral Line Catalog.* http:// spec.jpl.nasa.gov., 1996.

P. Uhd Jepsen, R. H. Jacobsen, and S. R. Keiding. Generation and detection of terahertz pulses from biased semiconductor antennas. *Optical Society of America*, 13(11):2424–2436, 1996.

Stephen E. Ralph and D. Grischkowsky. Trap–enhanced electric fields in semi–insulators: The role of electrical and optical carrier injection. *Applied Physics Letters*, 59(16):1972–1974, 1991.

M. N. Spencer, C. Chackerian Jr., and L. P. Giver. The nitric oxide fundamental band: Frequency and shape parameters for rovibrational lines. *J. Molec. Spec.*, 165:506–524, 1994.

F. G. Sun, G. A. Wagoner, and X.-C. Zhang. Measurement of free–space terahertz pulses via long–lifetime photoconductors. *Appl. Phys. Lett.*, 67(12):1656–1658, 1995.

C. H. Townes and A. L. Schawlow. *Microwave Spectroscopy.* McGraw–Hill Book Company, New York, Toronto, London, 1955.

M. van Exter, Ch. Fattinger, and D. Grischkowsky. Terahertz time–domain spectroscopy of water vapor. *Optics Letters*, 14(20):1128–1130, 1989.

Martin van Exter and Daniel R. Grischkowsky. Characterizaton of an Optoelectronic Terahertz Beam System. *IEEE TRANSACTIONS ON MICROWAVE THEORY AND THECHNIQUES*, 38(11):1684–1691, 1990.

Q. Wu and X.-C. Zhang. 7 terahertz broadband GaP electro–optic sensor. *Appl. Phys. Lett.*, 70(7):1784–1786, 1997.

Q. Wu and X.-C. Zhang. Free–space electro–optics sampling of mid–infrared pulses. *Appl. Phys. Lett.*, 71(10):1285–1286, 1997.

X.–C. Zhang, B. B. Hu, J. T. Darrow, and D. H. Auston. Generation of femtosecond electromagnetic pulses from semiconductor surfaces. *Appl. Phys. Lett.*, 56(11):1011–1013, 1990.

X.-C. Zhang and D. H. Auston. Optoelectronic measurement of semiconductor surfaces and interfaces with femtosecond optics. *J. Appl. Phys.*, 71(1):326–338, 1992.

Coherent time-domain far-infrared spectroscopy

D. H. Auston and K. P. Cheung

AT&T Bell Laboratories, Murray Hill, New Jersey 07974

Received December 11, 1984; accepted December 14, 1984

A new approach to far-infrared spectroscopy is described that uses extremely short far-infrared pulses to measure the dielectric properties of materials. Optical rectification of femtosecond optical pulses is used to produce a Čerenkov cone of pulsed far-infrared radiation of approximately one cycle in duration in the terahertz spectral range. The coherent detection of the electric field of these far-infrared pulses by electro-optic sampling provides a capability for measuring precise changes in the shape of the waveform following reflection or transmission from materials. This method, which is equivalent to having a tunable laser in the spectral range from 0.1 to 2 THz, is illustrated by the measurement of the dielectric response of a solid-state plasma in *n*-type germanium and a GaAs/GaAlAs multiquantum-well superlattice.

INTRODUCTION

The far-infrared region of the electromagnetic spectrum is of crucial importance to the study of elementary excitations in solids.[1] Superconducting band gaps, lattice resonances, and impurity levels are examples of material properties whose excitation energies lie in the spectral range from a fraction of 1 TH to a few terahertz (1 THz ≡ 10^{12} sec^{-1} ≡ 4.14 mV ≡ 300 μm ≡ 33 cm^{-1} ≡ 48 K). Although the introduction of Fourier-transform spectrometers has greatly aided the exploration of the far infrared, it is clear that tunable coherent sources of radiation with greater brightness are needed. This is particularly true for the study of nonlinear and transient phenomena. For this reason, extensive work has been done on the development of free-electron lasers operating in the far infrared, and it is expected that these instruments will soon be available to the spectroscopist. The detection of far-infrared radiation also allows considerable room for improvement with regard to both sensitivity and speed of response.

In this paper we describe a new approach to far-infrared spectroscopy that uses nonlinear optics and femtosecond optical pulses to generate and measure extremely short electromagnetic transients whose frequency spectra span a large portion of the entire far-infrared spectral range. A novel feature of this method is the use of these coherent continuum far-infrared pulses to make measurements in the time domain that are entirely equivalent to having a tunable monochromatic source covering the same spectral range. The first part of the paper summarizes the generation and detection of far-infrared pulses in electro-optic materials. The use of these pulses for coherent time-domain far-infrared spectroscopy is then described in detail, followed by two illustrations of its application to the measurement of the dielectric response of semiconductors. The paper concludes with a discussion of the unique advantages of this approach, its limitations, and further improvements and applications.

FAR-INFRARED GENERATION BY THE ELECTRO-OPTIC ČERENKOV EFFECT

It was recently proposed[2,3] and demonstrated[4] that, under suitable conditions, the propagation of femtosecond optical pulses in electro-optic materials should be accompanied by the radiation of an extremely fast electromagnetic transient. This phenomenon, which arises from the inverse electro-optic effect,[5] produces a Čerenkov cone of pulsed radiation having a duration of approximately one cycle and a frequency in the terahertz range. Although this effect closely resembles the classical Čerenkov radiation from relativistic charged particles in dielectric media, its physical basis has some unique distinguishing features. Most important, it is a nonlinear optical effect, arising from a second-order nonlinear polarization, and consequently requires a lack of inversion symmetry in the host material. Also, the charge state of the effective source is neutral, being a dipole moment rather than a point charge. The velocity of the source, however, does exceed the radiation velocity because of the additional contribution to the low-frequency dielectric response from the infrared lattice vibrations. As is indicated in Fig. 1, this is expected to produce a characteristic cone of radiation in the form of a shock wave. Unlike with classical Čerenkov radiation, however, the radiation source is spatially extended, being proportional to the intensity envelope of the optical pulse. Consequently the details of the radiation field are expected to depend sensitively on both the duration and the beam waist of the optical pulse. A discussion of these effects, based on an analysis of this phenomenon, is given in Refs. 2 and 3. We summarize here only the salient features of this work.

An analysis of the electro-optic Čerenkov radiation process[2,3] predicts the following expression for the time variation of the electric field:

$$E(t) = \frac{n_0^2 r_{33} W_p}{c^2 \tau^2}\left(\frac{\sqrt{2}\cot\theta_c}{v\tau r_\perp}\right)^{1/2} \times U\left(-2, -\frac{\sqrt{2}t}{\tau}\right)\exp\left(-\frac{t^2}{2\tau^2}\right), \quad (1)$$

where W_p is the optical pulse energy, n_0 and v are the optical index of refraction and the group velocity, $r_\perp$ is the radial distance from the beam axis, θ_c is the Čerenkov cone angle [$=\cos^{-1}(c/v\sqrt{\epsilon_3})$], r_{33} is the electro-optic coefficient, $U(-2, x)$ is the parabolic cylinder function of order -2, and the parameter τ is defined by the relationship

0740-3224/85/040606-07$02.00

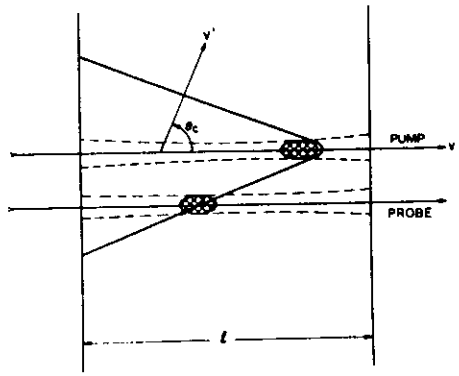

Fig. 1. Schematic of the experiment used to generate and detect short far-infrared bursts by Čerenkov radiation from femtosecond optical pulses in lithium tantalate. The Čerenkov cone of radiation propagates away from the pump pulse in a direction θ_c with a velocity that is determined by the ratio of the low-frequency index of refraction to the optical group velocity. A probe pulse measures the small birefringence that is due to the electro-optic effect induced by the electric field of the far-infrared transient as it moves in synchroniam with the Čerenkov wave front.

$$\tau = \left(\tau_p^2 + \frac{w^2\tan^2\theta_c}{v^2}\right)^{1/2}, \quad (2)$$

where τ_p is the $1/e$ half-width of the duration of the optical pulse and w is the $1/e$ beam radius (both assumed to have Gaussian profiles). The theory neglects dispersion and assumes that the point of observation is much greater than the optical beam waist. A unique feature of this result is the variation of the electric-field amplitude with the inverse 5/2 power of the pulse-width parameter τ (the field intensity varies as the inverse fifth power of τ). This makes the efficiency of this process as well as its speed much more attractive when extremely short optical pulses are used. A second aspect of the theory is the contribution to the infrared pulse duration from the beam waist of the optical pulse, as illustrated by expression (2). This means that tight focusing is necessary to produce extremely fast pulses.

The frequency spectrum of the pulse is given by the expression

$$E(\omega) = \omega^{3/2}\exp\left(-\frac{\omega^2\tau^2}{4}\right). \quad (3)$$

Since the pulse is of the order of one cycle in duration, the spectrum is extremely broad. It peaks at a frequency equal to

$$f_m = \sqrt{3}/(2\pi\tau). \quad (4)$$

Although many electro-optic materials can be used for this purpose, lithium tantalate has some particularly desirable features. First, it has a relatively large electro-optic coefficient along its polar axis equal to 2.8×10^{-11} m/V.[6] Second, it has a very low anisotropy of both its optical and low-frequency dielectric constants (0.2 and 0.5%, respectively). Third, it has a relatively large region of transparency in the far infrared, extending from dc to the transverse optic lattice resonance at 6 THz.[7]

Femtosecond optical pulses were obtained from a colliding-pulse mode-locked ring dye laser.[8] Their duration, measured by second-harmonic autocorrelation, was 100 fsec (full width at half-maximum), and their center wavelength was 625 nm. A relatively low pulse energy of only 10^{-10} J at a repetition rate of 150 MHz was sufficient for the experiments described in this paper.

COHERENT FAR-INFRARED DETECTION

The detection of the infrared pulses is accomplished with the use of a second femtosecond optical pulse, which is synchronized and delayed with respect to the generating pulse, as illustrated in Fig. 1. This configuration exploits a novel symmetry arising from the use of the electro-optic effect for both generation and detection. In the case of the generating pulse it is the inverse electro-optic effect that produces the nonlinear polarization responsible for the radiation field, and in the detection process it is the direct electro-optic effect that is used to measure the small birefringence produced by the electric field of the radiation pulse. This latter technique, known as electro-optic sampling,[9] was previously used to measure subpicosecond electrical transients in traveling-wave electro-optic transmission lines.

An example of the waveform measured by this technique is shown in Fig. 2. It is extremely fast and represents a single cycle of a frequency of approximately 1 THz. Its shape closely resembles the theoretical waveform predicted by expression (1). By calibrating the detection method, the electric-field amplitude was estimated to be 10 V/cm. For this measurement both optical pulses were focused on a sample of lithium tantalate through a common lens and were carefully aligned to propagate parallel through the crystal. The generating pulse was polarized parallel to the *c* axis of the crystal (out of

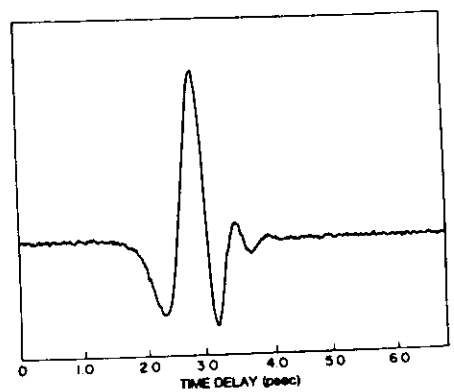

Fig. 2. Experimental observation of the electric-field waveform of the far-infrared transient measured by the method illustrated in Fig. 1. A lithium tantalate crystal 1 mm in length was used with 100-fsec optical pulses focused to a beam waist of approximately 7 μm. The peak amplitude of the electric field was approximately 10 V/cm. The true shape of the far-infrared pulse is faster than the result shown here because of the convolution with the probe pulse.

Spatiotemporal shaping of terahertz pulses

Jake Bromage, Stojan Radic, G. P. Agrawal, and C. R. Stroud, Jr.

The Institute of Optics, University of Rochester, Rochester, New York 14627

P. M. Fauchet and Roman Sobolewski

Department of Electrical Engineering and Laboratory for Laser Energetics, University of Rochester, Rochester, New York 14627

Received January 10, 1997

We report temporal shaping of few-cycle terahertz pulses, using a slit in a conductive screen as a high-pass filter. The filter's cutoff frequency was tuned by changing the width of the slit; the slope of the cutoff transition was altered by changing the thickness of the screen. We measured the transmission function of the filters, using large-aperture photoconducting antennas to create and detect the incident and transmitted electric field. Our experimental results were in excellent agreement with the performed finite-difference time-domain simulations of the propagation of the pulse through the slit. When the screen thickness was greater than the slit width, the filter was well modeled by a short, planar waveguide. Using a simple transfer function, we accurately describe the sharp cutoff and dispersion of such a filter. © 1997 Optical Society of America

Recently terahertz (THz) pulses have proved useful for a wide variety of applications, including far-infrared[1]/time-domain spectroscopy,[2] study and control of Rydberg atoms,[3] T-ray imaging of optically opaque materials,[4] and impulse-ranging studies.[5] Applications exploit the features of THz pulses that distinguish them from optical pulses, namely their broad bandwidth and long center wavelength. The broad bandwidth allows for the exciting possibility for sculpting the pulses to meet a desired goal by modifying their spectra. Although shaped THz pulses have been made by modifying the optical pump intensity profile[6] or by manufacturing more complex emitters,[7] there are advantages to sculpting the THz field directly.[8,9] Because of the long wavelengths, fabricating quasi-optical components for THz pulses is easier than for optical pulses. Further, we can directly characterize the effect of the THz shaping elements on the pulse, using sampling techniques to measure the electric field rather than the intensity.

In this Letter we report experiments in which we shaped THz pulses using a slit in a conductive screen as a high-pass filter.[10] We show that the shape of the electric-field pulse transmitted through such a slit filter depends on the slit width and the screen thickness. The filter's high-pass cutoff frequency, ν_c, is inversely proportional to the slit width, d, and so it can easily be tuned. Varying the screen thickness, l, leads to two modes of operation: If the screen thickness of the filter is much less than the cutoff wavelength, the filtering results from lower frequencies' diffracting more severely. On the other hand, if the filter's thickness is greater than the cutoff wavelength, the filter behaves like a short planar waveguide. This produces a much sharper cutoff transition and pulse dispersion, which we describe with a simple transfer function. We also show the highly accurate results of finite-difference time-domain (FDTD) simulations of pulses propagating through both types of slit filter.

The experimental configuration is shown in Fig. 1. Both the emitter and detector of the THz radiation were large-aperture photoconductive antennas.[11] We made the emitter of 1-cm^2 ⟨100⟩ semi-insulating GaAs biased with a field of 2 kV/cm via parallel Au–Ge–Ni electrodes. A 150-fs, 810-nm Ti:sapphire optical pulse triggered the THz emission by uniformly illuminating the GaAs wafer with a fluence of 20 μJ/cm^2. We fabricated the detector by depositing parallel Au–Ge–Ni electrodes, spaced 2 mm apart, upon an epilayer of low-temperature molecular-beam-epitaxy-grown GaAs (LT-GaAs). The 1.5-μm-thick LT-GaAs layer was grown at 200 °C and annealed *in situ* at 600 °C to produce a short carrier lifetime of ~1 ps. A delayed Ti:sapphire pulse gated the detector by uniformly illuminating the 2-mm^2 active area with a fluence of 0.5 mJ/cm^2. When the optical and the THz pulses were present in the LT-GaAs at the same time, the carriers produced by the optical pulse were accelerated by the electric field of the THz pulse. The component of the THz field perpendicular to the detector electrodes caused a current to flow in an external circuit. We measured this small current (~1 pA) by chopping the 1-kHz optical pulse train that triggers the emitter and using a lock-in amplifier. By varying the delay between the arrival of the THz pulse and the optical gating pulse at the detector,

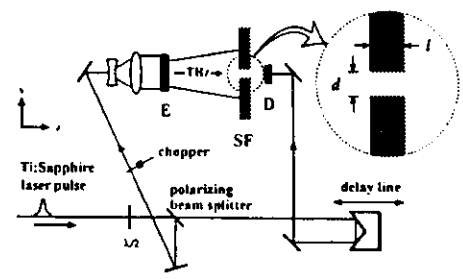

Fig. 1. Schematic of the experimental setup showing the THz emitter (E), the dimensions of the slit filter (SF), and the detector (D). The THz radiation is polarized along the y axis.

0146-9592/97/090627-03$10.00/0

Terahertz emission of population-inverted hot-holes in single-crystalline silicon

E. Bründermann[a] and E. E. Haller
Lawrence Berkeley National Laboratory and University of California, Berkeley, California 94720

A. V. Muravjov
Institute for Physics of Microstructures, Russian Academy of Science, Nizhny Novgorod 603600, Russia

(Received 20 April 1998; accepted for publication 8 June 1998)

We report THz emission of hot-holes in p-type silicon doped with a boron acceptor concentration of $N_A = 1.5 \times 10^{15}$ cm^{-3}. We apply crossed electric (E) and magnetic (B) fields to the crystal cooled to liquid helium temperature. Optical gain is found for field ratios E/B in the range 0.5–1 kV cm^{-1} T^{-1}. We calculate optical gain spectra in Si and identify possible laser transitions.
 [S0003-6951(98)01832-4]

Bulk single-crystalline silicon is not expected to function as a laser material due to its indirect band gap. However, Krömer pointed out in 1958 that microwave amplifiers based on hot-holes in p-type germanium and silicon could be built by using the warped valence band structure and optical phonon emission.[1] Andronov *et al.*[2] suggested that superposing a magnetic field perpendicular to an electric field can create conditions for heavy holes to emit optical phonons and to convert with a finite probability into light holes while light holes do not emit optical phonons and are trapped in cyclotron orbits. This leads to a hot-hole population inversion in the valence band between light- and heavy-hole Landau levels or within the light-hole Landau levels. The first observation of such an inversion[3] in Ge was followed by the demonstration of the hot-hole p-type Ge laser in 1984.[4,5] Those lasers were doped with $N_A = 10^{14}$ cm^{-3} acceptors, had a low compensation ($< 10\%$) and operated in crossed electric and magnetic ($\mathbf{E} \perp \mathbf{B}$) fields. Low compensation is required to minimize impurity scattering which reduces the light-hole lifetime. Acoustical phonon scattering is another process which significantly limits the light-hole lifetime. Therefore, the operating temperature for Ge lasers is limited to below 20 K. Modern Ge hot-hole lasers with nonhydrogenic acceptors can be tuned continuously between 1 and 4 THz.[6,7]

Several theoretical papers[8–12] report calculations of Si hot-hole laser parameters but no reliable experimental proof of a population inversion has been published. The advantageous predictions for Si in comparison to Ge lasers involve a wider frequency tuning range up to 10 THz[8,10] and optical gain at temperatures as high as 77 K.[8,12] Operation of THz lasers at such high temperatures will have a major impact on future astronomical studies from satellites. Those lasers could be used as local oscillators in heterodyne receivers to measure radiation from molecules involved in star formation. Here we present the first observations of THz emission from population-inverted hot-holes in p-type silicon.

Two boron doped Si samples ($N_A = 1.5 \times 10^{15}$ cm^{-3}) were cut and polished similar to Ge laser crystals.[6] The dimensions are $30 \times 5 \times 4.1$ mm^3 and $3 \times 3 \times 4.0$ mm^3. The ohmic contacts were formed by implantation of boron ions with a dose of 3×10^{15} cm^{-2} at 33 keV on two opposite faces at 77 K followed by annealing at 500 °C for 1 h.[13] Finally, the crystals were metallized by sputtering of 20 nm Cr, 20 nm Pd and 200 nm Au. The inter-contact distances were 4.1 and 4.0 mm. All crystal surfaces were oriented parallel to (100). The crystals were immersed in liquid helium (LHe) at 4.2 K. A dc magnetic induction B up to 7 T perpendicular to the electric field was applied by a superconducting coil in the ⟨001⟩ direction along the 30 or 3 mm long sample axis, respectively. The heavy-hole current flows in the vicinity of the heaviest hole mass direction along the ⟨110⟩ axis due to the Hall field component. This orientation was predicted to be preferable for a population inversion.[9] The applied electric field E was pulsed with variable pulse length (1–20 μs) and repetition rate (1–20 Hz). The high refractive index of Si facilitates amplification of internal reflection modes. Emission pulses were measured by a Ge:Ga photodetector mounted above the Si crystal in LHe in the Faraday configuration and observed on a 500 MHz digital oscilloscope.

Figure 1 shows the emission signal of the 30 mm long Si crystal. We interpret the increase in emission below 1 kV cm^{-1} T^{-1} with spontaneous emission of accumulated light holes. The further nonlinear steep increase in the 0.6–0.75 kV cm^{-1} T^{-1} range corresponds to optical gain. We find the maximum emission for $B = 3$ T at $E/B = 0.65$ kV cm^{-1} T^{-1}.

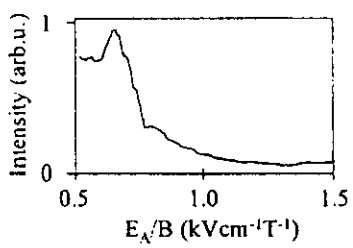

FIG. 1. Emission from the 30 mm Si crystal vs the applied electric field (E_A) and magnetic induction (B) ratio E_A/B. The applied electric field was 1.8 kV/cm.

[a]On leave from DLR, Institute of Space Sensor Technology, Berlin, Germany. Electronic mail: E_Brundermann@lbl.gov

Ultrafast carrier trapping and slow recombination in ion-bombarded silicon on sapphire measured via THz spectroscopy

Stuart D. Brorson, Jucheng Zhang,[a] and Søren R. Keiding
Odense Universitet, DK-5230 Odense M, Denmark

(Received 29 November 1993; accepted for publication 8 February 1994)

We have performed two different types of femtosecond pump and probe measurements on THz transmitting antennas fabricated on ion-bombarded silicon-on-sapphire chips. We find evidence that the decay of the photoexcited current occurs on a time scale of less than 1 ps. Simultaneously, we observe unambiguous evidence of screening originating from carriers trapped in long-lived trap states. A simple model of carrier transport and screening in the presence of fast trapping and slow recombination is discussed.

The fastest electrical pulses obtainable are produced using Auston switches (photoconductive gaps) fabricated on photoconductors having relaxation times on the order of 1 ps or less.[1] One such material of great technological importance is ion-bombarded silicon on sapphire (SOS), which has been measured having relaxation times as fast as 600 fs.[2,3] It is ordinarily supposed that the relaxation is due to extremely fast carrier trapping and/or recombination at localized defect sites caused by ion bombardment.[1,2] In this letter we describe results obtained from two different types of femtosecond pump and probe measurements on THz transmitting antennas fabricated on ion-bombarded SOS. The results of these measurements show unequivocally the presence of screening in the irradiated region of the Auston switch over nanosecond time scales. Simultaneously, we observe that the relaxation time of the photoexcited current is <1 ps. Our measurements are consistent with ultrafast trapping of mobile carriers dominating over recombination, followed by slow recombination of the trapped carriers.

The experiments were performed using miniature dipole antennas fabricated on SOS chips. Similar devices are commonly used in THz spectroscopy; the set up is reviewed in detail in Ref. 4. We used "10-30-10" antennas for our experiments. The electrode spacing in the photoconducting gap was 5 μm; the width of the "tabs" forming the antenna was 10 μm. The silicon layer was 0.5 μm thick. The photoconductive region was ion bombarded with a dosage of 10^{14} cm^{-2} using 100 keV O^+ ions, giving a mean implantation depth of 0.22 μm and a straggle of 0.053 μm.[5] The transmitting and receiving antennas were pumped with $\approx$200 fs, $\lambda = 750$ nm pulses from a mode-locked $TiAl_2O_3$ laser. All data were obtained using synchronous detection techniques (i.e., chopper and lock in).

Both experiments discussed here were pump and probe measurements on the transmitting antenna similar to those reported in Ref. 6. In the first measurement, the transmitting antenna is excited by two laser pulses—called "pump" and "probe"—which are separated by a fixed time delay T. The time behavior of the *emitted THz signal* is measured at the receiving antenna by scanning the arrival time t of a laser pulse—called the "gate"—at the receiver. Below, we will call this the "THz measurement." In the second measurement, we monitor the *current flowing in the transmitting antenna*, and sweep the time delay T between pump and probe pulses. We will refer to this as the "current measurement" below. It is similar in principle to measurements previously reported by Carruthers in ultrafast photodiodes,[7] and by Hall *et al.* in semiconductor laser amplifiers.[8]

In the THz measurement, we chopped only the pump laser beam at frequency f_1 (typically $\approx$1 kHz), and detected the THz signal at the receiver using a lock-in amplifier tuned to the same frequency. Then, scans were taken of the received THz signal for different time delays between pump and probe. Representative data are shown in Fig. 1, where the probe pulse has been delayed over a range $T \approx -6$ to $+6$ ps. The data shown were taken for equal powers in pump and probe beams, $P_{pu} = 13.4$ mW, $P_{pre} = 13.8$ mW. The THz pulse radiated by the pump beam is clearly visible at $t = 0$.

Also visible is a signal due to the probe which can be

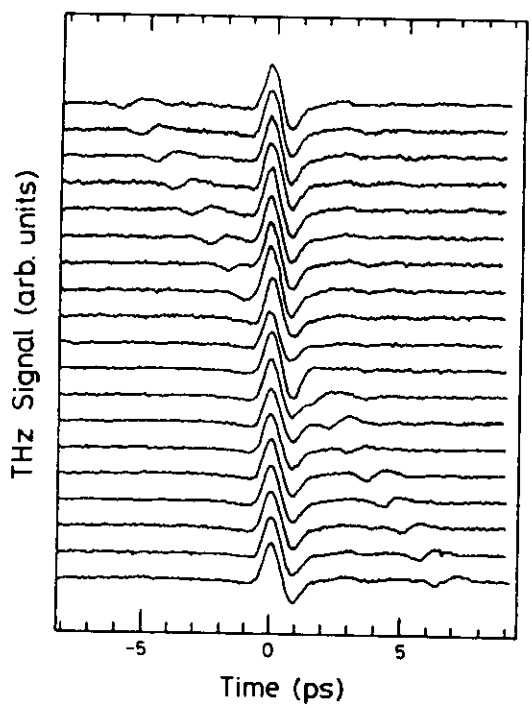

FIG. 1. THz pulse amplitude vs time t at the receiving antenna. The THz pulse produced by the chopped pump is visible at $t = 0$. Also visible is the smaller signal caused by the probe pulse at the transmitter, running from ≈ -6 ps (upper left) to $\approx +6$ ps (lower right).

[a]Permanent address: Laser Research Institute, Hebei Academy of Sciences, Shijiazhuang, China.

 0003-6951/94/64(18)/2385/3/$6.00

Coherent terahertz radiation detection: Direct comparison between free-space electro-optic sampling and antenna detection

Y. Cai, I. Brener,[a] J. Lopata, J. Wynn, L. Pfeiffer, and J. B. Stark
Bell Laboratories, Lucent Technologies, Murray Hill, New Jersey 07974

Q. Wu and X. C. Zhang
Physics Department, Rensselaer Polytechnic Institute, Troy, New York 12180

J. F. Federici
Department of Physics, New Jersey Institute of Technology, Newark, New Jersey 07102

(Received 19 March 1998; accepted for publication 26 May 1998)

We compare the use of free-space electro-optic sampling (FSEOS) with photoconducting antennas to detect terahertz (THz) radiation in the range of 0.1–3 THz. For the same average THz power and low-frequency modulation, signal-to-noise ratio and sensitivity are better with antenna detection at frequencies smaller than 3 THz. When the modulation frequency is increased to more than 1 MHz in FSEOS, both detection schemes have comparable performance. Using a singular-electric-field THz emitter, we demonstrate the feasibility of a THz imaging system using real-time delay scanning in FSEOS and only 20 mW of laser power. [S0003-6951(98)03930-8]

Traditional coherent terahertz (THz) radiation detection schemes involve the use of gated photoconducting antennas as detectors for freely propagating THz electromagnetic waves. This is true both for THz spectroscopy[1–5] and for THz imaging systems.[6] Recently, some groups have used free-space electro-optic sampling (FSEOS) as an alternate detection scheme.[7–13] The advantage of the latter is the higher detection bandwidth that can be as high as 37 THz.[12] Although previous reports of FSEOS measurements showed reasonable signal-to-noise ratios (SNR), a detailed comparison between both techniques for the *same* laser power is still missing. It is the purpose of this letter to present such a comparison, especially in the limit of low laser power and to show the feasibility of a fast delay scan, single-pixel imaging system based on FSEOS.

In order to carry out this comparison, we use a compact THz system with a common generator and dual detection capability as shown in Fig. 1. Both pump and probe beams are derived from a mode-locked Ti:sapphire laser (100 fs, 800 nm). The emission of freely propagating THz waves is achieved by exciting a singular-electric-field photoconductive antenna[2,3] with pulses from this laser. These emitters were fabricated on low-temperature GaAs (LTG) with dipole lengths of 45 and 60 μm and a 5 μm gap biased at ~40 V. The excitation power is kept fixed at ~20 mW. The detection side consists of a dual setup. Figure 1(a) shows the FSEOS setup where the detector is a 2.2 mm thick ZnTe crystal. A pair of balanced silicon photodiodes (OSD 5-5TR with TMO-16-1 transformer for impedance matching) is used to analyze the polarization rotation that the THz field induces on the visible probe beam. Figure 1(b) shows the antenna (75 μm LTG dipole with a 5 μm gap) detection scheme. The probe power used in the FSEOS detection is 1.8 mW (0.9 mW on each photodiode). In order to maximize the SNR, the photocurrent in each photodiode has to be maximized but be kept below saturation. In the antenna detection scheme, we use a ~20 mW laser beam to gate the antenna.

Both detection schemes rely on lock-in detection, chopping the laser beam that generates the THz radiation. When the chopping frequency is kept at a few kilohertz, the antenna detection scheme always has a better SNR (by almost two orders of magnitude in our system). The electro-optic sampling technique is very sensitive to laser noise (which can be quite substantial in an Ar-pumped Ti–sapphire laser at low frequencies) and to low-frequency mechanical and acoustical disturbances. This is because one has to detect very small changes in polarization (typically, $\sim 10^{-4}$–10^{-5}) in the probe beam. On the other hand, photoconducting antennas directly detect a photocurrent induced by the incident THz field. The laser noise influence can be overcome by modulating the visible pump beam at high frequencies (>1 MHz); This typically lowers the laser noise by ~30 dB.

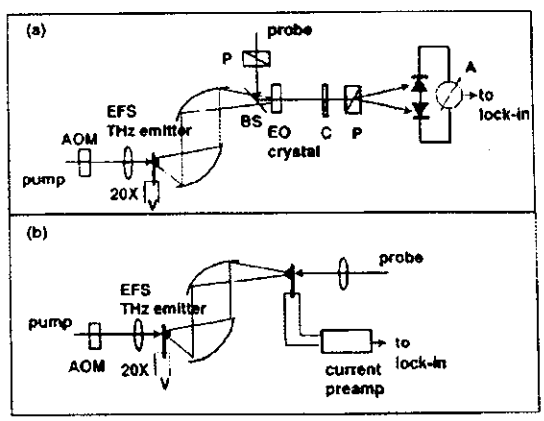

FIG. 1. Experimental setup: (a) free-space electro-optic sampling; (b) photoconductive antenna. In both cases the THz source is a singular-electric-field emitter with 20 mW pump and 40 V bias (~80 μA photocurrent).

[a]Electronic mail: igal@bell-labs.com

Design and performance of singular electric field terahertz photoconducting antennas

Y. Cai[a)]
Department of Electrical and Computer Engineering, New Jersey Institute of Technology, 161 Warren Street, Newark, New Jersey 07102

I. Brener, J. Lopata, J. Wynn, and L. Pfeiffer
Bell Laboratories, Lucent Technologies, 700 Mountain Avenue, Murray Hill, New Jersey 07974

J. Federici
Department of Physics, New Jersey Institute of Technology, 161 Warren Street, Newark, New Jersey 07102

(Received 5 May 1997; accepted for publication 12 August 1997)

We present new designs of more efficient terahertz (THz) radiation emitters and detectors enhanced by electric field singularities using sharp and laterally offset electrodes. We compare the performances of the terahertz emission and different polarization properties resulting from these structures. An average THz radiation power of 3 μW is achieved under 20 mW excitation, calibrated by free space electro-optic sampling. We also study the gap size dependence of the THz radiation, and find an absence of a positive electrode effect in the small gap limit. © *1997 American Institute of Physics.* [S0003-6951(97)03341-X]

We have recently shown that singular electric fields occurring near sharp metal electrode structures can significantly enhance the THz radiation emanating from photoexcited photoconductive switches.[1] This enhancement is due to both the acceleration of carriers in very high electric fields and to optical rectification through field enhanced $\chi^{(2)}$. In that previous work, we used electrode gaps larger than 75 μm, and most of the enhancement appeared near the anode. We also observed that a saturation in the THz emission intensity was reached for a given electrode spacing, thus limiting the efficiency of these emitters. In this work we describe even more powerful THz emitters and detectors by using new electrode geometries in the limit of small gaps that optimize the singular electric fields experienced by the photogenerated carriers. We compare the relative THz radiation power of various new dipole designs, and calibrate the absolute average power of the THz beam using free space electro-optic sampling.

The new THz emitters consist of two coplanar striplines with sharp indentations facing each other, as depicted in the inset of Fig. 1. We vary the separation between the parallel striplines d and the gap distance g. If g is small, then d is approximately equal to the dipole length. Two dimensional electrostatic calculations were carried out during the design process. Invariably, the strongest fringing electric fields are found near the triangular tips (i.e., structure TTM and TT0 in Fig. 1 inset). The sharpness of the electrodes determines the peak value of the singular electric field. Moreover, the fringing fields are enhanced when laterally offset electrodes are used (i.e., structure TT0 in Fig. 1 inset). The offset angle provides additional control in maximizing the overlap of high electric field regions with the laser excitation spot.

The photoconducting antennas are fabricated by conventional lithography on low temperature (LT) GaAs grown at ~250 °C and post-annealed at 600 °C for 1 min. The metal patterns are deposited using one of the usual schemes for ohmic contacts on n-type GaAs (Au–Ge, Ni, Ti, Au). Figure 1 (inset) shows a schematic diagram of the metal electrodes deposited on the structures.

First we measure and compare the THz emission intensity of each structure by using a standard coherent THz detection system with scanning capabilities on the emitter side.[1] The peak and average THz power are calibrated with free space electro-optic sampling.[2] On the emitter side, a short laser pulse (780 nm, ~100 fs) excites the sample through a 50× objective. The emitter is scanned with a spatial resolution of 0.4 μm, and the terahertz signals are recorded for each pixel. The generated THz radiation is then collected with a pair of off-axis paraboloids. The detection side consists of a dual setup, antenna and free space electro-optic sampling. In the antenna detection scheme, the THz dipole antenna is fabricated on LT GaAs using a 75-μm-long and 20-μm-wide conventional dipole structure FF as shown

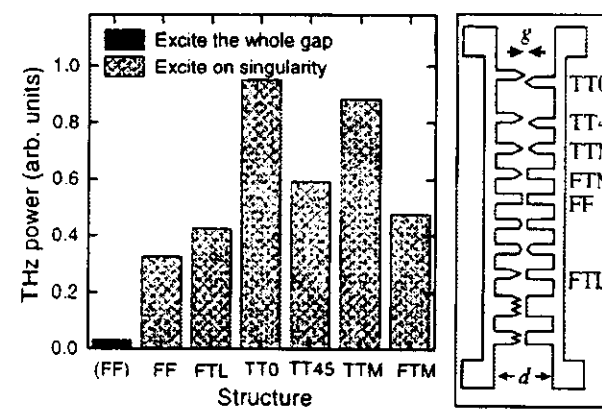

FIG. 1. THz radiation power as a function of dipole structures measured in a 60 μm dipole, 5 μm gap, under 20 V bias and 20 mW excitation. Shown in the inset is a schematic diagram of the metal electrodes used in the new THz emitters and detectors.

[a)]Electronic mail: yicai@physics.bell-labs.com

 0003-6951/97/71(15)/2076/3/$10.00

Far-infrared terahertz time-domain spectroscopy of flames

R. A. Cheville and D. Grischkowsky

School of Electrical and Computer Engineering and Center for Laser Research, Oklahoma State University, Stillwater, Oklahoma 74078

Received March 13, 1995

We present what is to our knowledge the first comprehensive far-infrared absorption measurement of flames. These measurements, covering the region of 7–88 wave numbers (0.2–2.65 THz) are only now made possible by the technique of terahertz time-domain spectroscopy. We observe a large number of absorption lines—including those of water, CH, and NH_3—in a stationary, premixed, propane–air flame. The absorption strength permits the determination of species concentration along the beam path. The flame temperature is determined by comparison of the relative strengths of the water vapor lines. © 1995 Optical Society of America

For commercial as well as scientific reasons, combustion processes have been the subject of intensive investigation. Important questions for understanding and accurately modeling combustion are the species present in the flame and the spatial distribution and temperature of these species. A wide variety of laser-based techniques, such as laser-induced fluorescence, four-wave mixing, and various Raman processes, have been used to measure one or more of these parameters.[1] Nonlinear techniques offer excellent spatial resolution but provide data that can be difficult to interpret, and the high intensities required may perturb the flame. Fluorescence methods have excellent sensitivity but are often affected by quenching and broadband emission from soot. Since no method is capable of providing a complete characterization of flames, alternative techniques are often used in conjunction.

Here we report what is to our knowledge the first panoramic far-infrared [terahertz (THz)] absorption measurement of combustion products in a premixed laminar hydrocarbon–air flame. The comprehensive spectra that we obtain provide a survey of the relative abundance of the constituents of the flame. Such overview data are also valuable in guiding higher-resolution methods to spectral regions of interest and in determining absolute concentrations of important constituents for application of other techniques having better spatial and temporal resolution. We also determine the flame temperature by comparing relative populations of rotational states of water vapor. Previous studies that used diode lasers to monitor vibrational–rotational transitions[2] and coherent anti-Stokes Raman spectroscopy of the ν_1 band[3] have demonstrated the importance and accuracy of water vapor thermometry.

Before the research described in this Letter, comprehensive far-infrared (THz) absorption spectroscopy of flames had not been possible. This situation is due mainly to the fact that alternative methods such as Fourier-transform spectroscopy use incoherent bolometric (liquid-helium-cooled) detection, which is overwhelmed by the copious amounts of far-infrared radiation emitted by flames. In contrast, our newly developed THz time-domain spectroscopy (THz-TDS) technique[4] uses a time-gated coherent receiver, which is immune to the THz radiation emitted by the flame. At the same time the coherent detection is 1000 times more sensitive to THz radiation than a helium-cooled bolometer. Another important advantage is that the THz source generates a well-collimated, low-divergence beam for which the receiver has a corresponding small acceptance angle. Amplitude signal-to-noise ratios in THz-TDS can exceed 10^4:1 (10^8:1 in power). Finally, the bandwidth of THz-TDS can extend continuously over a wide spectral range, from 0.1 to greater than 6 THz, permitting the simultaneous detection of many species.

The THz-TDS setup shown in Fig. 1(a) was described previously.[4] As depicted in Fig. 1(a), the collimated 1-cm-diameter THz beam passed through a premixed laminar flame. The atmospheric pressure flame was stabilized on a water-cooled porous sintered bronze burner,[5] 2.5 cm wide by 12.5 cm long. Such flames are stationary—the spatial geometry and composition remain constant in time. Our flame was stable over the duration of the experiment. Propane and dry air in a near-stoichiometric 1:22 ratio were supplied to the burner at a 20-L/min total flow rate. The entire apparatus was contained in an airtight box purged with dry air to eliminate the effects of ambient water vapor.[6] The burner was isolated in a metal chimney separate from the airtight box and vented to air through a metal baffle to prevent contamination of the dry air by combustion products. The windows separating the flame from the enclosure were thin quartz plates (~0.16 mm thick) fused onto quartz tubes that extended the windows into the flame.

A measured THz pulse envelope for this system with 12.5 cm of laboratory air (15% relative humidity) between the windows is partially shown in Fig. 1(b). The complete measurement extended to 290 ps. Shorter scans provide less spectral resolution but a better signal-to-noise ratio. All the structure following the excitation pulse is signal from water vapor. The noise level on this scan is <0.1 pA, resulting in a signal-to-noise ratio of more than 10,000:1. To obtain a better numerical spectral resolution, we extended the full 290-ps time-domain data with zeros[7]—increasing the length by a factor of 16 before taking the Fourier transform shown in Fig. 1(c). The n-fold extension of a data set by zeros at equally

0146-9592/95/151646-03$6.00/0

Generation of 10-THz transients from a subpicosecond optical pulse and a 1-THz field in quantum wells

D. S. Citrin[a)]
Department of Physics, Semiconductor Optics Theory Group, Washington State University, Pullman, Washington 99164-2814

(Received 26 September 1996; accepted for publication 1 November 1996)

A quantum well simultaneously subjected to a 1 kV/cm, 1 THz field, and a 100 fs optical pulse is shown to result in emission of a sub-ps strong upshifted ~10 THz transient. © *1997 American Institute of Physics.* [S0003-6951(97)01601-X]

In the following, we propose the simultaneous exposure of a quantum well (QW) to a broadband $\tau \lesssim 100$ fs optical pulse (τ is the pulse duration)—to excite both free and Coulombically bound electron-hole (e–h) pairs (excitons) from the crystal ground state—[1]and a $\mathscr{E}_0 \sim 1$ kV/cm, $\omega_0 \sim 1$ THz driving field to enable the generation of sub-ps ~10 THz electromagnetic (EM) transients.[2] The 10 THz emission is due to the time-varying dipole moment of the photoexcited radial e–h wavepacket in the 1 THz field, and arises from the quantum beating between the $1s$ exciton and continuum contributions of the wavepacket. We show that the amplitude of the emitted field is expected to be a factor of 10 larger than submillimeter fields generated from QWs via charge oscillations or optical rectification.[3] The use of a QW rather than a bulk semiconductor is beneficial since with compressive strain we can conveniently further increase the splitting of the heavy- and light-hole excitons thus eliminating undesired quantum beats between these levels and the ensuing complications for the strong-field dynamics.

We begin with a discussion of the excitation of the wavepacket which supplies the initial conditions for the strong-field dynamics and then consider the generation of EM transients by the wavepacket in the presence of an intense THz field. In the QW, an optical pulse centered near the QW bandedge E_0 and with a bandwidth that exceeds the $1s$-exciton binding energy E_b coherently excites from the crystal ground state exciton s states with principle quantum numbers ranging from $n=1$ through the continuum.[1] The wavepacket dynamics subsequent to impulsive optical excitation can be reconstructed theoretically from the linear optical susceptibility $\chi(t)$ in the time domain. The e–h radial wavepacket $\psi(\mathbf{r}=0,t)=\int_{-\infty}^{t} dt' \chi(t-t')\mathscr{E}_{\rm opt}(t')$, up to a normalization constant, where $\mathscr{E}_{\rm opt}(t)$ is the electric field of the excitation optical pulse with $\mathbf{r}$ in the in-plane relative e–h coordinate.[4] By working in the Lehman representation of the Hamiltonian H for an electron and hole interacting via their mutual Coulomb interaction, we can reconstruct the entire $\mathbf{r}$ and t dependence of $\psi(\mathbf{r},t)$. The e–h wavepacket for arbitrary $\mathbf{r}$ is $\psi(\mathbf{r},t)=\int_{-\infty}^{t} dt' D(\mathbf{r},0;t-t')\mathscr{E}_{\rm opt}(t')$, where $D(\mathbf{r},\mathbf{r}';t)$ is the Green's function, with a normalization defined below, for the e–h relative motion in the presence of the e–h Coulomb interaction, i.e., $D^{-1}=\epsilon - H$, where ϵ is the energy variable and $H\varphi_k(\mathbf{r})=E_k\varphi_k(\mathbf{r})$ with φ_k the exciton envelope function with quantum numbers k and E_k the energy of the state.

To calculate the response to the strong THz field, we assume that we can apply to $\psi(\mathbf{r},t)$ the classical equations of motion $\mathbf{x}(t)=-x_0\hat{\mathbf{n}}_x[\cos(\omega t+\phi)-\cos\phi+\omega t\sin\phi]$ for a free electron of reduced mass μ subject to initial conditions $\mathbf{x}(0)=\dot{\mathbf{x}}(0)=0$ in the time-varying electric field $\mathscr{E}(t)\hat{\mathbf{n}}_x = \mathscr{E}_0\hat{\mathbf{n}}_x\cos(\omega t+\phi)$, where $x_0=e\mathscr{E}_0/\mu\omega^2$ is the amplitude of the induced displacement, $\hat{\mathbf{n}}_x$ is a unit vector in the x direction which lies in the QW plane, and ϕ is the phase of the driving field at the time $t=0$ of photoexcitation.[5,6] Both quiver and drift contributions are included in $\mathbf{x}(t)$.[6] In fact, we shall see that the treatment below applies to more general cases, such as pulsed THz fields since the upshifted emission occurs within the first THz cycle. The remaining step is to calculate the electric-dipole response $ed(t)=\langle\psi(t)|ex|\psi(t)\rangle$, and hence the EM emission $\propto\ddot{d}(t)$, associated with the wavepacket. We only consider the $1s$ $[\psi_{1s}(\mathbf{r},t)]$ and continuum $[\psi_c(\mathbf{r},t)]$ terms in the wavepacket. (Our calculations have shown that the wavepacket dynamics under broadband excitation are dominated by the $1s$ and continuum states.[7]) Moreover, we take $\psi_{1s}(\mathbf{r},t)=\int_{-\infty}^{t} dt' D_{1s}(\mathbf{r},0,t-t')\mathscr{E}_{\rm opt}(t')$ to be given by the zero-field expression, and we make a semiclassical approximation for $\psi_c(\mathbf{r},t)$, namely, we take for the time-dependent continuum part of the wavefunction in the presence of the driving field to be $\psi_c(\mathbf{r},t)=\int_{-\infty}^{t} dt' D_c(\mathbf{r},0,t-t')\mathscr{E}_{\rm opt}(t')$.[5] Here $D_{1s}(\mathbf{r},0,t)=\varphi_{1s}(\mathbf{r})e^{-iE'_{1s}t/\hbar}\theta(t)$ with $E'_{1s}=E_{1s}-i\Gamma_{1s}$, where E_{1s} is the energy of the $1s$ exciton and Γ_{1s} is its homogeneous width, and $D_c(\mathbf{r},0,t)=-i[(2\pi)^2\mu/(\hbar t)]\varphi_{1s}^{-1}(0)\exp[i\mu|\mathbf{r}-\mathbf{x}(t)|^2/(2\hbar t)]\times\exp\{-i[E'_0-\frac{1}{2}\mu\dot{x}^2(t)]t/\hbar\}\theta(t)$ is the 2D free-particle propagator with $E'_0=E_0-i\Gamma_0$, where E_0 is the energy of the edge of the e–h continuum and $\Gamma/\hbar$ its dephasing rate assumed energy and state independent.[8] We have neglected the Sommerfeld factor in the continuum, which for realistic QWs has a rather weak effect. One finds for $t>\tau$ that the upshifted portion of the dipole moment is dominated by $d(t)\approx 2\mathrm{Re}\langle\psi_c(t)|x|\psi_{1s}(t)\rangle$. In the following, we assume an excitation optical pulse $\mathscr{E}_{\rm opt}(t)=\delta(t)$, i.e., the pulse duration is much less than ω_b^{-1}. In addition, we neglect the effect of dephasing while the pulse is present. To facilitate the evaluation of the matrix element, we approximate $\varphi_{1s}(\mathbf{r})=(\eta\pi^{1/2})^{-1}\exp(-r^2/\eta^2)$, where $\eta\approx a_0/2$ (a_0 is the bulk exciton Bohr radius) may be determined variationally. Provided x_0 and the spatial width of $\psi_c(\mathbf{r},t)$ far exceeds

a)Electronic mail: citrin@wsu.edu

 0003-6951/97/70(10)/1189/3/$10.00

Optical Rectification at Semiconductor Surfaces

Shun Lien Chuang

Department of Electrical and Computer Engineering, University of Illinois at Urbana-Champaign, Urbana, Illinois 61801

Stefan Schmitt-Rink,[a] Benjamin I. Greene, Peter N. Saeta, and Anthony F. J. Levi

AT&T Bell Laboratories, Murray Hill, New Jersey 07974

(Received 16 July 1991)

We show that far-infrared radiation can be generated in the depletion field near semiconductor surfaces via the inverse Franz-Keldysh effect or electric-field-induced optical rectification. This mechanism is conceptually different from those previously proposed and accounts for many recent experimental observations.

PACS numbers: 78.20.Jq, 42.65.Bp, 73.25.+i

A significant body of work dating back to the early days of pulsed lasers has explored the generation of far-infrared (FIR) radiation using visible-light sources and electro-optic materials. In such materials, the nonlinear interaction between two optical fields produces a static or slowly varying electric field at the beat frequency, with an intensity determined by the instantaneous intensity of the optical fields. This phenomenon has been designated as the "inverse electro-optic effect," "optical rectification," or, more generally, "difference frequency mixing" [1]. A number of picosecond time scale demonstrations of this effect have appeared in the literature [2]. More recently, the generation and detection of picosecond and subpicosecond FIR transients has taken a new direction, utilizing photoconductive media coupled to antenna structures [3]. In these experiments the FIR generation process has been explained as Hertzian radiation from time-varying electric currents.

Very recently, it has been shown experimentally that ultrashort pulses of FIR radiation can also be generated from ultrashort optical pulses incident on a semiconductor surface [4,5]. This observation opens up new and exciting possibilities for terahertz spectroscopy and characterization of electronic properties of semiconductor surfaces. These studies have culminated in the observation of FIR transients as short as 120 fs [5]. The commonly accepted explanation for the effect has remained in the domain of "current surges" occurring in the surface depletion field [4]. In the present work, however, we wish to reexamine this most recent phenomenon in the original context of optical rectification and second-order optical nonlinearities. Our model quantitatively takes into account both the above band-gap (resonant) nature of the excitation process as well as the presence of a surface depletion field. In so doing, we find that we can satisfactorily account for many key experimental observations, most importantly the absolute intensity of the detected light and its dependence on crystallographic orientation.

Figure 1 shows a simple representation of the energy-band extrema of a semiconductor near the surface. In a conventional transport picture one assumes that electron-hole (e-h) pairs are created by vertical transitions in real space within the penetration depth of the incident optical field. Subsequently, as indicated by the solid arrows in Fig. 1, electrons are accelerated by the surface depletion field, while holes remain confined to the surface. The resulting current surge $\partial J/\partial t$ then gives rise to FIR radiation, where J is proportional [4] to the photoelectron population n and material mobility μ. However, as indicated by the dashed arrow in Fig. 1, there exists an alternative approach to the problem, based on nonvertical transitions in real space. Because of spatial separation of final electron and hole states, this process leads to an instantaneous FIR polarization P_0 whose second time derivative $\partial^2 P_0/\partial t^2$ determines the radiated signal. This stationary-state picture also underlies some theoretical descriptions of the Franz-Keldysh effect, i.e., the modification of optical properties by a static electric field [6].

In lowest order in the optical field E_ω and neglecting nonlocal effects, the FIR (static) polarization P_0 induced perpendicular to the surface may be written as

$$P_0 = \chi^{(2)}(0;-\omega,\omega)|E_\omega|^2 , \qquad (1$$

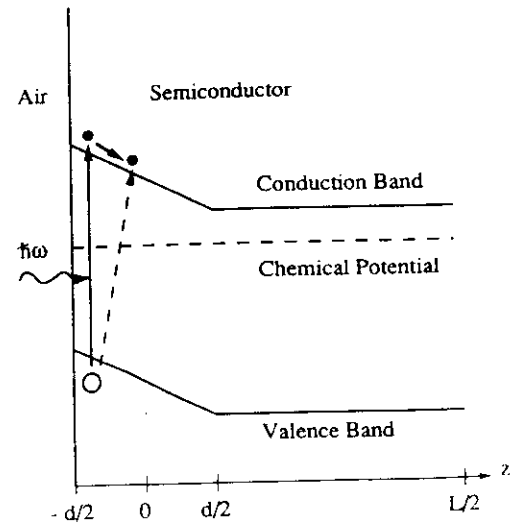

FIG. 1. Energy-band extrema near a semiconductor surface

Optical and electronic properties of doped silicon from 0.1 to 2 THz

Martin van Exter and D. Grischkowsky
IBM Watson Research Center, P.O. Box 218, Yorktown Heights, New York 10598

(Received 11 December 1989; accepted for publication 14 February 1990)

Using a source of freely propagating subpicosecond pulses of THz radiation, we have measured the absorption and dispersion of both *N*- and *P*-type, 1 Ω cm silicon from 0.1 to 2 THz. These results give the corresponding frequency-dependent complex conductance over the widest frequency range to date. The data provide a complete view on the dynamics of both electrons and holes and are well fit by the simple Drude relationship.

The dynamics of carriers in semiconductors is important from both the scientific as well as the technical point of view. The most interesting phenomena occur at frequencies comparable to either the plasma frequency or the damping rate.[1-7] Unfortunately, this usually occurs in the submillimeter region, which is difficult to reach with microwave[2,6] as well as with far-infrared[1,7] techniques. Below 100 GHz, microwave techniques have been used for single-frequency studies. The high-frequency behavior of semiconductors has been investigated with classical far-infrared spectroscopy.[1,4,7] However, for moderate doping, the strongest absorption of the free carriers lies below 2 THz, where classical far-infrared spectroscopy becomes very difficult. Consequently, the investigation of the most important frequency range from 0.1 to 2 THz has remained incomplete (1.5 THz = 50 cm^{-1} = 6.2 meV).

Recently a new system has become available for spectroscopic studies in the range from 0.1 to 2.0 THz.[8,9] This system is based on the optoelectronic generation and reception of a beam of subpicosecond THz pulses. By inserting a sample in the beam and comparing the shape of the original subpicosecond THz pulses with the shapes of pulses that have propagated through the sample, one is able to deduce the frequency-dependent absorption and dispersion.

In this letter we describe an application of the above time-domain spectroscopy technique to a complete measurement of the absorption and dispersion due to carriers in doped silicon. The measured samples were *N*- and P-doped, 1 Ω cm silicon. The dopants were phosphorus and boron, respectively, and the flat wafers had a (111) orientation. The frequency-dependent properties are shown to be completely due to the carriers and not to the host crystal. Our measurements extend from 0.1 to 2 THz and allow for the most comprehensive determination of the complex conductivity to date. To first order the results are well fit by the simple Drude theory, although slight deviations indicate that further refinements in the theory are needed.

The setup used to generate and detect the short pulses of THz radiation is depicted in Fig. 1(a) and has been described earlier.[8,9] The transmitter and receiver are identical, each consisting of a micron-sized dipole antenna imbedded in a coplanar transmission line and optoelectronically driven by 70 fs pulses from a colliding-pulse mode-locked dye laser. A large fraction of the generated pulses of THz radiation is captured by a silicon lens attached to the transmitting chip and is directed onto a paraboloidal mirror that recollimates the radiation into a low divergence beam. This THz beam is directed towards the receiver where it is focused onto th receiving antenna. The amplitude and time dependence c the transient voltage induced across the receiving antenn are obtained by measuring the collected charge (current versus the time delay between the THz pulses and the lase pulses that synchronously gate the receiver. Such a mea sured transmitted THz pulse with no sample in place i shown in Fig. 1(b). The corresponding amplitude spectrur of this 0.5 ps full width at half maximum pulse is presented i Fig. 1(c) and illustrates the 2 THz bandwidth available fo spectroscopy.

Figure 2(a) shows a THz pulse transmitted through 283-μm-thick sample of 1.15 Ω cm, *N*-type silicon. The firs

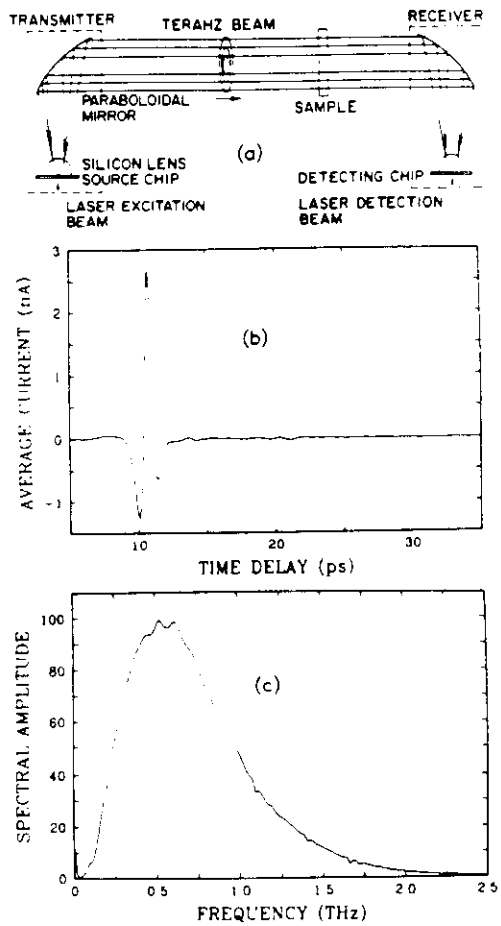

FIG. 1 (a) Schematic of the experiment; (b) measured transmitted T pulse; (c) amplitude spectrum of (b).

 0003-6951/90/171694-03$02.00

Terahertz time-domain spectroscopy of water vapor

Martin van Exter, Ch. Fattinger, and D. Grischkowsky

IBM Watson Research Center, P.O. Box 218, Yorktown Heights, New York 10598

Received April 24, 1989; accepted August 3, 1989

We describe the application of a new high-brightness, terahertz-beam system to time-domain spectroscopy. By analyzing the propagation of terahertz electromagnetic pulses through water vapor, we have made what we believe are the most accurate measurements to date of the absorption cross sections of the water molecule for the nine strongest lines in the frequency range from 0.2 to 1.45 THz.

Recently several new sources of freely propagating electromagnetic pulses have been demonstrated[1–3]; the spectral content of these sources extends from low frequencies to the terahertz frequency range. Using an optical approach in which a transient Hertzian dipole was tightly coupled to a sapphire collimating lens, we produced beams of single-cycle 0.5-THz pulses.[3] With the addition of paraboloidal focusing and collimating mirrors,[4] the resulting system has high brightness and extremely high collection efficiency.

In this Letter we describe the application of this new high-brightness system to time-domain spectroscopy[5–8] by studying the propagation of terahertz beams through water vapor. Fourier analysis of the directly measured electric fields of the propagated pulses, with and without water vapor in the beam path, yields the absorption and dispersion of water vapor as a function of frequency. This technique has some powerful advantages in producing results that appear to be equivalent to those of traditional cw spectroscopy. First, the detection of the far-infrared radiation is extremely sensitive. Although the energy per terahertz pulse is very low (1 aJ), the 100-MHz repetition rate and the coherent detection allow us to determine the electric field of the propagated pulse with a signal-to-noise ratio of ~3000 for an integration time of 125 msec. In terms of average power this sensitivity exceeds that of liquid-helium-cooled bolometers[9] by more than 1000 times. Second, because of the gated and coherent detection, the thermal background that plagues traditional measurements in this frequency range[9] is observationally absent. These two advantages have enabled us to make what we believe are the most accurate measurements to date of the absorption cross sections of the nine strongest rotational transitions of water vapor in the frequency range from 0.2 THz (6.6 cm^{-1}) to 1.45 THz (48.4 cm^{-1}).

The terahertz radiation source[4] is illustrated in Fig. 1(a). The emitting dipolar antenna was located in the middle of a 20-mm-long transmission line consisting of two parallel 10-μm-wide aluminum lines separated from each other by 30 μm. The pattern was fabricated on an ion-implanted, silicon-on-sapphire wafer. The antenna was driven by photoconductively shorting the 5-μm antenna gap with 70-fsec pulses coming at a 100-MHz rate in a 1.5-mW beam from a colliding-pulse, mode-locked dye laser. The terahertz radiation detector[4] uses the same ultrafast antenna and terminating transmission line as the transmitter. During operation the antenna is driven by the incoming terahertz radiation pulse polarized parallel to the antenna. The induced time-dependent voltage across the antenna gap is measured by shorting the gap with the 70-fsec optical pulses in the detection beam and monitoring the collected charge (current) versus the time delay between the excitation and detection laser pulses.

The terahertz optics[4] illustrated in Fig. 1(b) consists of two matched crystalline magnesium oxide (MgO) spherical lenses in contact with the sapphire side of the silicon-on-sapphire chips located near the foci of two identical paraboloidal mirrors. The combination of the MgO lens and the paraboloidal mirror collimated the emitted radiation to beam diameters (10–70 mm) proportional to the wavelength and with a frequency-independent divergence of only 25 mrad. The second identical combination on the receiving end focused the terahertz beam onto the detector. The total path length from transmitter to receiver was 88 cm, of which 86 cm was located in an airtight enclosure in which the water-vapor content could be controlled.

Figure 2(a) displays the detected terahertz radiation pulses after propagating through 1 atm of pure nitrogen. This high signal-to-noise measurement with millivolts of signal was made in a single 10-min scan of the 200-psec relative time delay between the

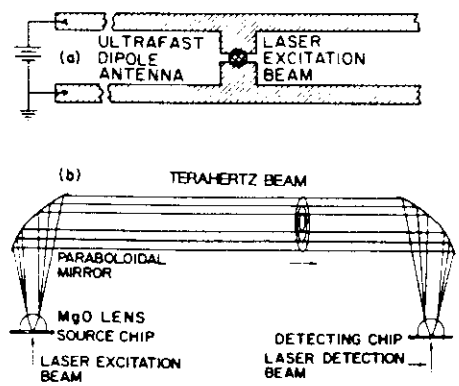

Fig. 1. (a) Ultrafast dipolar antenna. (b) Terahertz optics.

0146-9592/89/201128-03$2.00

Characterization of an Optoelectronic Terahertz Beam System

MARTIN VAN EXTER AND DANIEL R. GRISCHKOWSKY, SENIOR MEMBER, IEEE

Abstract—**We describe the performance of an optoelectronic THz beam system. The transmitter operation is based on the repetitive, subpicosecond laser excitation of a Hertzian dipole antenna embedded in a charged coplanar line. With this transmitter electromagnetic beams of 1/2 cycle THz pulses at a repetition rate of 100 MHz are produced. The associated optoelectronic receiver is gated in synchronism with the excitation of the transmitter by subpicosecond pulses from the same laser source. With this receiver, the 10 nW beams of THz pulses were observed with a signal-to-noise ratio greater than 10000:1. Several sources contributing to the noise of the receiver are discussed, together with ways to reduce them. With an integration time of 125 ms, a signal-to-noise ratio of 1 is obtained for a THz beam with an average power of 10^{-16} W. The receiver operates in the sampling mode and has a time resolution of 0.5 ps.**

I. Introduction

IN A SERIES of recent papers, the features and applications of a new high-brightness pulsed THz beam system have been reported [1]–[4]. The highest performance version of the system is based on repetitive, subpicosecond optical excitation of a Hertzian dipole antenna [3]–[5] embedded in a charged coplanar transmission line structure. The burst of radiation emitted by the resulting transient dipole is collimated by a THz optical system into a diffraction-limited beam and focused onto a similar receiver structure, where it induces a transient voltage and is detected. The THz optical system gives exceptionally tight coupling between the transmitter and receiver, while the excellent focusing properties preserve the subpicosecond time dependence of the source.

As mentioned previously [2]–[4], the combination of THz optics with the synchronously gated, optoelectronic detection process has exceptional sensitivity for repetitively pulsed beams of THz radiation. With lenses and mirrors it is possible to direct a large fraction of the radiation, emitted during the excitation of an optoelectronic device, onto a distant device. The transmitted waveforms have been measured with subpicosecond resolution and with signal-to-noise ratios of more than 10000:1. This result was obtained with a repetition rate of 100 MHz, an integration time of 125 ms, and a average power of 10 nW in the THz beam.

In this paper we present measurements and analysis of the total emitted power, the beam collection efficiency and the limiting noise properties of the THz receiver. In particular, we show how the combination of THz optics with the optoelectronic, subpicosecond, synchronous gating of the receiver allows for the measurement of incident THz beams with peak powers far less than the incident room-temperature thermal radiation in the same frequency range. Methods to further improve the performance of the receiver are also discussed.

The exceptional sensitivity is due in part to the high performance of the THz optics. Via two stages of collimation a THz beam with a frequency-independent divergence of 25 mrad is obtained from the THz transmitter. The THz receiver with identical optical properties collects essentially all of this beam. The resulting tightly coupled system of the THz transmitter and receiver gives strong reception of the transmitted pulses of THz radiation after many meters of propagation.

Another reason for the exceptional sensitivity is that the optoelectronic gating changes the effective resistance of the receiving antenna from 22 MΩ in the off state to 550 Ω in the on state. The gating window of the on state lasts for approximately 0.6 ps. The duty cycle of 0.6×10^{-7} is given by the ratio of the 0.6 ps gating time to the period of the 100 MHz sampling rate. Consequently, the average resistance seen by a current amplifier directly connected to the receiving antenna is about 7 MΩ. Therefore, with respect to the current amplifier, the receiver has a high impedance together with a subpicosecond response.

A final important feature of the detection method is that it is a coherent process; the electric field of a repetitive pulse of THz radiation is directly measured. Because we synchronously detect a repetitive signal, the total charge (current) from the signal increases linearly with the number of sampling pulses, while the charge (current) from noise increases only as the square root of the number of pulses.

II. Experimental Setup

The setup used to generate and detect beams of short pulses of THz radiation is presented in Fig. 1. The transmitting and receiving antennas are identical, each consisting of the metallic pattern shown in Fig. 1(a) [3], which

Manuscript received October 18, 1989; revised June 25, 1990. This work was supported in part by the U.S. Office of Naval Research.

M. van Exter was with the IBM Watson Research Center, P.O. Box 218, Yorktown Heights, NY 10598. He is now with the Huygens Laboratories, Postbus 9504, 2300 RA Leiden, the Netherlands.

D. R. Grischkowsky is with the IBM Watson Research Center, P.O. Box 218, Yorktown Heights, NY 10598.

IEEE Log Number 9038470.

High-brightness terahertz beams characterized with an ultrafast detector

Martin van Exter, Ch. Fattinger, and D. Grischkowsky
IBM Watson Research Center, P. O. Box 218, Yorktown Heights, New York 10598

(Received 9 March 1989; accepted for publication 15 May 1989)

We have significantly improved the emission and detection of electromagnetic beams of single-cycle 0.5 THz pulses, through the use of new dipolar antenna structures. The frequency response was extended to well beyond 1 THz, and the beam power was increased by more than 15 times. The antennas were located at the foci of sapphire lenses and were photoconductively driven by ultrafast laser pulses. An additional collimation by a paraboloidal mirror produced a beam with a 25 mrad divergence, and subsequent focusing by a second identical mirror improved the coupling between the transmitting and receiving antenna by orders of magnitude.

Since the initial experiments of Hertz,[1] the Hertzian dipole has been known to be an important emitter and receiver of radiation with wavelengths large compared to the dipole. Modern integrated circuit techniques have now made possible the precise fabrication of micron-sized dipoles, which when driven with subpicosecond excitation can radiate well into the terahertz regime. The importance of these integrated-circuit versions of the Hertzian dipole as generators and detectors of terahertz radiation was first demonstrated by Auston *et al.*[2] Recent work has introduced an optical technique to collect, collimate, and focus the terahertz radiation emitted by Hertzian dipoles,[3,4] produced by shorting a charged coplanar transmission line with ultrashort laser pulses.[5] When these dipole sources were located at the foci of spherical mirrors or lenses, most of the emitted radiation was captured and could be focused on detectors or collimated to produce relatively large diameter diffraction limited beams. Besides the high coupling efficiency, the excellent focusing properties preserved the subpicosecond time dependence of the source.

The above optical approach represents an alternative and complementary method to recent works extending radio and microwave techniques into the terahertz regime through the use of antennas.[6-10] For example, Mourou *et al.*[6] used a subpicosecond laser pulse to trigger a GaAs photoconductive switch driving a coaxial cable terminated by a millimeter-sized dipole antenna. This combination produced a microwave transient of several picoseconds. Later, Heidemann *et al.*[7] demonstrated the importance of planar antennas by exciting a larger, exponentially tapered, slot-line antenna with a laser-driven photoconductive switch to obtain nanosecond bursts of radiation. As discussed in their paper, this planar design is readily adaptable to integrated circuit fabrication with a consequent increase in bandwidth as the size is reduced. Defonzo *et al.*[8] demonstrated picosecond performance of an integrated circuit version of an antenna similar to that of Ref. (7). Later, Defonzo *et al.* developed and demonstrated an improved impedance-matched antenna consisting of an exponentially flared transmission line.[9] This design reduced antenna reflections and produced clean 10 ps bursts of radiation. In the most recent work, subpicosecond pulses have been generated, transmitted, and detected by Smith *et al.*,[10] who used integrated circuit techniques to fabricate ultrafast dipolar antennas terminated by coplanar transmission lines.

In this letter we report the use of a new ultrafast dipole antenna structure, optimized for photoconductive excitation, as the radiation source for the optical method.[3,4,11] Using this antenna we achieve an increase in transmitted beam power of more than 15 times, compared to the earlier work.[4] The antenna was located at the focus of a collimating sapphire lens in contact with the sapphire side of an ion-implanted,[12] silicon-on-sapphire (SOS) chip on which the antenna was fabricated. In addition, when the simple gap structure initially used for detection[3,4] was replaced with this antenna, the frequency response was significantly extended. In fact, we show that the signal measured by the antenna is the time derivative of the signal measured by the gap. Through the use of paraboloidal collimating and focusing mirrors, we have obtained a frequency-independent divergence of only 25 mrad and have increased the coupling between the transmitter and receiver by orders of magnitude. This tight coupling is evidenced by the fact that we measure electrical signals of many millivolts after a free-flight path of 80 cm.

The terahertz radiation source is illustrated in Fig. 1(a). Because this antenna directs all of the photocurrent into the antenna arms, it performs somewhat better than a dipole antenna at the end of a transmission line.[10] For comparable dimensions, more power is radiated and the noise level is lower due to the larger separation between the lines. A simple scaling argument compares the efficiency of the new antenna with that achieved by the earlier "sliding contact" technique[3,4] of simply shorting-out a coplanar transmission line. For this case the photocarrier density is inversely proportional to the area of the focused laser spot with a diameter approximately equal to the spacing between the lines. The area of contact of the photoconductive spot with the lines is proportional to the diameter of the laser spot. Consequently, with the same electric field between the lines, the photocurrent is inversely proportional to the line separation. Therefore, the main advantage of the new antenna design is that the total photocurrent from a 5 μm gap is put into a 30 μm antenna. Directly shorting a coplanar line with 30 μm separation between the two lines and with a six times higher bias voltage, would produce a current only 1/6 of that obtained by the antenna. The 20-μm-wide antenna structure was located in the middle of a 20-mm-long transmission line consisting of two parallel 10-μm-wide, 1-μm-thick, 5 Ω/mm, aluminum lines separated from each other by 30 μm. The antenna was driven by photoconductive shorting the 5 μm antenna gap with 70 fs pulses coming at a 100 MHz rate in a

 0003-6951/89/300337-03$01.00

Terahertz beams

Ch. Fattinger and D. Grischkowsky
IBM T. J. Watson Research Center, P. O. Box 218, Yorktown Heights, New York 10598

(Received 10 October 1988; accepted for publication 29 November 1988)

We have generated freely propagating, diffraction-limited beams of single-cycle 0.5 THz electromagnetic pulses from a 5-mm-diam coherent source. After propagating 100 cm in air, there was little change in the measured subps pulse shape, even though the signal strength was reduced by 20 times compared to the strength at 10 cm.

The importance of integrated circuit versions of the Hertzian dipole as generators and detectors of terahertz radiation was first demonstrated by Auston *et al.*[1] In a recent paper an optical approach was introduced to focus and to manipulate the terahertz radiation emitted by the Hertzian dipole source with an ultrafast time dependence.[2] The dipole had small dimensions compared to any of the radiated wavelengths and was produced by shorting a charged coplanar transmission line with an ultrashort laser pulse. When this dipole source was located at a focal point of a spherical mirror, essentially all of the emitted radiation was captured by the mirror and could be focused on an ultrafast optically driven photoconductive switch. Besides the extremely high coupling efficiency, the excellent focusing properties preserved the subps time dependence of the source. This approach represents an alternative and complementary method to recent works extending radio and microwave techniques into the terahertz regime through the use of antennas.[3,4]

In this letter we report the application of the optical technique to the generation of diffraction-limited terahertz beams with a relatively large source size, by locating the ultrafast dipole source at the focal point of a collimating lens. This technique allowed us to produce, for the first time, diffraction-limited beams of single-cycle 0.5 terahertz pulses from a coherent source (the time dependence is much faster than the transit time across the source) of 5 mm diameter. Because of their relatively low divergence, the single-cycle pulses were easily measured after a propagation distance of 100 cm. The detection was accomplished by focusing the terahertz beam on a photoconductive switch driven by a subpicosecond laser pulse.

The terahertz radiation source is similar to that used before[2,5,6] and is illustrated in Fig. 1(a). Here, the 20 μm sized subps electric dipoles are created by photoconductive shorting of the charged coplanar transmission line with 70 fs pulses from a colliding-pulse, mode-locked dye laser. As described previously, the electrical pulse coupled to the transmission line has the same time dependence as the transient electric dipole responsible for the terahertz radiation.[6] This electrical pulse on the line was measured by a fast photoconductive switch (driven by the monitor beam, a time-delayed beam of the same 70 fs laser pulses), which connected the transmission line to the electrical probe. The 20-mm-long transmission line had a design impedance of 125 Ω and consisted of two parallel 5-μm wide, 0.5-μm-thick aluminum lines separated from each other by 15 μm. The measured dc resistance of a single 5 μm line was 10 Ω/mm. The transmission line was fabricated on an undoped silicon-on-sapphire (SOS) wafer, which was heavily implanted to ensure the required short carrier lifetime.[7]

The terahertz radiation detector shown in Fig. 1(b) is simply a photoconductive gap of 5 μm spacing with a width of 25 μm. This gap was fabricated as above on a separate SOS chip. One side of the gap is grounded, and a current amplifier is connected across the gap as indicated. During operation the gap is biased by the incoming terahertz radiation pulse polarized across the gap. The measurement is made by shorting the gap via the 70 fs ultrashort optical pulses in the detection beam and measuring the collected charge (current) versus the time delay between the excitation and detection pulses.

The terahertz optics illustrated in Fig. 1(c) consist of two crystalline sapphire, spherical lenses contacted to the backside (sapphire side) of the SOS chips. For the radiation

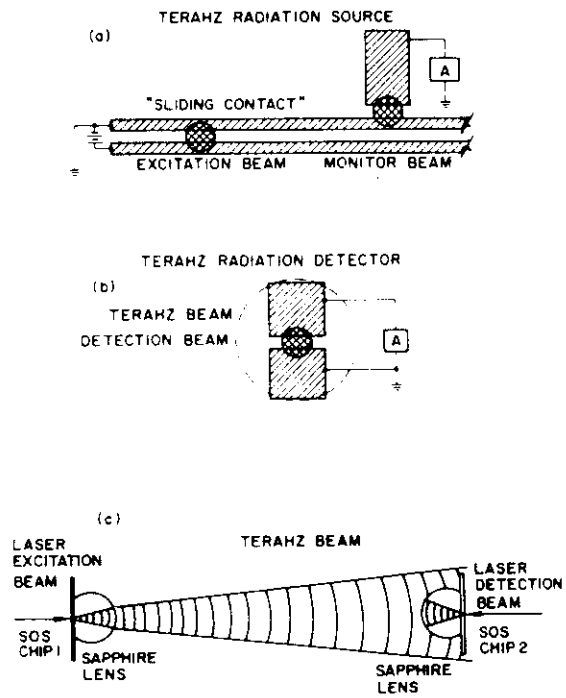

FIG. 1. (a) Schematic diagram of the charged coplanar transmission line. The laser excitation beam spot defines the location of the transient electric dipole. The monitor beam measures the electrical pulse coupled to the line. (b) Schematic diagram of the terahertz detector. The laser detection beam spot is shown centered on the gap in the focal spot of the terahertz radiation. (c) Schematic diagram of the collimating and focusing optics consisting of crystalline, sapphire lenses in contact with the backside (sapphire side) of the SOS chips.

 0003-6951/89/060490-03$01.00

Gouy shift and temporal reshaping of focused single-cycle electromagnetic pulses

Simin Feng and Herbert G. Winful

Department of Electrical Engineering and Computer Science, University of Michigan, 1301 Beal Avenue, Ann Arbor, Michigan 48109-2122

Robert W. Hellwarth

Departments of Physics and Electrical Engineering, University of Southern California, Los Angeles, California 90089-0484

Received October 3, 1997

We discuss exact solutions of Maxwell's equations that describe the evolution of single-cycle electromagnetic pulses. The solutions are applied to recent observations of the diffraction transformation of terahertz pulses. In particular, we elucidate the role of the Gouy shift in the temporal reshaping and polarity reversals of single-cycle terahertz pulses. © 1998 Optical Society of America

OCIS codes: 320.0320, 320.5550, 320.5540.

Advances in ultrafast optical technology have made possible the generation of single-cycle and half-cycle electromagnetic pulses of subpicosecond temporal duration.[1] These pulses have center frequencies in the terahertz range and spectra that extend from zero to several terahertz. This extraordinarily large bandwidth results in significant temporal reshaping of focused terahertz pulses even when they propagate through free space or pass through apertures.[2,3] Analysis of this diffraction-induced pulse shaping is usually carried out through numerical solution of Maxwell's equations.[3] On another front there is much interest in exact solutions of Maxwell's equations that describe the localized transmission of electromagnetic energy.[4–6] One particularly interesting class of solutions termed electromagnetic directed-energy pulse trains by Ziolkowski[5,6] has finite total energy and could prove useful in describing ultrashort-pulse phenomena in regimes beyond the slowly varying envelope and the paraxial approximations.

In this Letter we show that a certain subset of Ziolkowski's electromagnetic directed-energy solutions of Maxwell's equations can describe most of the observed features of focused single-cycle electromagnetic pulses. These exact solutions demonstrate how the Guoy phase shift of focused beams leads to temporal reshaping and polarity reversals as terahertz pulses propagate through free space.

The modified power spectrum pulse discovered by Ziolkowski[5,6] is an exact solution of the free-space wave equation:

$$\left(\nabla^2 - \frac{1}{c^2}\frac{\partial^2}{\partial t^2}\right) f(\mathbf{r}, t) = 0. \tag{1}$$

In terms of the variables $\rho^2 = x^2 + y^2$, $\tau = z - ct$, $\sigma = z - ct$, and $s = \rho^2/(q_1 - i\tau) - i\sigma$, the modified power spectrum solution is given by

$$f(\mathbf{r}, t) = f_0/(q_1 - i\tau)(s + q_2) \tag{2}$$

for a pulse propagating along the z direction. Here q_1 and q_2 are parameters with dimensions of length that can be shown to determine the peak wavelength and the Rayleigh range of the pulses, respectively. For the typical terahertz pulse q_1 is a few orders of magnitude smaller than q_2. Vector field solutions of Maxwell's equations are then readily obtained by use of the method of Hertz potentials.[6] In this Letter we construct a Hertz vector that is transverse to the direction of propagation $\Pi = \hat{x} f(\mathbf{r}, t)$, where $\hat{x}$ is a unit vector. The electric and the magnetic fields are then found from $\mathbf{E} = -\mu_0 \nabla \times \partial \Pi/\partial t$ and $\mathbf{H} = \nabla \times \nabla \times \Pi$, respectively. In Ref. 7, the use of a z-directed Hertz potential was reported to result in toroidal wave packets, termed focused doughnuts. We find here that the transversely oriented Hertz potential results in oblate wave packets that resemble focused pancakes.

For the case in which $q_1 \ll q_2$ (which means that the effective wavelength of the pulse is much shorter than the Rayleigh range), it can be shown that the dominant field components are

$$E_y(\mathbf{r}, t) = 2f_0\sqrt{\frac{\mu_0}{\epsilon_0}}\,\frac{(q_1 + i\tau)^2 - (q_2 - i\sigma)^2}{[\rho^2 + (q_1 + i\tau)(q_2 - i\sigma)]^3}, \tag{3}$$

$$H_x(\mathbf{r}, t) = 2f_0\,\frac{2\rho^2\cos(2\varphi) + (q_1 + i\tau)^2 - (q_2 - i\sigma)^2}{[\rho^2 + (q_1 - i\tau)(q_2 - i\sigma)]^3}, \tag{4}$$

where $\varphi = \tan^{-1}(y/x)$. The E_x component is exactly zero owing to the x orientation of the Hertz vector. The other components are such that E_z/E_y and H_z/H_x are of the order of $O(\sqrt{q_1/q_2})$, whereas H_y/H_x is of the order of $O(q_1/q_2)$.

Equations (3) and (4) are exact, finite-energy solutions of Maxwell's equations that describe the spatiotemporal evolution of focused single-cycle electromagnetic pulses with diffraction effects included. Owing to the linearity of Maxwell's equations, the real and the imaginary parts of Eqs. (3) and (4) separately

0146-9592/98/050385-03$10.00/0

Coherent, broadband midinfrared terahertz beam sensors

P. Y. Han and X.-C. Zhang[a)]
Physics Department, Rensselaer Polytechnic Institute, Troy, New York 12180-3590

(Received 12 March 1998; accepted for publication 24 September 1998)

With proper selection of the electro-optic terahertz (THz) wave emitter and sensor crystals, we demonstrate the coherent measurement of free-space broadband radiation spanning 100 GHz to over 30 THz. This effort supports the feasibility of midinfrared time-domain spectroscopy. © *1998 American Institute of Physics.* [S0003-6951(98)03347-6]

The generation of midinfrared pulses through the optical rectification extended the radiation frequency from a few THz to several tens of THz.[1–3] The coherent measurement of a detection frequency greater than 5 THz was demonstrated using a GaP[4] and a ZnTe electro-optic sensor.[5] This optoelectronic technique opens the door to the midinfrared (mid-IR) region for coherent emission spectroscopy, time-domain spectroscopy, and ultrafast pump-probe spectroscopy.

In this letter, we report the recent study of coherent, broadband midinfrared THz beam sensors. We focus on free-space electro-optic sampling of the THz pulse in the frequency range higher than the optical phonon levels of the sensor crystals. Experimental results of midinfrared THz pulse measurements indicate that the thickness of the electro-optic crystals (both emitter and sensor) is a crucial factor influencing the temporal wave form and spectral bandwidth of the measured THz pulse. With proper selection of the emitter and sensor, taking proper consideration of their phonon bands, it is feasible to achieve a useable frequency bandwidth ranging from 100 GHz to 30 THz. We present the experimental results of the coherent generation and detection of femtosecond THz midinfrared pulses.

The experimental setup of the electro-optic mid-IR detection system is depicted in Fig. 1. A 12 fs Ti:sapphire laser delivers an average power of nearly 500 mW at a center wavelength of 800 nm. Electro-optic crystals (including GaAs, InP, ZnTe, CdTe, GaP, BBO, and $LiTaO_3$) with different thickness were used as the emitters and sensors. Three hundred and fifty milliwatts of the laser power were focused on the emitter by a gold-coated off-axis parabolic mirror with a 5 cm effective focal length. The broadband THz radiation generated from the emitter by optical rectification was collimated and then focused on the sensor by a pair of *f*/0.6 off-axis parabolic mirrors. The laser probe beam was combined to collinearly travel with the THz beam through a 2-μm-thick pellicle, which had a negligible effect on the laser pulse width and THz beam. If the emitter crystal is transparent to the optical excitation beam, such as for ZnTe, GaP, or $LiTaO_3$, a silicon wafer is placed after the emitter crystal to block the optical beam but transmit the THz beam. The electro-optic modulation induced by the ultrafast Pockels effect was detected by using a pair of balanced photodiodes. By varying the time delay between the optical pump and probe pulses, the temporal wave form of the midinfrared transient was sampled.

Previous research on ZnTe indicates a good velocity-matching range between the laser pulse (centered at 800 nm) and far-infrared THz beam (centered at 2 THz or 150 μm).[6,7] However, broadband velocity matching from far-IR to mid-IR is not possible. Therefore, a sensor crystal with proper thickness is a crucial condition for the optimization of generating and detecting midinfrared pulsed radiation. Limited by the coherence length and propagating dispersion of the THz beam in both emitter and sensor crystals, a ZnTe crystal of a few millimeters in length might be the ideal length for a far-IR THz measurement, but it is not the optimal length for a mid-IR THz measurement. The dispersion of the THz beam in the crystal is the major factor influencing the shape and spectrum of the measured mid-IR beam.

In order to reduce the propagating dispersion in the midinfrared, a thin emitter and sensor is crucial. Figure 2(a) shows a typical temporal waveform obtained from a 30 μm (110) ZnTe emitter and 27 μm (110) ZnTe sensor. Weak structures in the waveform before and after the main peak are due to optical beam and THz beam reflections within the ZnTe crystals. Since both emitter and sensor are very thin, the chirp of the temporal wave form due to the propagating dispersion is minimized. The Fourier transform of the THz wave form is shown in Fig. 2(b). Since both the emitter and sensor are ZnTe crystals, there is only one transverse optical phonon band centered at 5.3 THz. The spectral modulation in the spectrum is due to the multiple reflection of the THz field in the ZnTe crystals. The dip around 17 THz in the spectrum is the response cutoff due to velocity mismatching. The index difference between optical group index and midinfrared index in ZnTe is 0.6, which corresponds to a group-velocity mismatch of 60 fs in a 30-μm-thick ZnTe crystal.[8] According to the response cutoff modeling,[7] the frequency cutoff

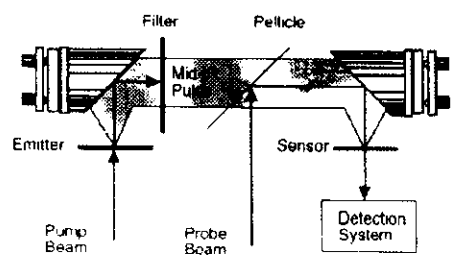

FIG. 1. Schematic illustration of the experimental setup for the generation and detection of a midinfrared THz beam.

[a)]Electronic mail: zhangxc@rpi.edu

J. Phys. Chem. A **1997**, *101*, 3646−3660

FEATURE ARTICLE

Terahertz Studies of Collision-Broadened Rotational Lines

H. Harde

Universität der Bundeswehr Hamburg, Holstenhofweg 85, 22043 Hamburg, Germany

R. A. Cheville and D. Grischkowsky*

School of Electrical and Computer Engineering and Center for Laser and Photonics Research, Oklahoma State University, Stillwater, Oklahoma 74078

Received: September 26, 1996; In Final Form: March 7, 1997[⊗]

Via terahertz (THz) coherent transients and THz time-domain spectroscopy, we have measured the far-wing absorption line profile of the ensembles of collision-broadened ground state rotational lines of methyl bromide, methyl chloride, and methyl fluoride vapors out to more than 200 line widths from resonance, corresponding to frequency offsets as much as 5 times the resonant frequency. On these far wings the measured absorption is approximately an order of magnitude less than that predicted by the van Vleck−Weisskopf theory. Our observations show that as the offset frequency is increased, a transition occurs from the regime of the van Vleck−Weisskopf theory to the regime of the Lorentz theory. These measurements are fit to a new molecular response theory which explicitly includes the molecular orientation time during a collision. Due to the broad bandwidth of the THz pulses, we demonstrate the validity of this molecular response theory for the far-wing absorption of methyl fluoride, chloride, and bromide. The excellent theoretical fit to our measurements encompassing the frequency range over which this transition occurs indicates a molecular response time on the order of 200 fs. These measurements also permit determination of the line-width dependence on the rotational quantum number J.

I. Introduction

Important information on the collision behavior and intermolecular forces is obtained through the width and shape of broadened spectral lines from optical to microwave frequencies.[1−3] The near-resonance part of the line shape is mainly determined by the collision frequency or time between collisions. However, the far wings of the resonance lines are strongly influenced by the interaction forces between molecules which occur during the collision itself.

The analysis of most spectroscopic data is performed using two line shapes based on two different orientational distributions after a collision. The line shape of Lorentz[4] assumes that after a collision the molecules are oriented randomly with respect to the applied electromagnetic field. This assumption prevents the Lorentz theory from reducing to that of Debye in the zero-frequency resonant case. This discrepancy was removed by van Vleck and Weisskopf, who developed a line-shape theory based on the assumption that after a collision the molecules are oriented along the direction of the applied field with a Boltzmann distribution. This assumption requires the duration of the collision be short compared to the period of oscillation of the field. For the higher frequencies of optical and infrared transitions, the Lorentzian line shape[4] provides excellent agreement with experiment, particularly for the central region of the line. As the frequencies are reduced to those of the microwave or far-infrared region, and under conditions when a line width becomes comparable with the transition frequency, the absorption profile of a spectral line is better represented by the van Vleck−Weisskopf line shape.[5−8]

Studies of collisionally broadened line shapes have impact beyond understanding molecular interactions during collisions for a wide variety of problems of practical interest. These include applications for electromagnetic propagation and remote sensing in the atmosphere where the broad continuum absorption from water vapor leads to higher than expected loss.[9] This continuum absorption is not yet completely understood; both anomalous far-wing absorption and water dimers or larger clusters have been proposed to explain the continuum absorption.[10] Determination of accurate line shapes is also important for analysis of astronomical data, where spectroscopy is often the only practical method of obtaining information about the celestial bodies of interest. The wide range of conditions of these observations, from the extremely low densities of interstellar space to high pressures and temperatures of planetary atmospheres, presents both theoretical and experimental challenges.

Using the techniques of THz coherent transients and THz time-domain spectroscopy (THz-TDS), we have extended such line-shape investigations to THz frequencies with the goal of gaining some insight into the actual collision process itself. Our investigations are now giving information on the duration of the strong state-changing collisional interaction since we are able to sensitively investigate the far wings of rotational lines.

To study the spectral line shapes of absorption and dispersion, we measure coherent transient effects in the time domain,[11,12] which result from the interaction of a short pulse of THz electromagnetic radiation with the resonant systems.[13−16] These experiments were based on exciting molecular vapors with freely propagating subpicosecond pulses of THz radiation and detecting the free induction decay (FID) reradiated by the vapors. The

[⊗] Abstract published in *Advance ACS Abstracts*, May 1, 1997

THz Commensurate Echoes: Periodic Rephasing of Molecular Transitions in Free-Induction Decay

H. Harde,[a] Søren Keiding,[b] and D. Grischkowsky
IBM Watson Research Center, P.O. Box 218, Yorktown Heights, New York 10598
(Received 20 September 1990)

We report the first study of coherent transients excited by ultrafast pulses of THz radiation. Using a newly developed optoelectronic source of well-collimated beams of subpicosecond pulses of THz radiation to excite N_2O vapor, we have observed the subsequent emission from the vapor of coherent THz pulse trains extending to as long as 1 nsec. The origin of these subpicosecond THz pulses (echoes) is a periodic rephasing, during the free-induction decay, of the more than fifty coherently excited rotational lines with commensurate transition frequencies. From the decay and reshaping of the echoes the coherent relaxation time T_2 and the anharmonicity factor for the N_2O molecule are evaluated.

PACS numbers: 42.50.Md, 42.50.Kb, 42.50.Qg

Coherent transients resulting from the interaction of electromagnetic radiation with resonant systems were first studied for nuclear and paramagnetic spin systems at radio and microwave frequencies.[1] Analogous studies in the optical regime were initiated with the photon-echo experiment,[2] and since that time there have been extensive studies of coherent effects in both the visible and infrared regimes.[3-5] While many of these phenomena are analogs of effects first observed in spin resonance, some of them do not have their spin-resonance counterpart because of propagation effects.

In this paper we report the first experimental and theoretical study of coherent transients excited by pulses of THz radiation. This newly accessible frequency range is important due both to the samples that can be investigated and to the unusual experimental conditions encountered with subpicosecond pulses of THz radiation. Commercially available submillimeter-wave microwave sources can only be modulated up to 0.2 nsec and can at most be tuned by 10% of their center frequency. In comparison the THz pulses used here are unique in terms of their pulse duration and corresponding bandwidth. They essentially consist of a single oscillation and are characterized by a transform-limited white spectrum in the THz range. This allows entire manifolds of resonance lines to be excited in the impact approximation. However, in contrast to ordinary absorption spectroscopy where only the spectral amplitudes are measured, and compared to infrared and optical investigations, where coherent transients are only detected as pulse intensities or as beat notes on a carrier,[4-6] our experiments directly measure the actual electric field of the transmitted signals. We thereby determine both the spectral amplitudes as well as the phase of the transmitted components. Compared to coherence effects for nuclear- and electron-spin systems,[1] the work reported here involves samples many wavelengths in length, so that in addition to the point response, propagation effects are also important. Because the subpicosecond pulses cannot be represented by a carrier frequency and a time-dependent pulse envelope, one cannot use the slowly varying envelope approximation of coherent optics,[3] and the concept of pulse area does not apply.

We have investigated coherent THz transients from N_2O vapor. The propagation of a subpicosecond THz pulse through such a molecular vapor excites a multitude of rotational transitions in the impact approximation and causes the molecules to reradiate a free-induction-decay (FID) signal.[1,3] Because the N_2O molecule has an almost constant frequency spacing between the rotational lines, a periodic rephasing and dephasing of the entire ensemble of the more than fifty excited transitions is observed. This situation contrasts to that of water vapor with a multitude of incommensurate resonance lines studied earlier by THz time-domain spectroscopy.[7] Consequently, after the initial excitation pulse, the N_2O-vapor sample emits a series of uniformly spaced (39.8 psec) subpicosecond THz pulses (for a related phenomenon of infrared pulses emitted after excitation see Refs. 8 and 9). The rephasing process has a close relationship to that of spin and photon echoes. Because of this and because the frequencies are numerical multiples of the fundamental frequency, equal to the spacing between adjacent rotational lines, we term these periodic pulses "THz commensurate echoes." Because of the experimental system's exceptionally high signal-to-noise ratio, we have measured, with a time resolution of better than 0.5 psec, trains of echoes extending to beyond 600 psec. These echoes decay with the coherent relaxation time T_2, while Doppler dephasing can be completely neglected. From these observations T_2 can be directly determined. As will be described later in the paper, T_2 can still be measured when the absorption lines are so strongly overlapping that the rotational line structure is no longer observed in the frequency domain. From the echo repetition rate the frequency separation between the rotational lines is found, and because of the exceptionally high time resolution of the measurements, the anharmonicity in the line spacing can be detected as reshaping of the individual pulses.

The setup used to generate and detect the short pulse of THz radiation is depicted in Fig. 1(a) and has been

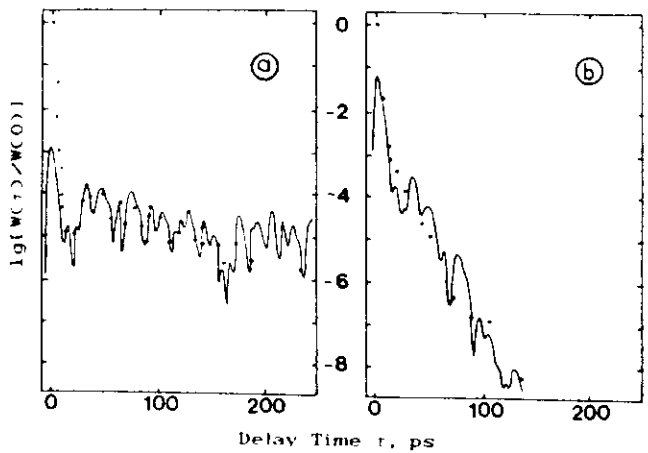

Fig 3 Conversion signal representing FID of the ν_3 Q-band of CH_4 (a) p=0.27 bar, τ_R=450 ps; (b) p=7 bar; τ_R=17.5 ps

5. CONCLUSION

We have considered application of the strong collisions model of frequency exchange for describing relaxation process in three various gases and have obtained values of rotationally inelastic collisions cross-sections. Theoretically calculated and experimentally obtained pulse responses satisfactorily agree, and it proves necessity of taking into account frequency exchange with help of more advanced models for obtaining precise numerical parameters of relaxation process.

6. REFERENCES

Akhmanov S A , Koroteev N I , Magnitskii S A , Morozov V B , Tarasevich A P , Tunkin V G 1985 JOSA B 2 640
Angsti R , Finsterholzl H , Frunder H , Illing D , Papousek D, Pracna P , Narahari Rao K , Schrotter H W , Urban S 1985 J.Mol.Spectrosc. 114 454
Barnes W L, Suskind J, Hunt R H, Plyler E K 1972 J.Chem.Phys. 56 5100
Bratengeier K, Purucker H-G, Laubereau A 1989 Opt.Comm. 70 393
Burshtein A I, Kolomoitsev D V, Nikitin S Yu, Storozhev A V 1991 Chem. Phys. 150 231
Gerzberg G 1949 Vibrational and Rotational Spectra of Diatomic Molecules (Moscow: IL)
Kolomoitsev D V, Nikitin S Yu 1986a Opt.Spectr.(Sov.) 60 559
Kolomoitsev D V, Nikitin S Yu 1986b Opt.Spectr.(Sov.) 61 1201
Kolomoitsev D V, Nikitin S Yu 1989 Opt.Spectr.(Sov.) 66 286
Kolomoitsev D V, Nikitin S Yu 1991 Proc.SPIE 1402 11
Magnitskii S A 1983 Ph.D.Thesis (Moscow: MSU)
Nikitin S Yu 1985 Vestn.Mosc.Univ. Ser.3 26 48
Tarasevich A P 1985 Ph.D.Thesis (Moscow: MSU)

Inst. Phys. Conf. Ser. No 126: Section III
Paper presented at Int. Symp. on Ultrafast Processes in Spectroscopy, Bayreuth, 1991

Time-domain spectroscopy of molecular vapors with subpicosecond pulses of THz radiation

H. Harde*, D. Grischkowsky

IBM Watson Research Center, P.O. Box 218, Yorktown Heights, New York 10598

A newly developed optoelectronic beam system generating subpicosecond pulses of THz radiation was used for time-domain studies of N_2O vapor. After the excitation the molecules were observed to radiate coherent transients on the free induction decay originating from the periodic rephasing of coherently excited rotational absorption lines. Numerical simulations of the terahertz pulse propagation through the sample, based on the linear dispersion theory, exactly reproduce the measured pulse structures. Additional calculations of terahertz pulses interacting with OCS and HCN vapor are presented.

1. INTRODUCTION

While in recent years spectroscopy with ultrashort pulses was restricted to optical and infrared frequencies, with the newly developed terahertz beam sources, producing subpicosecond pulses of terahertz radiation (van Exter *et al* 1989a, Zhang *et al* 1990), a new frequency range is becoming accessible for time domain spectroscopy and the studies of fast transients. At IBM an optoelectronic terahertz transmission and detection system has been developed and used for measurements of dielectrics and semiconductors (Grischkowsky *et al* 1990a) as well as high T_c substrates (Grischkowsky *et al* 1990b). Also molecular vapors of H_2O (van Exter *et al* 1989b) and N_2O (Harde *et al* 1991a, Harde and Grischkowsky 1991b) have been investigated with this setup. The teraHz pulses are unique in terms of their pulse duration and corresponding bandwidth. They essentially consist of a single oscillation and are characterized by a transform limited white spectrum extending to beyond 2 THz. The radiation is well collimated into a low-divergence beam and can be detected with a signal to noise ratio of better than 20,000.

In this paper we report an experimental and theoretical study of time resolved terahertz spectroscopy of N_2O vapor, where we refer to some of the results presented in an earlier publication (Harde and Grischkowsky 1991b), and we add numerical simulations of the pulse propagation through OCS and HCN vapor. These molecules with a similar structure to N_2O but with larger electric dipole moment are interesting candidates for studies of propagation effects through optically dense media. Terahertz pulses passing through one of these vapors excite a multitude of pure rotational transitions in the impact approximation and cause the molecules to teradiate a free induction decay (FID) signal that consists of a series of well defined ultrashort pulses (for similar observations in the infrared see, Forster *et al* 1971, Heritage *et al* 1975, Woerner *et al* 1989, and Bratengeier *et al* 1989). These pulses have their origin in a periodic rephasing of the equally spaced rotational lines. For N_2O vapor we have measured trains of coherent transients extending to beyond 600 ps which are compared with theoretical simulations that we derived from calculations based on the linear dispersion theory. Owing to the exceptionally

* Permanent address: Universität der Bundeswehr, Holstenhofweg 85, 2 Hamburg 70, Germany

functions with pion transverse momentum, leading to a decrease in the extracted "source radii" for higher p_t or k_t. This effect was demonstrated by theoretical investigations [5] to be a sensitive test of collective expansion: Pratt considered the isentropic expansion of a hadron-filled sphere initially at an energy density of 2 GeV/fm^3 and freezing out at 120 MeV (not an unreasonable formation and decay scenario). He found both R_O and R_S to fall by more than a factor of 2 in going from $k_t = 0$ to $k_t = 600$ MeV/c due to a pronounced radial collective flow. Such behavior was indeed seen at the much lower Bevalac energies [20]. Our data do not exhibit such a dramatic k_T dependence. The dependence is stronger at midrapidity than at forward rapidity. Our S + Au data at $y = 3$ agree with the S + Pb results of NA44 [21]. What we observe is consistent with earlier predictions for both string-motivated and Bjorken or thermal descriptions of the reaction dynamics [7] and with recent hydrodynamic calculations that include a phase transition with a modest latent heat difference [22]. On the other hand, our data for the longitudinal direction (Fig. 1) are indeed perfectly compatible with a collective, isentropic longitudinal "scaling" expansion, showing effects that are as strong as expected [5,6]. We are led to the conclusion that different mechanisms appear to drive the longitudinal and transverse expansions of the initial reaction volume: Collective transverse flow depends on rapidity and average, its signals are weaker than those, supporting longitudinal flow. The observed qualitative agreement of the microscopic RQMD model with the momentum evolution of both the longitudinal and transverse source parameters (Figs. 1 and 3) may suggest a first plausible explanation. The correlation between longitudinal momentum and position may result, not from a pressure driven hydrodynamic expansion, but from the relativistic kinematics of particle production from decaying strings which are oriented along the beam direction at the high SPS energy. RQMD seems to even overestimate this effect (see Fig. 1). The net outcome may well resemble that of a Bjorken-Sinyukov collective model. The transverse expansion, however, may indeed be thermal (i.e., driven by rescattering) and of relatively short duration (the density falling rapidly because of the predominantly longitudinal expansion). This scenario is implied by the RQMD model. These observations at 200A GeV may also be reconcilable with recent reports of a more pronounced transverse expansion at the lower Brookhaven AGS energy [23], where longitudinal collectivity should be less predominant. We note, however, that a second tentative explanation stems from the agreement of the hydrodynamical model calculations of Bolz *et al.* [22] with our data [16]. In this calculation the longitudinal expansion is manifestly collective but the transverse expansion is slowed down by the inward shock wave mechanism, characteristic of a mixed phase of plasma and hadrons. Intuitively one hesitates to apply such a model to collisions induced by the surface-dominated, small sulphur projectile. The next generation of experiments, with lead beams at the same energy, will help to finally clarify the expansion scenario.

This work was supported by the Director, Office of Energy Research, Division of Nuclear Physics of the Office of High Energy and Nuclear Physics of the U.S. Department of Energy under Contract No. DE-AC03-76SF00098 and by the Bundesminister für Forschung und Technologie, German Federal Republic, as well as by the Leibniz grant of Deutsche Forschungsgemeinschaft. We thank Dr. H. Sorge, Dr. S. Pratt, and Dr. B. R. Schlei for permission to use their codes.

[a] Alexander von Humboldt Foundation Fellow.
[b] Alexander von Humboldt Foundation U.S. Senior Scientist Award Recipient.

[1] A. Sandoval *et al.*, Nucl. Phys. **A461**, 465c (1987).
[2] D. Ferenc *et al.*, Nucl. Phys. **A544**, 531c (1992); P. Seyboth *et al.*, *ibid.*, **A544**, 293c (1992).
[3] A preliminary stage of this work has been presented elsewhere: G. Roland *et al.*, Nucl. Phys. **A566**, 527c (1994).
[4] G. Goldhaber *et al.*, Phys. Rev. **120**, 300 (1960); G. Cocconi, Phys. Lett. **49B**, 459 (1974).
[5] S. Pratt, Phys. Rev. Lett. **53**, 1219 (1984); Phys. Rev. D **33**, 1314 (1986); G. Bertsch *et al.*, Phys. Rev. C **37**, 1896 (1988).
[6] K. Kolehmainen and M. Gyulassy, Phys. Lett. B **180**, 203 (1986); A. N. Makhlin and Y. M. Sinyukov, Z. Phys. C **39**, 69 (1988); Y. M. Sinyukov, Nucl. Phys. **A498**, 151c (1989).
[7] S. Pratt *et al.*, Phys. Rev. C **42**, 2646 (1990).
[8] S. S. Padula *et al.*, Nucl. Phys. **B329**, 357 (1990).
[9] J. Sullivan *et al.*, Phys. Rev. Lett. **70**, 3000 (1993).
[10] H. Sorge, H. Stocker, and W. Greiner, Nucl. Phys. **A498**, 567c (1989); we employed RQMD version 1.08.
[11] J. W. Harris *et al.*, Nucl. Instrum. Methods Phys. Res., Sect. A **315**, 33 (1992).
[12] J. Bächler *et al.*, Z. Phys. C **52**, 239 (1991).
[13] W. A. Zajc *et al.*, Phys. Rev. C **29**, 2173 (1984).
[14] M. Gyulassy and S. K. Kauffmann, Nucl. Phys. **A362**, 503 (1981).
[15] T. Abbott *et al.*, Phys. Rev. Lett. **69**, 1030 (1992).
[16] Th. Alber *et al.*, (to be published).
[17] J. Bartke, Phys. Lett. B **174**, 32 (1986).
[18] Other investigations [9,13] have preferred a description in terms of rms values referring to a Gaussian ansatz. In that case our radius parameters should be divided by $\sqrt{2}$.
[19] M. Herrmann and G. F. Bertsch, Institute for Nuclear Theory Report No. DOE/ER/40561-141-INT94-00-57, 1994.
[20] D. Beavis *et al.*, Phys. Rev. C **34**, 757 (1986).
[21] H. Beker *et al.*, CERN Report No. PPE/94-119, 1994.
[22] J. Bolz *et al.*, Phys. Lett. B **300**, 404 (1993); B. R. Schlei, Thesis Marburg University, 1994.
[23] J. Barette *et al.*, Phys. Lett. B **333**, 33 (1994).

Line-Shape Transition of Collision Broadened Lines

H. Harde,[1] N. Katzenellenbogen,[2] and D. Grischkowsky[2]
[1]*Universität der Bundeswehr Hamburg, Holstenhofweg 85, 22043 Hamburg, Germany*
[2]*Oklahoma State University, Stillwater, Oklahoma 74078*
(Received 19 July 1994)

Using the newly developed technique of THz time-domain spectroscopy, we have measured the far wing absorption line profile of the ensemble of collision broadened ground state rotational lines of methylchloride vapor out to more than 200 linewidths from resonance, corresponding to frequency offsets as much as 5× the resonant frequency. On these far wings the measured absorption is approximately an order of magnitude less than that predicted by the van Vleck–Weisskopf theory. Our observations show that at higher frequencies a transition occurs from the regime of the van Vleck–Weisskopf theory to the regime of the Lorentz theory.

PACS numbers: 32.70.Jz

The study of molecular collisions has led to a relatively complete understanding of collision broadening phenomena in gases [1–3]. Important information on the collision behavior and intermolecular forces is obtained through the width and shape of broadened spectral lines from optical to microwave frequencies. For the higher frequency range of optical and infrared transitions, the simple Lorentzian line shape [4] provides excellent agreement with experiment, particularly for the central region of the line. As the frequencies are reduced to those of the microwave or far-infrared region, and under conditions when a linewidth becomes comparable with the transition frequency, the absorption profile of a spectral line is better represented by a van Vleck–Weisskopf line shape [5–8].

The line-shape theory of Lorentz [4,5] assumes that after a collision the molecules are oriented randomly with respect to the applied electromagnetic field. Later, it was shown by van Vleck and Weisskopf [5] that this assumption prevents the Lorentz theory from reducing to that of Debye for the zero resonant frequency case. This discrepancy was removed by the van Vleck–Weisskopf theory based on the assumption that after a collision the molecules are oriented with a Boltzmann distribution along the applied electromagnetic field [1,5]. This assumption required that the duration of the collision be short compared to the period of oscillation of the applied field.

In the THz experiments reported here, we measured the absorption line shapes in the ground state rotational band of methylchloride vapor from relatively near resonance to frequency offsets as much as 5× the resonant frequency and to as much as 200 linewidths away. These experimental conditions are unprecedented. Our measurements are well fit using a van Vleck–Weisskopf line shape for an individual transition out to frequencies of the order of 1 THz. Further, increasing the frequency leads to a much reduced absorption compared to that of the van Vleck–Weisskopf line shape. In fact, we find that at higher frequencies the measured absorption is almost an order of magnitude less than that given by the van Vleck–Weisskopf line shape.

We have observed, for the first time, the switching between the van Vleck–Weisskopf and Lorentz collision theories. Our observations are well explained by the following picture [1,5]. At lower frequencies our measurements satisfy the condition that the collision duration is short compared to the period of oscillation of the applied field. However, as the frequency is further increased, the above condition is violated and the original approximation of Lorentz becomes applicable, the molecules become randomly oriented with respect to the applied field after a collision. We obtain an excellent fit to our measurements by using the van Vleck–Weisskopf theory for relatively low frequencies and with a weighting function switching to the Lorentz theory for the high frequency part.

For our investigations we used the powerful new technique of THz time-domain spectroscopy (TDS) [9–15]. With this technique two electromagnetic pulse shapes are measured, the input (reference) pulse and the propagated pulse, which has changed shape due to its passage through the sample under study. Consequently, via Fourier analyses of the input and propagated pulses, the frequency dependent absorption and dispersion of the sample can be obtained. Because of the broad bandwidth of the THz pulses, a spectral range extending from low frequencies up to more than 5 THz can be investigated.

The high-performance optoelectronic setup used to generate and detect the subpsec pulses of freely propagating THz electromagnetic radiation is shown in Fig. 1 and has been described elsewhere [9–11]. A GaAs transmitting antenna with simple coplanar transmission line geometry [11] and a silicon on sapphire receiving antenna consisting of a micron size dipole antenna imbedded in a coplanar transmission line were both optoelectronically driven by 65 fs pulses from a colliding-pulse mode-locked dye laser. The generated pulses of THz radiation are collimated by a silicon lens attached to the back of the trans-

0031-9007/95/74(8)/1307(4)$06.00

Imaging with terahertz waves

B. B. Hu and M. C. Nuss

AT&T Bell Laboratories, 101 Crawfords Corner Road, Holmdel, New Jersey 07733-3030

Received May 11, 1995

We present what is to our knowledge the first imaging system based on optoelectronic terahertz time-domain spectroscopy. Terahertz time-domain waveforms are downconverted from the terahertz to the kilohertz frequency range, and the waveform for each pixel is frequency analyzed in real time with a digital signal processor to extract compositional information at that point. We demonstrate applications to package inspection and chemical content mapping in biological objects. © 1995 Optical Society of America

Optoelectronic terahertz time-domain spectroscopy (THz-TDS) has come a long way since the first demonstration of free-space THz transmitters and detectors a few years ago.[1] In particular, it has proven to be a powerful tool for spectroscopic measurement of far-infrared properties of materials such as dielectrics and semiconductors,[2] superconductors,[3] liquids,[4] and gases.[5] Unlike in traditional Fourier-transform far-infrared spectroscopy, in which a blackbody radiation source and a bolometer are used, both the generation and the detection are optically gated in THz-TDS. This offers extraordinary noise rejection, and signal-to-noise ratios as high as 10,000:1 are achieved.[6] Also, the detection is coherent—both the amplitude and the phase of the THz waveform are measured, allowing one to extract the full complex dielectric constant of the material under investigation without having to resort to the Kramers–Kronig relations. In general, most chemical compounds show very strong, highly specific frequency-dependent absorption and dispersion in the THz range. This is particularly true for gases that have characteristic narrow absorption lines in this range. But liquids and solids also have rather specific frequency-dependent absorption and dispersion characteristics in this frequency range, leading to characteristic time-domain waveforms when THz radiation passes through different materials. Accordingly, it should be feasible to a certain degree to apply THz-TDS to determine the chemical content of an unknown object. Together with the ability to collimate and focus THz waves down to the diffraction limit of a few hundred micrometers at the sample,[7] imaging of chemical compositions should be possible with reasonable spatial resolution by the THz-TDS technique. However, until now, acquisition of THz waveforms has required lock-in detection and low-pass filtering with a 100–300-ms time constant per data point. With resulting acquisition times of a few minutes for a single THz waveform at each image point, imaging with THz transients has so far been impractical.

In this Letter we demonstrate practical terahertz imaging for what is to our knowledge the first time. THz transients are focused to a diffraction-limited spot on the sample, and the transmitted THz waveforms are acquired and processed in real time at each point of the sample while the sample is scanned in x and y at a rate of currently 10–20 pixels/s. We analyze the temporal waveform transmitted through the sample at every pixel of the object in real time, from which information on the chemical composition of the sample can be inferred in many cases. This new application of THz-TDS is permitted by the following advances in the technology: (i) a reduction of the acquisition time for each THz waveform from minutes down to less than 5 ms with a signal-to-noise ratio of still more than 100:1, (ii) downconversion of the THz waveforms into the audio (kilohertz) range with a scanning delay line, and (iii) real-time acquisition, processing, frequency analysis and display of the spectral data of the THz transients by a digital signal processor (DSP). As first examples of this novel technology, we show that this system can be used for safe terahertz-ray (T-ray) package inspection, chemical content mapping, and food inspection.

Figure 1 shows a schematic setup of the THz imaging system. An Ar-ion-pumped self-mode-locked Ti:sapphire laser delivering pulses of 100-fs duration at $\lambda \approx 800$ nm is used as a femtosecond optical source. Roughly 80 mW from this source is used to excite a THz transmitter. This photoconducting transmitter consists of two strip lines spaced by 50 μm that are lithographically defined on a semi-insulating GaAs substrate, with a bias of 80–100 V applied to the strip lines. In our initial experiment, the imaging optics consists of two pairs of off-axis paraboloid reflectors. The THz radiation from the transmitter is first collimated and then focused down to a diffraction-limited spot on the object by the first pair of paraboloids, and another pair of paraboloids is used to collect and focus the THz radiation from the sample onto the optically gated THz dipole detector. The detector is a 50-μm-wide radiation-damaged silicon-on-sapphire photoconducting dipole antenna with a 5-μm gap.[1] The THz detector is optically gated by approximately 60 mW of the laser beam. Both the transmitter and the receivers have high-resistivity silicon hyperhemispherical substrate lenses attached to the backs of their substrates to improve coupling of the THz radiation to air. A 20-Hz scanning delay line temporally downconverts the THz waveforms into the audio (kilohertz) range, with the downconversion ratio given by twice the ratio of the speed of the delay line to the speed of light. In our example the scanning delay line with a speed of 15 cm/s converts a 1-THz waveform exactly to a 1-kHz waveform. The amplitude of the scan is approximately 0.75 cm, resulting in a spectral resolution of 20 GHz. The signal is then amplified by a current preamplifier, digitized, and processed by the DSP on the flight for each pixel. Both the analog-to-digital (A/D) converter and the DSP are integrated on a commercial signal processing board (Data Translation DT3818). The spectral information at each pixel is obtained and processed by the board in less than 5 ms. The typical real-time THz signal has an amplitude of 10 V after passing the 10^9 V/A current preamplifier with a signal-to-noise ratio of greater than 100:1. In this first implementation of the THz imaging experiment, the sample, rather than the THz beams, is scanned. Currently the THz image is acquired, analyzed, and displayed at a rate of 12 pixels/s. Simple modifications are expected to increase this rate into the neighborhood of 100 pixels/s, so that a 100 × 100 image can be obtained in little over a minute.

As a first application we demonstrate the use of this novel technique for industrial inspection. In a manner similar to x-ray inspection, an image is formed from the differences in transmittance through different materials inside a concealed package. However, unlike x-ray inspection, our T-ray technique is safe, nondestructive, and free of hazardous effects and can therefore potentially provide an alternative solution for security checking, package inspection, etc. Plate I shows a THz image of a semiconductor integrated-circuit chip package. The THz image contains 50,000 pixels, and the THz transmission is color coded according to the total intensity of the transmitted THz signal integrated over a 1–3-THz frequency range. The plastic packaging material of the chip shows only little absorption in the THz spectral range, whereas metals are fully absorbing and doped semiconductors are partially absorbing.[2] Hence, the image clearly shows the silicon chip area as well as the metal leads connecting to the package pins. A spatial resolution of roughly 250 μm is achieved. Even better spatial resolution can be obtained by having the DSP process only higher THz frequencies, of course at the expense of signal strength.

Another application of the T-ray imaging technique is to detect and map out chemical compositions within an object. To demonstrate this application, we apply this technique to obtain the water distribution within a leaf. The water content inside the leaf causes strong absorption of THz light in the high-frequency range (>500 GHz). To map out the water content of the leaf, we compare the amplitude spectrum of the THz signal passing through the leaf with the reference spectrum without the sample by the DSP. For a leaf approximately 4.5 cm × 2.3 cm, spectral information at 30,000 pixels is recorded with a spatial resolution of roughly 400 μm. Plate II shows a THz image of a fresh leaf (left) and a THz image of the same leaf after 48 h (right). Also shown at the right is a color scale for the relative water concentration. Although the visible appearance of the leaf (not shown) does not change appreciably within this time span, the THz image shows a very prominent change, indicating that the water distribution has changed dramatically over 48 h as the water has gradually evaporated from the leaf. In particular, we see that water has largely disappeared from the bulk of the leaf, whereas appreciable water content still remains in the stems of the leaf.

Similar measurements have also been successfully performed on a variety of other samples. For example, meat absorbs THz radiation because of its moisture content, whereas fat is nearly transparent to THz radiation. Thus from a THz image of a piece of bacon we are able to map out the fat distribution, indicating some possible applications to food inspection. This technology could also be extended to medical tissue and biomedical studies, for example, for skin cancer detection, as the water retention of tumors may be different from that for healthy tissue. We can also see the technology potentially applied to gas monitoring and industrial process control, such as in a combustion chamber or in a reactive-ion etcher. The

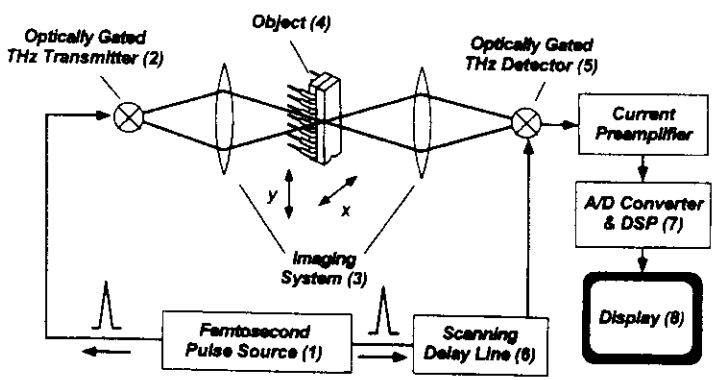

Fig. 1. Schematic of the THz imaging system. In our experiments the object is raster scanned by a two-axis motorized stage.

0146-9592/95/161716-03$6.00/0

Terahertz coherent transients from methyl chloride vapor

H. Harde

Universitaet der Bundeswehr, Holstenhofweg 85, 22043 Hamburg, Germany

N. Katzenellenbogen* and D. Grischkowsky*

IBM Watson Research Center, P.O. Box 218, Yorktown Heights, New York 10598

Received September 14, 1993; revised manuscript received December 17, 1993

A newly developed optoelectronic source for generating well-collimated beams of subpicosecond pulses of terahertz radiation was used to study coherent propagation effects in a spectrally thick medium of methyl chloride vapor. After the passage of the excitation pulse, we observe the subsequent emission of a coherent terahertz pulse train in the free-induction decay of the molecular vapor. The individual pulses of the train are separated by 38 ps, corresponding to the frequency separation between adjacent rotational lines of the excited manifold of more than 70 transitions. An analysis of the data determines the rotational constants and anharmonicity factors of the two naturally abundant methyl chloride isotopes. From the decay and reshaping of the pulse train the coherence relaxation time T_2 is obtained as a function of vapor pressure. Our observations indicate a strong nonmonotonic collision broadening and a van Vleck–Weisskopf line shape of the individual rotational lines.

1. INTRODUCTION

The experimental and theoretical study of coherent transient effects resulting from the interaction of electromagnetic radiation with resonant systems[1,2] was recently extended to the terahertz frequency range.[3,4] These experiments were based on exciting molecular vapors with freely propagating subpicosecond pulses of terahertz radiation and detecting the free-induction decay (FID) reradiated by the vapors. This newly accessible frequency range, midway between the frequencies used for spin resonance and those of infrared and optical studies, is important both because of the samples that can be investigated and because of the unusual experimental conditions encountered with subpicosecond pulses of terahertz radiation. The recently developed optoelectronic terahertz-beam system used in these experiments produces well-collimated beams of subpicosecond pulses of freely propagating terahertz radiation.[5–9] These pulses of terahertz electromagnetic radiation can be detected with signal-to-noise ratios of better than 10,000. Compared with studies of coherence effects in the radio frequency and the microwave regimes for nuclear- and electron-spin systems, the terahertz experiments involved samples that were of many wavelengths in length, so that in addition to the point response, propagation effects were also important. In contrast to investigations at infrared and optical frequencies, in which coherent transients are detected only as pulse intensities or as beat notes on a carrier,[10–12] the terahertz experiments directly measure the actual electric field of the transmitted radiation pulse and that radiated by the coherent response of the sample. This feature allows for experimental studies with unprecedented precision, and both the amplitude and the phase are measured within the broad bandwidth of the terahertz pulse extending from low frequencies up to 5 THz.

In this paper we extend the terahertz coherence studies to methyl chloride, which is a symmetric top molecule with a large electric dipole moment. This molecule is an interesting candidate for observation of coherent propagation effects under extreme conditions for which the vapor is an optically dense sample for the terahertz radiation. Owing to the high sensitivity and the excellent signal-to-noise ratio of the measuring system, additional molecular information can be obtained. Our measurements indicate that the individual rotational transitions have van Vleck–Weisskopf line shapes, with a strong nonmonotonic J dependence for the collision-broadening coefficient.

The propagation of a terahertz excitation pulse through methyl chloride vapor simultaneously excites a manifold of rotational transitions, thereby causing the molecules to radiate a FID signal consisting of a series of uniformly spaced subpicosecond terahertz pulses.[3,4] For a similar phenomenon of infrared pulses emitted after excitation, see Refs. 13–16. Since the methyl chloride molecule is distinguished by absorption lines with an almost constant frequency spacing, after the initial excitation a periodic rephasing and dephasing of the entire ensemble of more than 70 excited transitions occurs during the FID and is manifest as a train of subpicosecond terahertz pulses with a repetition rate equal to the frequency separation between adjacent lines. This situation is quite similar to the mode locking of lasers. A coherent signal radiated by dipoles coming into phase and forming a macroscopic dipole moment is known from spin and photon echoes. Because of this and the fact that the frequencies are numerical multiples of the difference frequency between two lines, we term the periodic pulses terahertz commensurate echoes.[3]

These echoes carry almost complete information about the molecular system. From their temporal separation and pulse shapes we obtain the parameters of the molecule, and from their decay the coherence relaxation time

0740-3224/94/061018-13$06.00

Chemical recognition of gases and gas mixtures with terahertz waves

R. H. Jacobsen,* D. M. Mittleman,† and M. C. Nuss

Bell Labs, Lucent Technologies, 101 Crawfords Corner Road, Holmdel, New Jersey 07733

Received August 9, 1996

A time-domain chemical-recognition system for classifying gases and analyzing gas mixtures is presented. We analyze the free induction decay exhibited by gases excited by far-infrared (terahertz) pulses in the time domain, using digital signal-processing techniques. A simple geometric picture is used for the classification of the waveforms measured for unknown gas species. We demonstrate how the recognition system can be used to determine the partial pressures of an ammonia–water gas mixture. © 1996 Optical Society of America

The analysis of chemical compositions is a fundamental issue in molecular spectroscopy. In the far-infrared region of the electromagnetic spectrum, time-domain spectroscopy has been facilitated by a novel development of pulsed broadband sources. This spectroscopic technique, commonly known as terahertz (THz) time-domain spectroscopy, is based on optoelectronic techniques[1,2] that use photoconductive antennas excited by femtosecond laser pulses to generate and detect subpicosecond electromagnetic pulses. The THz waveforms consist of a single-cycle oscillation of the electromagnetic field and have spectra covering frequencies from 100 GHz to more than 2 THz, and signal-to-noise ratios as high as $10^6:1$ have been obtained.[3]

The impulse character of the THz waveforms has motivated studies of the coherent transient response of resonantly excited gases[4,5] and gas mixtures.[6] The coherent transient phenomena show up in the time-domain spectra as free induction decays[7] (FID's) characterized by fast oscillations[4] and commensurate echoes[5] that occur after the impulse excitation. The FID is a unique time-domain representation of the absorption and dispersion characteristics of the sample and serves as a fingerprint of its chemical composition. However, despite its time-resolved nature, THz spectroscopy has so far been based on conventional Fourier-transform techniques.

In this Letter we demonstrate a time-domain chemical-recognition system for the analysis of the chemical compositions of infrared active gas systems. We model the action of a resonantly excited gas or gas mixture by a linear digital filter that reshapes an incident THz waveform to produce the corresponding FID. These circumstances strongly resemble the basic problems of spectral estimation for phonetic recognition,[8] and theory and algorithms from speech recognition systems have been adopted. In particular, we apply a correlation type of analysis known as linear predictive coding[9,10] (LPC) to extract and parameterize the spectral features of a waveform. A simple geometric picture permits the use of these parameters for classification of individual gas species as well as mixture analysis.

In linear prediction, subsequent values in a time series of a digital signal, $s(n)$, can be generated from a weighted sum of the past M values:

$$s(n) = \sum_{k=1}^{M} a_k s(n-k) + e(n),$$

where $e(n)$ is the residual, and a_k are the parameters of the linear prediction. To illustrate the basic physics involved we introduce the z transform of Eq. (1):

$$S(z) = \sum_{k=1}^{M} a_k z^{-k} S(z) + E(z), \tag{2}$$

where $z = \exp(i2\pi f\Delta)$ and Δ^{-1} is the sampling frequency. We find that the signal $S(z)$ is constructed from the residual $E(z)$ by an all-pole filtering:

$$S(z) = H(z)E(z), \tag{3}$$

where

$$H(z) = \frac{1}{1 - \sum_{k=1}^{M} a_k z^{-k}}. \tag{4}$$

The LPC coefficients a_k contain the information on the spectral content of the waveform. The advantages of using LPC for chemical recognition of gases are twofold: (1) Poles provide an accurate representation for an underlying power spectrum that has sharp spectral lines. This is in contrast to Fourier analysis, in which a signal waveform is expanded into a Fourier series. Such series can have only zeros, not poles, and must attempt to fit sharp spectral features with a polynomial that requires a large number of coefficients. (2) By using the LPC we can always rely on the same number of coefficients M, regardless of the number of resonances excited. This enables us to use simple geometric pictures instead of complicated template-matching techniques for the classification of waveforms.

The optimum values for the LPC coefficients are calculated from least-squares principles, i.e., we wish to minimize the total squared residual: $\mathcal{E} = \sum e(n)^2$. The analysis yields a system of normal equations[10] that relates the LPC coefficients to values of autocorrelation function $\sum_k s(k)s(k-n)$ of the time series representing the waveform.

The parameters from a LPC analysis are treated as a vector, $\mathbf{a} = (a_1, a_2, \ldots a_M)$, in an M-dimensional vector space. Vectors representing known gas species are stored in a codebook, and the codebook is built by

0146-9592/96/242011-03$10.00/0

Generation and detection of terahertz pulses from biased semiconductor antennas

P. Uhd Jepsen, R. H. Jacobsen, and S. R. Keiding

Department of Chemistry, Aarhus University, Langelandsgade 140, DK-8000 Aarhus C, Denmark

Received November 2, 1995; revised manuscript received April 26, 1996

We propose a simple model based on the Drude–Lorentz theory of carrier transport to account for the details of the ultrashort terahertz pulses radiated from small photoconductive semiconductor antennas. The dynamics of the bias field under the influence of the space-charge field from the accelerated carriers is included in the model. We consider in detail the optical system used to image the terahertz radiation onto the terahertz detector, and we calculate the frequency-dependent response of the detector. The proposed model is compared with several different experiments, each focusing on different parameters of the model. Agreement between experiment and model is found in all cases, supporting the validity of this simple and appropriate model.

1. INTRODUCTION

The use of ultrafast lasers to generate subpicosecond pulses of electromagnetic radiation, terahertz (THz) pulses, has evolved during the past 5 years into a very active research field. When an ultrafast laser interacts with a material to generate a dc polarization, the polarization acts as a source for the THz pulses. The dc polarization can have its origin in either a simple flow of free carriers in a photoconductive switch, $P_{dc} = \int j\,dt$, where j is the current density, or from a nonlinear optical χ^2 process, $P_{dc} = \chi^2(0, -\omega, \omega)E(\omega)E^*(-\omega)$. The resulting THz pulses generally consist of only a few cycles of the electric field and consequently have a very high bandwidth. Centered around 1 THz with frequencies extending beyond 5 THz, the pulses have proven to be very useful in time-domain spectrometers and, equally important, as probes of fundamental carrier transport processes in the semiconductors from which they originate or as probes of phonon dynamics in crystals.

Several reviews exist covering different aspects of the THz field. The generation of THz pulses from semiconductor surfaces and from large-aperture photoconducting antennas was reviewed by Zhang.[1,2] Grischkowsky reviewed the high-bandwidth THz systems that used small photoconducting antennas and their applications to time-domain spectroscopy.[3,4] The generation of THz pulses from semiconductor quantum wells was recently reviewed by Nuss and Lou,[5,6] and applications of THz spectroscopy in atomic and molecular physics were discussed by us.[7] Recently, a special issue of the *Journal of the Optical Society of America B* covering THz pulses was published.[8]

In this work we focus on a detailed description of all the elements in a standard time-domain spectrometer, from the THz emitter by means of the THz optical system to the THz detector. The THz setup is illustrated in Fig. 1, in which the emitter, the THz optics, and the detector are shown. The inset shows the detailed geometry of the emitter and the detector antennas. With a 100-fs laser pulse from a mode-locked Ti:Sapphire laser we generate the THz pulse shown in Fig. 2(a), with its Fourier transform shown in Fig. 2(b). The weak oscillations on the trailing edge of the pulse are caused by free-induction decay of pure rotational transitions in the residual H_2O vapor present in the optical path of the beam. The spectral resolution is 6 GHz (0.2 cm^{-1}). The sharp water lines and the moderate structure in the spectrum are caused by weak reflections and are completely reproduced from scan to scan.

The characteristic of a THz system was previously described by van Exter and Grischkowsky.[9] We have used very simple models to describe the different components of the spectrometer, and we show by comparison with different experiments that the system is very well described by these simple models. To describe the THz emitters, we use the simple Drude–Lorentz model, modified to take into account ultrafast changes in the bias field owing to screening effects. From the calculations and the experiments it is evident that the screening process is the key factor determining the properties of the radiated THz pulses. The THz pulses are imaged onto the detector by lenses and mirrors. Owing to the extreme bandwidth, a frequency range covering two orders of magnitude, the optical system plays an important role in shaping the THz pulse. At the detector the electric field of the THz pulse acts as a transient bias, polarizing free carriers generated by a femtosecond laser pulse. Describing the detection process thus requires a detailed understanding of ultrafast carrier transport dynamics. Furthermore, the active size of the receiver also plays a central role in evaluating the response function of the detector.

2. TERAHERTZ EMITTERS

To illustrate the physical properties of a THz emitter system, we consider the THz antenna shown in the inset of Fig. 1. This particular antenna geometry was first introduced by Grischkowsky *et al.*[10,11] and proved to be a very efficient THz source with high bandwidth. As the emitter chips, we use a high-resistivity chromium-compensated GaAs substrate wafer (Sumitomo) and use a

0740-3224/96/1102424-13$10.00

Electro-optic measurement of THz field pulses with a chirped optical beam

Zhiping Jiang and X.-C. Zhang[a)]
Physics Department, Rensselaer Polytechnic Institute, Troy, New York 12180-3590

(Received 8 December 1997; accepted for publication 18 February 1998)

Using a linearly chirped optical probe pulse in free-space electro-optic measurements, a temporal wave form of a co-propagating THz field is linearly encoded onto the frequency spectrum of the optical probe pulse, and then decoded by dispersing the probe beam from a grating to a detector array. We achieve acquisition of picosecond THz field pulses without using mechanical time-delay device. We also demonstrate a *single-shot* electro-optic measurement of the temporal wave form of a THz pulse. © *1998 American Institute of Physics.* [S0003-6951(98)00916-4]

Conventional time-domain optical measurements, such as THz time-domain spectroscopy in pump/probe geometry, use a mechanical translation stage to vary the optical path between the pump and probe pulses.[1-4] The intensity or polarization of the optical probe beam which carries information generated by the pump beam is repetitively recorded for each sequential time delay. In general, this data acquisition in the temporal scanning measurement is a serial acquisition; the signal is recorded during the probe pulse sampling through a very small part of the THz wave form (roughly the pulse duration of the optical probe beam). Therefore, the data acquisition rate in this single channel detection is limited to less than 100 Hz for a temporal scan on the order of tens of picoseconds.[5] Clearly, this relatively slow acquisition rate cannot meet the requirement for real-time measurements, such as time-domain THz spectroscopy of fast-moving objects or flame analysis. To increase the acquisition rate, parallel data acquisition or multichannel detection is required. One possible method is to extend the novel design of "real time picosecond optical oscilloscopes" for the local-field characterization to the freely propagating THz field applications.[6-8]

In this letter, we present experimental results of electro-optic measurement of freely propagating picosecond electromagnetic pulses by using a linearly chirped (a linear ramp of frequency versus time) optical beam. The temporal wave form of a THz pulse is simultaneously recorded on the differential spectrum profile of the optical probe beam. By measuring the spectrum difference of the probe beam with and without pulsed electromagnetic field modulation, temporal measurement of THz wave form is obtained without a moving element for the time delay. We also demonstrate a single-shot electro-optic measurement of a freely propagating THz pulse.

Figure 1 schematically illustrates the experimental setup of the electro-optic measurement with a chirped optical probe beam. The geometry is similar to the conventional free-space electro-optic sampling setup,[9] except for the use of a grating pair for chirping and stretching the optical probe beam, and a grating-lens combination with a detector array for the measurement of the spectral distribution.[6] Two laser systems are used as the optical source; one is a Ti:sapphire laser oscillator (Spectra-Physics Tsunami) with an average power of 2 W and a pulse duration of 100 fs at an 82 MHz repetition rate, and the other is an amplified Ti:sapphire laser (Coherent Rega 9000) with an average power of 0.9 W and a pulse duration of 200 fs at 250 kHz. The center wavelength of the Ti:sapphire lasers is about 820 nm with a spectrum bandwidth from 7 nm (Rega) to 17 nm (Tsunami). The THz emitter is a 8 mm wide GaAs photoconductor. A polylens of 5 cm focal length focuses the THz beam onto a 4 mm thick ⟨110⟩ ZnTe crystal. The optical probe pulse is frequency chirped and time stretched from sub-picoseconds to over 30 ps by the grating pair. Due to the negative chirp of the grating (pulse with decreasing frequency versus time), the blue component of the pulse leads the red component. The fixed delay line is only used for the positioning of the THz pulse within the duration of the synchronized probe pulse (acquisition window) and for temporal calibration.

When the chirped optical probe pulse (approximately 30 ps long) and a THz pulse co-propagate in the ZnTe crystal, the polarization of different wavelength components of the chirped pulse is rotated by a different portion of THz pulsed field through the Pockels effect. The degree and direction of rotation is proportional to the THz field strength and polarity. After the optical analyzer, the polarization modulation is converted to the amplitude modulation on the spectrum. The grating-lens combination is used to disperse and focus the collimated probe beam on a linear diode array (LDA). The linear diode array (PI, ST-120) has 1024 pixels with a 14 bit dynamic range. Similar to the THz imaging experiment,[10] the electro-optic modulation must be operated near the zero op-

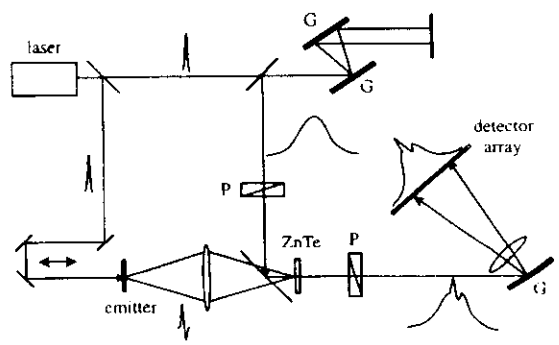

FIG. 1. Schematic of experimental setup of electro-optic measurement with a chirped optical probe beam.

a)Electronic mail: zhangx2@rpi.edu

Electrical characterization to 4 THz of *N*- and *P*-type GaAs using THz time-domain spectroscopy

N. Katzenellenbogen and D. Grischkowsky
IBM Watson Research Center, P.O. Box 218, Yorktown Heights, New York 10598

(Received 28 February 1992; accepted for publication 2 June 1992)

Using a high-performance optoelectronic THz beam system for time-domain spectroscopy, we have measured the absorption and index of refraction of *N*- and *P*-type doped GaAs from low frequencies to 4 THz. From these measurements the complex conductance was obtained over the same frequency range. All of the results were well fit by Drude theory.

In contrast to silicon, it is not possible to electrically characterize GaAs wafers with simple mechanical contacts, due to the Schottky barrier at the metal/GaAs interface. For such characterization ohmic contacts must be fabricated on the wafer itself. Accordingly, manufacturers specifications on device-grade GaAs wafers are relatively imprecise. This is especially true for *N*-type doping, due to the lower concentrations required. Therefore, a contactless method of electrical characterization of GaAs wafers would be extremely desirable. Previous work has proposed and demonstrated that far-infrared spectroscopy is a possible solution.[1] Pioneering far-infrared absorption measurements have been made on *N*-type GaAs at several different free carrier concentrations.[2] The measured absorption due to the free carriers agreed with Drude theory on the high-frequency wing and allowed for an "optical" determination of the free carrier density and mobility. However, the peak absorptions measured were only a fraction of that expected from Drude theory. Later measurements with discrete far-infrared laser sources showed that these early measurements were severely compromised by scattered far-infrared light, which placed a limit on the magnitude of the absorption that could be measured.[3]

The key parameters characterizing the dynamics of free carriers in semiconductors are the plasma frequency ω_p and the carrier damping rate $\Gamma = 1/\tau$, where τ is the carrier collision time. Because ω_p and Γ characteristically have THz values, measurements spanning the values of these parameters must be performed in the difficult THz frequency range.[4] The experiments described in this letter present such measurements on device-grade, *N*-type and *P*-type GaAs wafers, by the newly developed THz time-domain spectroscopy (TDS) technique.[4,5] Our results show, for the first time, the absorption and index of refraction due to the free carriers in GaAs measured over the peaks of their response and extending from low frequencies to beyond 4 THz. The fact that the measured frequency-dependent absorption and index of refraction are mostly due to the free carriers allows the complex conductivity to be determined from the measurements over the full frequency range. The results are fit to surprising accuracy by the Drude theory.

The THz-TDS measurements were performed by measuring freely propagating, THz electromagnetic pulses transmitted through the GaAs wafer under investigation. These transmitted pulses were then compared to the measured THz pulses with no sample in place. Analysis of the respective numerical Fourier transforms determines the frequency dependent absorption and index of refraction.[5] The 40-mm-diameter wafers were obtained from Sumitomo Electric, with the *P* type specified to be between 0.52 and 0.56 Ω cm with a zinc dopant, and the *N* type to be between 0.1 and 1 Ω cm with a silicon dopant. Because of the large absorptions, the *P*-type and *N*-type wafers were thinned to 230 and 190 μm, respectively.

Earlier THz-TDS measurements on doped silicon wafers were limited to the highest frequency of 2 THz.[4] Since then, the frequency range of the optoelectronic THz beam system, illustrated schematically in Fig. 1(a), has been extended by combining a new type transmitter[6] with a high-performance SOS receiver.[7] As shown in Fig. 1(b), this system can now generate and measure femtosecond pulses of freely propagating THz radiation with a signal-to-noise ratio of better than 1000. An expanded view of this input pulse [Fig. 1(b)] for the *N*-type measurements is presented in Fig. 1(c), where on the trailing edge rise and fall times faster than 160 fs can be observed. These values are consistent with the receiver response time of 150 fs.[7] The amplitude spectrum shown in Fig. 1(d) extends from low frequencies to 5 THz and is obtained by a numerical Fourier transform of the measured pulse of Fig. 1(b).

Our THz-TDS measurements of the exceptionally high absorption of the *N*-type GaAs sample are shown in Fig. 2(a) along with previous Fourier-transform-spectroscopy (FTS) measurements on a sample with an equivalent dopant concentration (triangles)[2] and discrete measurements on the same sample with far-infrared laser lines (squares).[3] As determined by a Drude theory fit, our sample has a free carrier concentration of $N_e = 7.8 \times 10^{15}/\text{cm}^3$, while for the sample of the earlier works,[2,3] $N_e = 7.1 \times 10^{15}/\text{cm}^3$. Surprisingly, where the absorption is high, these measurements on similar samples show quite different results. However, the measurements converge at the highest frequencies where the absorption is relatively low. As discussed in Ref. 3, we consider this to be mainly due to the sensitivity of the FTS measurements to scattered far-infrared light. Compared to the previous techniques which measure power, an advantage of THz time-domain spectroscopy is that it is a coher-

 0003-6951/92/320840-03$03.00

Efficient generation of 380 fs pulses of THz radiation by ultrafast laser pulse excitation of a biased metal-semiconductor interface

N. Katzenellenbogen and D. Grischkowsky
IBM Watson Research Center, P. O. Box 218, Yorktown Heights, New York 10598

(Received 10 September 1990; accepted for publication 12 November 1990)

We have demonstrated a new method of generating pulses of freely propagating THz electromagnetic radiation. The resulting 380 fs pulses are the shortest directly measured THz pulses in free space to date and are more powerful than those generated by Hertzian dipoles or by resonant dipole antennas. Temporal features as short as 190 fs were observed on these THz radiation pulses and thereby, illustrate an ultrafast receiver response time.

Recently, there has been a great deal of work demonstrating the generation of THz radiation via excitation with ultrashort laser pulses. Modern integrated circuit techniques have made possible the precise fabrication of micron-sized dipoles, which when photoconductively driven by subpicosecond laser pulses can radiate well into the THz regime.[1,2] An alternative and complementary approach has been to extend radio and microwave techniques into the THz regime through the use of antennas.[3-9] Other sources based on various physical systems and effects include the emission of an electromagnetic shock wave due to a moving volume dipole distribution, i.e., electro-optic Cherenkov radiation,[10,11] and the electromagnetic shock wave radiated by a propagating surface-dipole distribution.[12,13] Most recently, radiation has been generated by photoconductively driving the surface field of semiconductors[14,15] and of strained-layer superlattices[16] with ultrafast laser pulses.

In this letter we report a new mechanism of generating relatively powerful and extremely short pulses of freely propagating THz radiation. After propagating 88 cm in free space, these pulses were measured to have a (full width at half maximum) pulse width of 380 fs with no deconvolution. These are the shortest directly measured, freely propagating THz pulses in free space to date. This source is fully compatible with our recently developed optoelectronic THz beam system[8,9] and has thereby extended the frequency bandwidth of this system to beyond 3 THz. The THz pulse amplitudes are larger than those produced with our previously used antenna geometry.[9] Because of the ultrafast temporal features of these radiation pulses, we have been able to demonstrate that our ion-implanted, silicon-on-sapphire receiver can resolve features as short as 190 fs.

The source is based on a recently discovered optoelectronic effect,[17] initially used to generate a 350 fs electrical pulse on a coplanar transmission line by focusing an ultrashort laser pulse on the interface (edge) of a positively biased line. Here, we use the same technique with a different line geometry and an experimental arrangement designed to capture the radiation emitted into the substrate from the point of excitation.

The configuration used to generate the pulses of freely propagating THz electromagnetic radiation is shown in Fig. 1(a), where the coplanar transmission line structure consists of two 10-μm-wide metal lines separated b μm. The length of the entire transmission line is 20 and the laser excitation spot with a diameter of typical μm was located at the midpoint. This structure was f cated using standard liftoff procedures on silicon sapphire (SOS), GaAs, and InP intrinsic, high-resist wafers. For the SOS wafers the initial metal layer cor of 100 nm of Ti followed by 500 nm of Al. After liftoff gave a resistivity of 10 Ω/mm for a single 10-μm-wide For both GaAs and InP, the metallization consisted nm of Ni followed by 10 nm of Ge followed by 80 n Au followed by 10 nm of Ge followed by 30 nm o followed by 100 nm of Au. After this deposition the w was given a standard anneal to form an Ohmic con Liftoff was then performed. This procedure gave a resi ity of 120 Ω/mm for a single 10-μm-wide line.

Irradiating the metal-semiconductor interface (e of the positively biased line with focused ultrafast

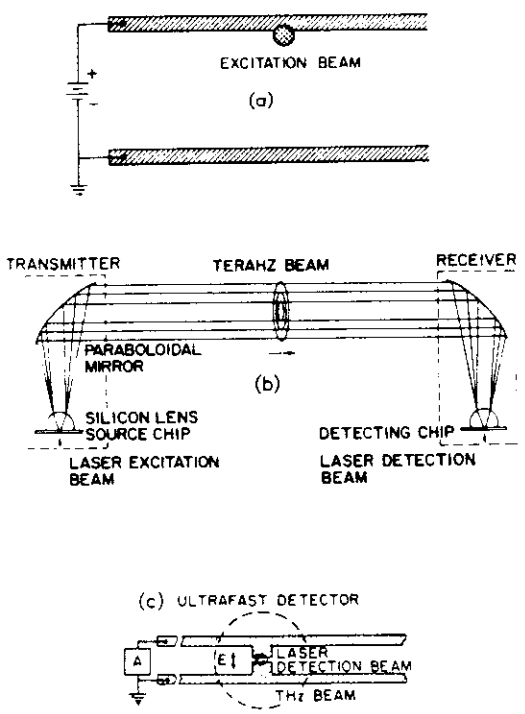

FIG. 1. (a) Configuration used to generate the freely propagating of THz radiation. (b) THz collimating and focusing optics. (c) Rec antenna geometry.

 0003-6951/91/030222-03$02.00

Unidirectional radiation of widely tunable THz wave using a prism coupler under noncollinear phase matching condition

Kodo Kawase,[a] Manabu Sato, Koichiro Nakamura, Tetsuo Taniuchi, and Hiromasa Ito
Research Institute of Electrical Communication, Tohoku University, 2-1-1, Katahira, Sendai 980-77, Japan

(Received 20 March 1997; accepted for publication 10 June 1997)

A widely tunable THz wave has been parametrically generated and reported recently by us utilizing a $LiNbO_3$ crystal with a monolithic grating coupler under a noncollinear phase matching condition. However, the output direction of the THz wave is strongly dependent on the generated frequency due to the nature of noncollinear phase matching, as well as the grating coupler. In this letter, a novel method for THz coupling is proposed using a low dispersion prism to eliminate almost completely the THz beam deflection for the entire tuning range. The unidirectional THz wave radiation was confirmed theoretically and experimentally for the range of 1–2 THz. © *1997 American Institute of Physics.* [S0003-6951(97)02632-6]

Over the last decade, several techniques involving the use of photoconductivity and optical rectification have been developed for the THz radiation.[1–4] Most studies have utilized ultra-broad-bandwidth characteristics of femtosecond optical pulses, so that the generated THz waves possess high temporal characteristics with the sacrifice of their temporal coherence.

In contrast to these methods, we have recently demonstrated a room temperature operated tunable THz-wave generation introducing a monolithic grating coupler onto a $LiNbO_3$ crystal which was pumped by a Q-switched Nd:YAG laser.[5,6] The process involved is an optical parametric oscillation (OPO) utilizing the polariton mode scattering of $LiNbO_3$ based on the 248 cm^{-1} A_1-symmetry soft mode.[7] Idler (near-infrared) and THz waves are parametrically generated by the pump, and three wave vectors ($\mathbf{k}_p, \mathbf{k}_i, \mathbf{k}_T$; p:pump, i:idler, T:THz) are noncollinearly phase matched (NCPM) as shown in the inset of Fig. 1. The generated wavelength of idler (λ_i) is a few nanometers longer than the pump wavelength ($\lambda_p = 1.064$ μm), and that of the THz wave (λ_T) is more than a hundred times longer than λ_p, so that the wave vectors have a relation $|\mathbf{k}_p| > |\mathbf{k}_i| \gg |\mathbf{k}_T|$. Consequently, the angle ϕ between the pump wave and the idler wave is small (~0.8°), and the angle δ between the idler and the THz wave is relatively large (~65°). Tunability ($\lambda_T = 150$–290 μm) is obtained by changing the angle ϕ between the pump and the idler. As the NCPM condition changes for the tuning, the direction angle δ of the generated THz wave inside the crystal changes. Furthermore, the THz wave suffers total internal reflection at the crystal-air interface due to a large refractive index of nonlinear crystals in the THz-wave region (~5.2 for $LiNbO_3$).

In the former experiments, two types of specially prepared crystals were used to avoid the total internal reflection. One was with a cut exit at the corner of the crystal so that the THz wave emerges approximately normal to the exit surface[7] (angled surface coupler: ASC). Another type was with a monolithic grating coupler (GC) fabricated on the crystal surface using a precise dicing saw.[5,6] For ASC, refractive index dispersion of the nonlinear material (e.g., $LiNbO_3$) and the change of the phase-matching angle δ directly influence the output direction θ_{air}. For GC, the output direction change is relatively large due to the Bragg condition and the wide tuning range of the THz wave. The average rates of these radiation angles change around $\lambda_T \approx 200$ μm for both methods are

$$\left(\frac{\Delta\theta_{air}}{\Delta\lambda}\right)^{ASC} \approx -0.017(\text{deg./}\mu\text{m}), \tag{1}$$

$$\left(\frac{\Delta\theta_{air}}{\Delta\lambda}\right)^{GC} \approx 0.65(\text{deg./}\mu\text{m}). \tag{2}$$

The stable output direction of the THz wave is usually desirable for many applications. Here we report a new method to fix the THz-wave direction by employing a semiconductor prism coupler (PC) sitting on the y surface of the $LiNbO_3$ as shown in Fig. 1. Inside the nonlinear crystal, the angle between the pump and the idler waves depicted in Fig. 1 is given by

$$\cos\phi \left(\cong 1 - \frac{1}{2}\sin^2\phi\right) = \frac{|\mathbf{k}_p|^2 + |\mathbf{k}_i|^2 - |\mathbf{k}_T|^2}{2|k_p|\,|k_i|} = \frac{n_p^2\upsilon_p^2 + n_i^2\upsilon_i^2 - n_T^2\upsilon_T^2}{2n_p\upsilon_p n_i\upsilon_i} \tag{3}$$

where υ_j and n_j ($j = p, i, T$) are frequencies and refractive indices for λ_j, respectively, satisfying the energy conserva-

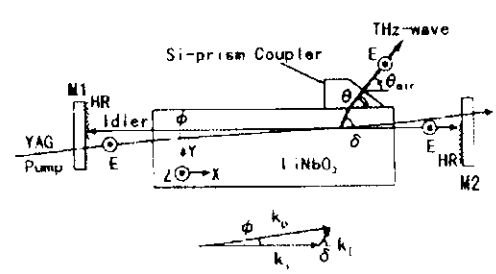

FIG. 1. Experimental cavity arrangement of unidirectional THz wave radiation using Si-prism coupler. The change of the angle θ is ≅0.01°, though the angle δ varies up to ≅1° as the THz wavelengths are tuned from 150 to 290 μm.

[a]Present address: Department of Applied Physics, Tohoku Gakuin University, Japan; Electronic mail: kawase@tjcc.tohoku-gaukuin.ac.jp

 0003-6951/97/71(6)/753/3/$10.00

Coherent tunable THz-wave generation from $LiNbO_3$ with monolithic grating coupler

Kodo Kawase, Manabu Sato, Tetsuo Taniuchi, and Hiromasa Ito[a)]
Research Institute of Electrical Communication, Tohoku University, 2-1-1, Katahira, Aoba-ku, Sendai 980-77, Japan

(Received 23 January 1996; accepted for publication 4 March 1996)

Coherent THz-wave generation is demonstrated utilizing a grating coupler fabricated on the surface of a $LiNbO_3$ crystal pumped by a Q-switched Nd:YAG laser. Wide tunability, sharp directivity, and high efficiency were achieved. © *1996 American Institute of Physics.* [S0003-6951(96)00318-X]

During the past several years, THz-wave generation and detection have attracted much attention from both the fundamental and applied points of view. Most studies have utilized ultrabroad bandwidth characteristics of femtosecond optical pulses based on recent progress in laser technology, so that the generated THz waves possess high temporal characteristics with the sacrifice of their temporal coherence.[1-4]

In contrast to recent studies, many research efforts had been carried out a couple of decades ago concerning the generation of tunable coherent far-infrared radiation based on optical technology.[5-9] Among them the efficient and wide tunable THz generation had been reported in the pioneering works of Pantell, Puthof, and others in the late 1960s to early 1970s.[7-9] This is based upon tunable light scattering from the long-wavelength side of the A_1-symmetry soft mode in $LiNbO_3$. The input (pump) photon at near-infrared stimulates a near-infrared Stokes photon (called an "idler" in this letter) at the difference frequency between the pump photon and the vibrational mode. At the same time, the THz wave (signal) is generated by the parametric process due to the nonlinearity arising from both electronic and vibrational contributions of the material. The tuning is accomplished by controlling the propagation direction. Although the interaction is highly efficient, it should be noted that most of the generated THz waves are absorbed or totally reflected inside the crystal due to a large absorption coefficient, as well as a large refractive index in the THz range (≈5.2). To allow the THz radiation a cut had been made in the corner of the crystal.[7-9]

It is to our surprise that as far as we know no research has been reported on this novel method since 1976. In this letter, we report an efficient and wide tunable generation of coherent THz wave based on the principle of the previous works, but far better efficiency by introducing the grating coupler on the $LiNbO_3$ crystal surface to couple out the THz wave directly to the free air space.

The experimental setup is depicted in Fig. 1. A 3.5-mm-thick $LiNbO_3$ z plate was cut to a dimension of $50(x) \times 10(y) \times 3.5(z)$ (mm^3). Two end surfaces of the x plane were cut parallel, polished, and AR coated at 1.07 μm. The relation between the grating period Λ and the nth-order radiation angle θ_N to the grating surface is given by

$$\theta_N = \cos^{-1}(n_T \cos\delta - N\lambda_T/\Lambda), \tag{1}$$

where δ is the incident angle to the grating, and n_T is a refractive index of $LiNbO_3$ at THz. The grating couplers were fabricated on the y surface by precise machining using a cutting saw (DISCO DAC-2SP/86), whose pitch, depth, and length were 125 μm, 60 μm, and 10 mm, respectively. The crystal was placed inside the cavity as shown in the figure, which was resonated at the idler wave using two high-reflection mirrors, $M1$ $(r=\infty)$ and $M2$ $(r=10$ m). The half-area of both mirrors were coated, and the pump beam was traversed at the uncoated portion.

The pump, the resonated idler, and the generated THz waves were set up to be consistent with the noncollinear phase-matching condition as shown in the inset of Fig. 1. The angle between the pump and idler is on the order of a few degrees. A Q-switched Nd:YAG laser (SOLAR LF113, 1.064 μm) was used as the pump source, whose electric field is along the z axis. Its pulse width, repetition, and typical pulse energy were 25 ns, 16.7 pps, and 30 mJ/pulse, respectively. The idler wave as well as the pump was aligned so as to pass through the crystal as close to the y surface as possible to minimize the absorption effect to the THz radiation. THz output was detected using a silicon bolometer (Infrared Lab.) operating at 4 K. In order to suppress its response at near-infrared and midinfrared regions, a Yoshinaga filter was installed inside. A Schottky barrier diode (SBD) was also utilized to detect the temporal characteristic of THz waves

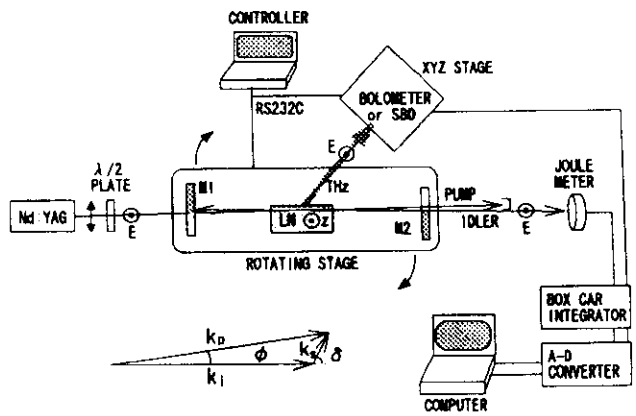

FIG. 1. Experimental setup for the generation of coherent tunable THz wave. The inset shows the momentum conservation relation among the pump, near-infrared idler, and THz signal.

a)Electronic mail: hiromasa@riec.tohoku.ac.jp

 0003-6951/96/68(18)/2483/3/$10.00

A photoconductive, miniature terahertz source

Richard K. Lai, Jiunn-Ren Hwang, Theodore B. Norris, and John F. Whitaker[a)]
Center for Ultrafast Optical Science, University of Michigan, Ann Arbor, Michigan 48109-2099

(Received 14 January 1998; accepted for publication 13 April 1998)

We discuss the performance of a micromachined, photoconductive terahertz emitter that is fabricated on low-temperature-grown GaAs. The device is mounted on a pair of single-mode optical fibers that allows the source to be freely positionable. A strong radiation burst is emitted due to the large magnetic moment created by the electrode. The emitter's small feature size of 300 μm by 300 μm with a photoconductive switch area of 30 μm by 30 μm suggests its application for terahertz, time-domain, near-field spectroscopy and imaging. © *1998 American Institute of Physics.* [S0003-6951(98)00724-4]

Sources for freely propagating terahertz (THz) radiation are important for spectroscopic studies of phenomena such as carrier and exciton dynamics in semiconductor structures and for THz emission from phonons and electron cyclotron oscillations.[1–4] Prospects for useful imaging applications using THz beams have also recently become evident.[5] One of the more common THz generation and detection systems consists of a pair of photoconductive switches defined by coplanar transmission lines on low-temperature-grown GaAs (LT-GaAs) or silicon-on-sapphire (SOS) substrates. One device then acts as an emitter and the other as a detector.[6] The picosecond electric dipoles necessary for THz generation are created by electrically shorting the coplanar lines with an ultrashort laser pulse. As a result, the accelerating electrons between the lines emanate a pulse of broadband radiation into the substrate, with spectral content extending into the THz regime. The THz pulse duration is determined by the electron transport and screening dynamics, which is typically on the order of a picosecond. High-resistivity-silicon or sapphire lenses and parabolic mirrors are used for collimating and focusing the THz radiation. The output radiation is focused onto the detector, where another ultrashort-laser pulse train, time delayed with respect to the laser emitter pulse, is employed for photoconductive gating. Focusing of the radiation onto a sample of interest results in a spatial resolution of several hundred microns limited by diffraction. Also, the focused beam diameter can be frequency dependent over a large THz bandwidth. On the other hand, a flexible, freely positionable point source in contact with a sample would have a resolution of tens of microns, determined by the size of the photoconductive switch. In this letter, we describe the fabrication and mechanism of the THz generation for such an emitter.

Recently, an epitaxial-layer, fiber-mounted photoconductive (PC) probe coupled to a JFET source-follower amplifier was developed to measure guided picosecond electrical signals with high sensitivity.[7] We now describe a micromachined THz emitter that is produced using similar fabrication techniques as those employed for the PC probe. The device, mounted on a pair of single-mode optical fibers, has been used to launch free-space THz signals from both electric and magnetic dipoles.

The emitter was fabricated on a GaAs layer grown by molecular beam epitaxy at 240 °C and annealed *in situ* at 600 °C for 10 min. The carrier relaxation of the LT-GaAs was measured by pump-probe transient absorption to be about 2 ps. In order to isolate the 1-μm-thick LT-GaAs layer and produce the free-standing PC device, mesa etching, titanium/gold metallization patterning, and backside etching have been used.[7,8] The resulting emitter consisted of a 500/3000 Å, Ti/Au, metal-semiconductor-metal (MSM) interdigitated structure with 2 μm finger size and spacing resulting in a switch area of 30 μm by 30 μm. This MSM structure acted as the PC switch (Fig. 1). Two gold electrodes provided the bias and ground connections across the PC switch.

A pair of single-mode optical fibers were glued onto the emitter using ultraviolet-curing cement. One of the fibers was polished with a 45° bevel to allow the guided laser pulses to internally reflect off the core surface to the backside of the emitter and into the MSM photoconductive switch. The other fiber provided only mechanical stability. Silver epoxy was placed along each of the fibers and onto the elec-

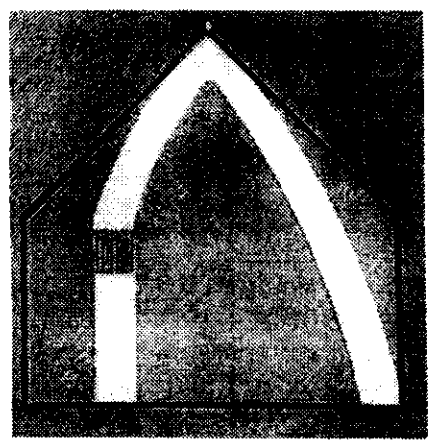

FIG. 1. Photomicrograph of the THz emitter before liftoff from the GaAs substrate. The emitter is 300 μm by 300 μm by 1 μm and consists of a Ti/Au interdigital MSM switch with finger size and spacing of 2 μm. The switch area is 30 μm by 30 μm. The left electrode was connected to a dc voltage source while the right electrode was connected to ground.

a)Electronic mail: whitaker@engin.umich.edu

0003-6951/98/72(24)/3100/3/$15.00

T-ray tomography

Daniel M. Mittleman,* Stefan Hunsche, Luc Boivin, and Martin C. Nuss

Bell Laboratories, Lucent Technologies, 101 Crawfords Corner Road, Holmdel, New Jersey 07733

Received March 24, 1997

We demonstrate tomographic T-ray imaging, using the timing information present in terahertz (THz) pulses in a reflection geometry. THz pulses are reflected from refractive-index discontinuities inside an object, and the time delays of these pulses are used to determine the positions of the discontinuities along the propagation direction. In this fashion a tomographic image can be constructed. © 1997 Optical Society of America

We recently described a new imaging modality, based on time-resolved measurements of picosecond bursts of electromagnetic radiation in the terahertz (THz) frequency range.[1] Although THz time-domain measurements have been used successfully for spectroscopy,[2,3] imaging with THz pulses has not been practical owing to the long (minutes) acquisition times for the THz waveforms. Our new T-ray imaging technique is made possible by reduction of the acquisition time of a single THz waveform from several minutes to several milliseconds, while a signal–noise ratio of >1000:1 is maintained.[4] In the original demonstration,[1] no explicit use of the time-domain nature of the THz pulses was made, and the images displayed only the transmitted power obtained by integration of the Fourier spectrum of the THz waveform with a digital signal processor. There is much more spectroscopic information available from the THz waveforms, such as timing, broadening, and other temporal distortions that result from the frequency-dependent absorption and dispersion of the object. These temporal distortions can be analyzed in real time to yield compositional information about the sample. For example, we recently demonstrated real-time recognition of gases and gas mixtures, using linear predictive coding as a waveform classification and recognition procedure.[5]

In this Letter we report on the extension of T-ray imaging to three-dimensional tomographic imaging by analyzing the temporal structure of THz waveforms returned from objects in a reflection geometry. The return time of reflected pulses directly correlates with the location of the dielectric interfaces along the propagation direction of the beam. Because the arrival time of the THz waveforms can be determined with an accuracy of a few femtoseconds, i.e., much less than the pulse duration, the positions of reflecting surfaces within the object under study can be determined with an accuracy of a few micrometers when successive reflections are well separated in time.[4] In contrast with the two-dimensional T-ray transmission images published earlier,[1] full volume images of many objects in the THz frequency range can now be obtained.

The experimental setup is described in detail in Ref. 4. The beam of THz pulses is incident upon the sample at nearly normal incidence and comes to a focus at the sample surface. The beam reflected from the object is recollimated and then captured by a pick-off mirror, which directs it to the receiver antenna. The generation, detection, and real-time processing of the THz waveforms are similar to what is described in the original transmission experiments.[1,4] For an object with multiple reflecting internal surfaces, the reflected waveform consists of a series of replicas of the input pulse of varying magnitude, polarity, and temporal distortion. We illustrate this, using the example of a 3.5-in. floppy disk, with the input and reflected THz waveforms from a single point on the floppy disk shown in Fig. 1. We obtain waveform (a) by replacing the object with a mirror, and thus the pulse that is incident upon the sample is represented. The small oscillations that follow the main pulse in this waveform are a result of residual water vapor in the beam path[6] and do not affect the measurement significantly. Curve (b), a representative reflected waveform, consists of a

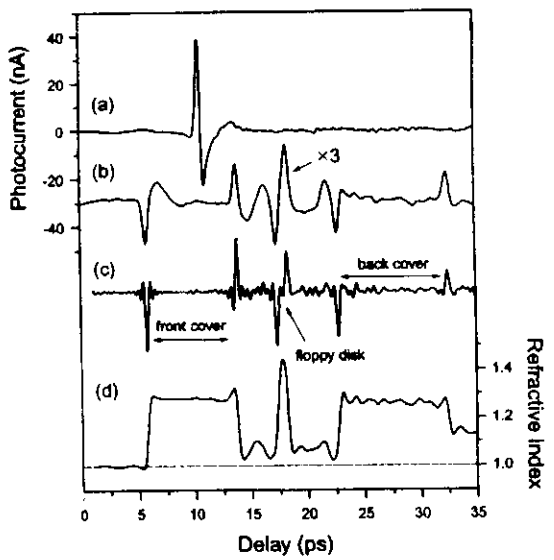

Fig. 1. (a) Input THz waveform and (b) reflected waveform from a single point on a 3.5-in. floppy disk. Each of the reflected pulses identifies a dielectric discontinuity along the propagation direction of the beam normal to the floppy disk, as labeled in the figure. Curve (c) is the reflected waveform after signal processing, as described in the text. Curve (d) is the refractive-index profile of the medium (right-hand axis), derived from curve (c) by Eqs. (3) and (4) below. Curve (b) has been scaled up by a factor of 3 relative to the left (photocurrent) axis and vertically offset for clarity.

0146-9592/97/120904-03$10.00/0

series of replicas of the input waveform. These correspond to reflections from the dielectric interfaces of the floppy disk from air to plastic, from plastic to air, or from surfaces of the magnetic recording material. The polarity and the magnitude of each reflection are given by the reflection coefficient at each interface and are related to the size and sign of the corresponding index step. The four reflections resulting from the front and back plastic covers are clearly resolved. However, the thickness of the magnetic recording material is so small that the waveforms returned from its front and back surfaces cannot be distinguished and appear as a single distorted waveform. In this example the temporal waveforms hardly change shape while traversing the object because the plastic material has little absorption and dispersion. In a more general situation, reflected waveforms may be significantly altered in shape.

In Fig. 1, (c) is the waveform of (b) after numerical Fourier deconvolution (i.e., division of the Fourier spectra of the incident and the reflected waveforms, with a low-pass filter to remove noise above ~2.5 THz). Subsequently, low-frequency background is removed by means of wavelet filtering.[7] This procedure produces a sharp spike at a time delay corresponding to the position of every reflecting interface. Thus it helps to determine more accurately the positions of the various interfaces. In contrast with (b) in Fig. 1, the front and back surfaces of the thin (~120-μm) magnetic recording material are clearly resolved in the deconvolved data (c). This is consistent with the expected resolution of $L_c/2$, where $L_c = 200$ μm is the coherence length of the THz pulse in the intervening material. In contrast, when no other reflections are nearby, we find that the position of a reflecting surface can be determined with a precision of only a few micrometers.[4]

Figure 2 shows a conventional T-ray image of a section of the floppy disk obtained in reflection [Fig. 2(a)] and a tomographic slice [Fig. 2(b)] at a fixed vertical position. We obtained the conventional T-ray image at the top by computing the total reflected power, using real-time processing of the reflected waveforms with a digital signal processor,[1,4] with the reflected power translated into a gray scale. The plastic cover with its various features, the circular recording disk, and the metallic hub in the center of the disk can be distinguished.

In Fig. 2(b) a tomographic T-ray slice of the floppy disk is shown at a particular vertical position (y = 15 mm), indicated by the dashed line in Fig. 2(a). For each horizontal (x) position a reflected waveform is acquired, processed as described above [curve (c), Fig. 1], and displayed as a function of delay in this tomographic image. The amplitude of the processed waveforms is translated into a gray scale so that each reflecting surface appears as a stripe. The positions of the various parts of the floppy disk along the propagation direction of the THz beam, such as the front and back covers, the magnetic recording disk, and the metal hub, can be observed clearly in this tomographic picture. The image also shows some artifacts of the technique that result from multiple reflections among the various interfaces, such as the features observed behind the (opaque) metal hub, as well as the apparent discontinuity in the magnetic recording medium caused by a change in the thickness of the front plastic cover at x = 12 mm.

Signal processing of the THz waveforms can be used to extract the layer structure of the medium at any given (x, y) position. The reflected waveform $B(t)$ is related to the input waveform $A(t)$ by a convolution with the impulse response $g(t)$ of the layered medium:

$$B_j = \sum_{k=0}^{M} g_{j-k} A_k . \tag{1}$$

In Eq. (1) discrete-time functions defined by digitization with a time step Δt [e.g, $B_k = B(k\Delta t)$] are used. M is the number of samples in the digitized waveforms, 1024 in these examples. The impulse response $g(t)$ is characteristic of the object and does not depend on the details of the input pulse. The coefficients g_k are determined by the reflection off the kth layer as well as by the transmission through the preceding layers, $j = 1, \ldots, k-1$, once in each direction. The distance d_j between two adjacent layers j and $j+1$ is related to the time separation of the two corresponding reflections $\Delta t = t_{j+1} - t_j$ by

$$d_j = \frac{c}{2n_j}\Delta t , \tag{2}$$

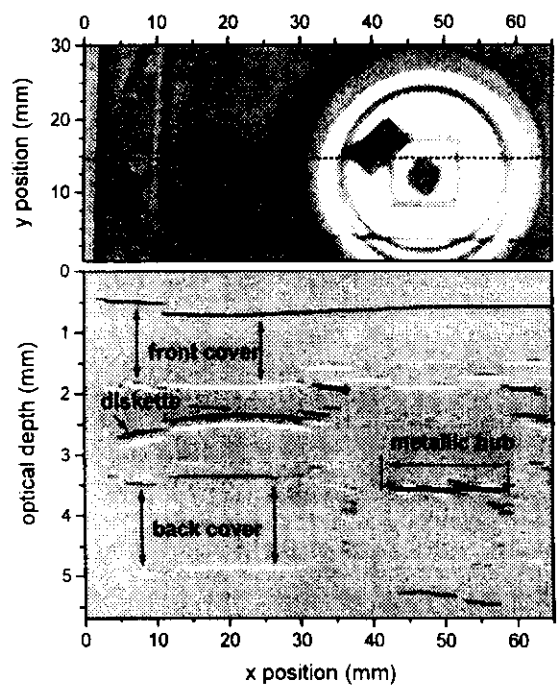

Fig. 2. (a) Conventional reflective T-ray image of the 3.5-in. floppy disk and (b) tomographic image of the same disk at a constant vertical position, indicated by the dashed line at y = 15 mm in (a). Darker stripes indicate positive refractive-index steps ($\Delta n > 0$), and lighter stripes indicate negative steps ($\Delta n < 0$). The vertical axis (optical delay) is related to the waveform delay by Eq. (2), neglecting all refractive-index variations.

A wideband coherent terahertz spectroscopy system using optical rectification and electro-optic sampling

Ajay Nahata,[a] Aniruddha S. Weling, and Tony F. Heinz
Departments of Electrical Engineering and Physics, Columbia University, New York, New York 10027

(Received 23 May 1996; accepted for publication 7 August 1996)

We present a scheme for exploiting the nonresonant second-order nonlinearities in electro-optic media to extend the bandwidth of coherent spectroscopy in the far-infrared using ultrafast laser pulses. Using optical rectification and electro-optic sampling in ⟨110⟩ ZnTe for the generation and coherent detection of freely propagating THz radiation, respectively, we have demonstrated spectral sensitivity beyond 3 THz. This was accomplished by achieving phase matching for both optical rectification and electro-optic sampling over a broad range of THz frequencies. © *1996 American Institute of Physics.* [S0003-6951(96)03542-5]

In recent years, remarkable progress has been made in the development of spectroscopic capabilities for coherent terahertz (THz) measurements.[1,2] A key ingredient in these advances is the development of broadband coherent sources and detectors of THz radiation. Much of the work reported to date relies on the use of photoconductive elements both as emitters and detectors.[1,3] While these devices are highly optimized in many respects, there are fundamental limitations in their frequency response associated with the natural time constants for carrier dynamics.[1] The ready availability of laser pulses with durations of ~10 fs[4,5] suggests the potential for extending the bandwidth of coherent spectroscopy to significantly higher frequencies. By using materials with an instantaneous optical response for both emission and detection, it may be possible to capture much of this enormous bandwidth. This suggests the use of materials with nonresonant second-order optical nonlinearities for these applications.

THz radiation may be produced in an electro-optic medium via difference-frequency mixing.[6-9] The generation process may be regarded as the beating of various Fourier components of the driving optical spectrum to produce an optically rectified baseband pulse.[10] Such a difference-frequency generation scheme is capable of producing electric fields with spectral content extending from dc[11] to the mid-infrared.[12] For detection of the THz electric field wave form, this mixing process can be reversed in an electro-optic medium. Valdmanis *et al.*[13] have shown that electro-optic sampling is a sensitive probe of localized electric fields in transmission lines and high-speed circuits. This approach has recently been extended to the coherent detection of freely propagating THz radiation.[14,15] In this letter, we describe a wideband coherent THz spectroscopy system using optical rectification for the generation of THz radiation and electro-optic sampling for the coherent detection of this radiation, both in ⟨110⟩ ZnTe. The electro-optic sampling measurement is performed in a transmission geometry. This geometry allows for the copropagation of the THz and probe beams over an extended path length while maintaining ultrashort response times. An important consideration which we address here is the use of phase matching to allow for greater interaction between the optical and THz pulses in the nonlinear medium in order to enhance the efficiency of both the generation and detection processes.

Both broadband optical rectification and electro-optic sampling have been demonstrated in thin $\chi^{(2)}$ media.[14,16] In order to enhance the sensitivity, longer interaction lengths are desirable, necessitating appropriate consideration of phase matching constraints.[10] The phase matching condition for the optical rectification process (collinear difference frequency mixing) is given by

$$\Delta k = k(\omega_{\rm opt}+\omega_{\rm THz})-k(\omega_{\rm opt})-k(\omega_{\rm THz})=0, \tag{1}$$

where $\omega_{\rm opt}$ and $\omega_{\rm THz}$ are the optical and THz frequencies, respectively, and $\omega_{\rm opt}$ and $(\omega_{\rm opt}+\omega_{\rm THz})$ lie within the spectrum of the optical pulse. An equivalent equation can be written for electro-optic sampling. If we neglect dispersion in the optical spectral range, we can express the coherence length $l_c(=\pi/\Delta k)$ as

$$l_c=\frac{\pi c}{\omega_{\rm THz}|n_{\rm opt}-n_{\rm THz}|}. \tag{2}$$

Here, c is the speed of light and $n_{\rm opt}$ and $n_{\rm THz}$ are the optical and THz refractive indexes, respectively. In inorganic nonlinear optical crystals, the difference between the optical and THz refractive indexes tends to be large, because of the contribution of low lying phonon resonances to the THz refractive index. The optical refractive indexes of ZnTe may be obtained from the equation[17]

$$n^2=4.27+3.01\lambda^2/(\lambda^2-0.142), \tag{3}$$

where λ is the optical wavelength in μm. The far-infrared (FIR) refractive indexes may be obtained from[18]

$$n^2=(289.27-6f_{\rm THz}^2)/(29.16-f_{\rm THz}^2), \tag{4}$$

where $f_{\rm THz}(=\omega_{\rm THz}/2\pi)$ is in THz. Using Eq. (3), the optical refractive index of ZnTe at 800 nm is 2.85. Figure 1 shows the coherence length as a function of FIR frequency, $f_{\rm THz}$, calculated using Eq. (2).

Birefringence has been employed to achieve long coherence lengths in optical rectification experiments.[10] However, the large refractive index difference between the optical and FIR results in a narrow phase matching bandwidth. Angle tuning in a noncollinear beam geometry has also been shown

[a]Electronic mail: an23@columbia.edu

 0003-6951/96/69(16)/2321/3/$10.00

Coherent detection of freely propagating terahertz radiation by electro-optic sampling

Ajay Nahata,[a] David H. Auston,[b] and Tony F. Heinz
Departments of Electrical Engineering and Physics, Columbia University, New York, New York 10027

Chengjiu Wu
AlliedSignal, Inc., Research and Technology, P. O. Box 1021, Morristown, New Jersey 07960

(Received 11 September 1995; accepted for publication 31 October 1995)

We report the demonstration of an electro-optic sampling technique that allows for the detection of freely propagating terahertz radiation. Coherent sampling is performed in a poled polymer device that is physically separated from the emitter. The poling electrodes in the sampling element are found to have an integrating effect on the incident terahertz field. The shot noise limited minimum detectable field in the polymer is 100 (mV/cm)/$\sqrt{\text{Hz}}$. We discuss methods by which the sensitivity may be significantly enhanced. © *1996 American Institute of Physics.* [S0003-6951(96)03502-7]

The use of ultrafast laser sources to generate and detect freely propagating pulses of coherent far-infrared radiation has stimulated significant interest in recent years. These coherent pulses have been used to examine ultrafast carrier dynamics in semiconductors[1] and to measure the far-infrared linear optical properties of a wide range of dielectric media.[2] The terahertz (THz) bandwidth pulses are typically generated by exciting radiative current transients in photoconductive media[2-4] or producing a nonlinear polarization via difference frequency mixing in nonlinear optical media.[5] To date, the only broadly applicable technique to coherently detect this radiation requires the use of synchronously gated photoconducting dipole detectors.[3] While these detectors exhibit excellent sensitivity, there is a strong speed versus sensitivity trade-off which is determined by the photoconductive response and antenna dimensions.[2]

Electro-optic sampling[6] is an attractive alternate approach for the detection of THz radiation. Significant advantages of this technique are the capability of detection that is limited primarily by the optical bandwidth and the ability to calibrate the detected electric field. These features have been exploited in extensive characterization of ultrafast electrical pulses propagating in transmission lines and circuits.[6-8] The technique has also been utilized in measurements where freely propagating THz radiation was generated and detected within the same device. Prominent examples of this include studies of Cherenkov radiation in $LiTaO_3$ (Ref. 9) and Bloch oscillations in GaAs/AlGaAs superlattices.[10]

In this letter, we demonstrate an electro-optic sampling technique that allows for the coherent detection of freely propagating submillimeter wave radiation. In this scheme, the emitter and detector are physically separated from one another by a large distance, making the system well suited for spectroscopic applications. As an electro-optic medium, we make use of a poled polymer. In contrast to traditional electro-optic media such as $LiTaO_3$,[9] polymers do not suffer from the complication of a large difference in the optical and far-infrared refractive indexes and absorption in the far infrared. Furthermore, the optical nonlinearity in poled polymers is expected to have negligible response time. In this work, electro-optic sampling is accomplished using a thin poled polymer film in a double pass geometry. The performance of this configuration, the influence of the poling electrodes, as well as possibilities for future experiments are discussed.

We fabricated the electro-optic sampling element (EOSE), shown schematically in Fig. 1, on an *R*-plane sapphire substrate. A high reflectivity dielectric coating centered at 800 nm was first evaporated onto one side of the substrate. Two coplanar 5 mm×5 mm×2000 Å thick aluminum pads separated by 50 μm, used for poling, were then photolithographically defined onto the coating. The polymer used in this study is composed of 20 mol % 2-*N*-[4-(4-nitrophenylazo) indolino] ethyl methacrylate (MA9) and methyl methacrylate (MMA), which we designate MA9:MMA. The chemical structure, synthesis, polymer properties, and linear and nonlinear optical properties are described elsewhere.[11] The polymer film in the EOSE was 10 μm thick and poled at its glass transition temperature with a field of 1.0 MV/cm.[12] A high resistivity silicon (>10 kΩ cm) hyperhemispherical lens[2] was attached to the sapphire substrate to focus the THz radiation into the electrode gap.

The experimental setup for generating and detecting THz radiation is shown in Fig. 2. A 76 MHz mode-locked Ti:sapphire laser operating at 800 nm served to generate and detect the transient submillimeter wave pulses. A collimated 2 mm

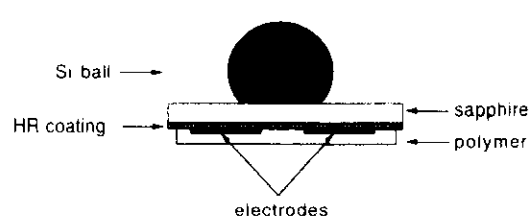

FIG. 1. Schematic drawing of the electro-optic sampling element.

[a]Electronic mail: an23@columbia.edu
[b]Current address: Office of the Provist, Rice University, Houston, TX 77005

 0003-6951/96/68(2)/150/3/$6.00

Generation of subpicosecond electrical pulses by optical rectification

Ajay Nahata* and Tony F. Heinz

Departments of Electrical Engineering and Physics, Columbia University, New York, New York 10027

Received February 3, 1998

We describe the generation of subpicosecond electrical pulses by optical rectification of ultrashort optical pulses. The electrical pulses are generated by the second-order nonlinear response of a $LiTaO_3$ crystal bonded to a coplanar transmission line. A bipolar temporal waveform with a width of 875 fs was measured after a propagation distance of 175 μm. This pulse width was limited by the response time of the photoconductive sampler. We observed both broadening and amplitude reduction in the temporal waveform owing to propagation. © 1998 Optical Society of America

OCIS codes: 320.5540, 350.5500, 160.5140.

The use of ultrashort electrical pulses is becoming increasingly important for applications ranging from high-speed electronics to wideband spectroscopy. With respect to the latter application, the analysis of pulse propagation characteristics on transmission lines offers a powerful approach for spectroscopic studies of materials.[1] In this geometry, long interaction lengths are possible, which is of particular value for probing thin films. Thus there is considerable incentive to increase the bandwidth of the generated electrical pulses. The established approach to producing electrical transients relies on the optical excitation of photoconductors by femtosecond optical pulses.[2,3] Other techniques for generating ultrashort electrical pulses include the use of exciton ionization in quantum-well structures[4] and the use of nonlinear transmission lines.[5] Although these techniques have significant utility, they exhibit a fundamental limitation in response time related to the transient dynamics of the photoexcited carriers or propagation characteristics of the device.

The use of nonlinear optical approaches seems well suited for circumventing these fundamental temporal limitations. Specifically, rectification of optical pulses is an attractive technique for generating ultrashort electrical pulses. Bass and co-workers[6] first observed optical rectification in the form of an induced dc voltage across a KDP crystal irradiated by an intense ruby laser. Generation of nanosecond electrical pulses was later demonstrated with an ADP crystal as the nonlinear medium.[7] Two additional techniques involving the absorption of the optical pump beam by impurities in polar crystals were found to be capable of generating intense picosecond electrical pulses.[8] However, the electrical pulses were limited to durations well in excess of 1 ps. Although optical rectification in nonlinear optical media has been suggested as a means of generating electrical pulses of picosecond duration on transmission lines,[2,9] there has not, to our knowledge, been any experimental demonstration of this effect.

In this Letter we describe the generation of subpicosecond electrical pulses by optical rectification, using the nonresonant second-order susceptibility of a nonlinear medium. The demonstration employs a coplanar strip-line geometry, shown schematically in Fig. 1, with a $LiTaO_3$ crystal superstrate acting as the nonlinear medium. Because of the nature of the generation process, we are able to vary the generation-to-detection distance. Detection of the electrical pulses on the transmission line is accomplished by use of a gated photoconductive switch integrated into the device.

We begin by examining the behavior of current produced on a transmission line through optical rectification. For this purpose we adapt the classic analysis of Ward.[7] For simplicity we neglect all finite response times and retardation effects in the system. We begin by considering the charge induced on the transmission line, $q(t)$, by a photogenerated dipole. The nonlinear polarization, $\mathbf{P}_{NL}$ ($= P_{NL}\hat{z}$), is given (in MKS units) by

$$P_{NL}(t) = -\frac{n^3 r_{33}}{2c} I_{opt}(t), \tag{1}$$

where n denotes the optical refractive index of the nonlinear medium; c, the speed of light in vacuum; r_{33}, the relevant electro-optic coefficient, and $I_{opt}(t)$, the intensity profile of the pump pulse. Here we have

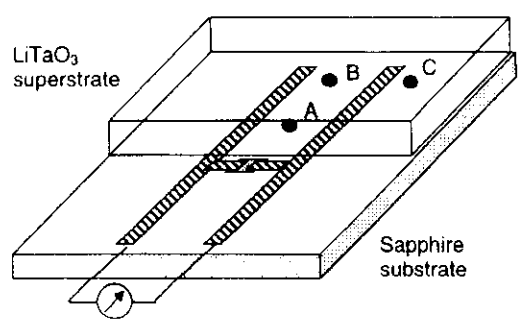

Fig. 1. Schematic drawing of the device with a coplanar strip-line transmission line and an integrated photoconductive switch. A $LiTaO_3$ crystal is bonded onto the device. Points A–C represent the positions of the pump beam used in the experiment.

0146-9592/98/110867-03$15.00/0

Generation of terahertz radiation from a poled polymer

Ajay Nahata[a] and David H. Auston[b]
Department of Electrical Engineering, Columbia University, New York, New York 10027

Chengjiu Wu and James T. Yardley
Corporate Research and Technology, AlliedSignal Inc., P.O. Box 1021, Morristown, New Jersey

(Received 10 January 1995; accepted for publication 27 June 1995)

We report the generation of terahertz radiation via optical rectification from a poled polymer using femtosecond optical pulses. We have measured the refractive index and power absorption in the terahertz frequency range. The corresponding difference frequency mixing coherence length in the poled polymer (1 mm at 1 THz) is ~20 times greater than that of $LiNbO_3$ (50 μm at 1 THz). The observed far-infrared electric field radiated from a 16 μm thick polymer sample is only 4 times smaller than that from a 1 mm thick y-cut $LiNbO_3$ crystal. We discuss conversion efficiencies for thicker polymer samples. © *1995 American Institute of Physics.*

With device speeds consistently increasing, intense broadband high frequency radiation sources are needed for the characterization of dielectric materials. Over the last decade, several different techniques involving the use of photoconductivity and optical rectification have been developed for the generation and detection of terahertz (THz) bandwidth free propagating electromagnetic radiation.[1–6] This latter process can be understood as difference frequency mixing, in which two different frequencies within the frequency spectrum of an optical pulse interact in a nonlinear medium to induce a polarization and radiate at the beat frequency. The bandwidth of the resulting radiation is limited by the bandwidth of the optical pulse and lies in the THz frequency range. Recently, a variety of nonlinear optical materials have been studied using non-phase-matched optical rectification.[7,8] Among these, the organic single crystal DAST has been shown to generate the most intense submillimeter wave radiation.[9] In general, organic media offer many attractive properties for nonlinear optical applications. A wide range of chromophores with donor- and acceptor-substituted moieties and extended π conjugation have been shown to possess large molecular hyperpolarizabilities. They can be chemically modified on a molecular scale to alter the dielectric constant, refractive index, and optical nonlinearity of the dye species. In polymeric form, these compounds offer many significant advantages over single crystals. In particular, they are readily processable, can be poled to induce noncentrosymmetry, and may possess nonlinear coefficients greater than that of lithium niobate.[10,11]

In this letter, we describe the generation of THz radiation from a model poled polymer. Using the measured THz signal, as well as refractive index and absorption measurements, we discuss the applicability of these materials for intense radiation sources. The nonlinear medium is a copolymer of 4-*N*-ethyl-*N*- (2-methacryloxyethyl)amine-4′-nitro-azobenzene (MA1) and methyl methacrylate (MMA), which we designate MA1:MMA. The samples used in this study contain 16.5 mol% MA1. The chemical structure, synthesis, polymer properties, and linear, and nonlinear optical properties are described elsewhere.[12]

We fabricated an unpoled sample for linear optical measurements and a poled sample for generation of THz radiation. Both samples were fabricated on Corning 7059 glass with a 2000 Å thick layer of indium tin oxide. We initially spun cast a 4 μm thick film of poly(acrylic) acid (PAA, Aldrich) from a solution containing 25 wt % solids in deionized water onto each substrate. The nonlinear copolymer was then cast from a solution containing 30 wt % solids in dimethyl-(ethyl)ether yielding film thicknesses between 15 and 200 μm. The sample to be poled was capped with another 4 μm thick film of PAA. This upper polymer layer was used to reduce damage to the MA1:MMA layer during the corona poling process, while the lower layer for each sample was used to produce a free-standing film, as described below. In the poled film, dipolar alignment was effected using corona poling.[13,14] The apparatus has been described elsewhere.[12] After initially heating the sample to the glass transition temperature of the MA1:MMA film (T_g=132 °C), an electric field was placed across the polymer structure using a corona voltage of −5000 V and a grid voltage of −3000 V. The indium tin oxide layer was used as the ground plane. After a 30 min poling period at T_g, the sample was cooled to room temperature in the presence of the field. The voltage was then removed, effectively freezing the dipole alignment. Since the PAA layers were highly conductive, we assumed that the poling voltage was primarily applied across the MA1:MMA layer. This effective poling voltage was confirmed using an electrostatic voltmeter. Free-standing MA1:MMA films were produced by dissolving the PAA layers of each sample in deionized water.

We used a conventional pump-probe experimental setup, shown in Fig. 1, for generating and detecting the THz radiation. In the figure, the xyz coordinate system corresponds to the laboratory frame, while the $x'y'z'$ system corresponds to the molecular coordinate frame. The external incidence angle θ is defined by a rotation in the y-z plane about the x-axis. The polar axis (z') of the uniaxial nonlinear medium is determined by the direction of the poling field. The optical pulses were provided by a cw Ar^+ laser pumped mode-locked Ti-sapphire laser (Coherent MIRA) operating at 800

[a]Electronic mail: an23@columbia.edu
[b]Current address: Office of the Provost, Rice University, Houston, TX 77005.

 0003-6951/95/67(10)/1358/3/$6.00

Comparison of terahertz waveforms measured by electro-optic and photoconductive sampling

Sang-Gyu Park,[a] M. R. Melloch, and A. M. Weiner
School of Electrical Engineering, Purdue University, 1285 EE Building, West Lafayette, Indiana 47907-1285

(Received 16 July 1998; accepted for publication 28 September 1998)

Terahertz waveforms measured by free-space electro-optic sampling and a photoconductive dipole antenna were carefully compared. We show that the difference between the waveforms could be explained quantitatively in terms of carrier lifetime and frequency dependent response of the photoconductive receiver antenna. © *1998 American Institute of Physics.* [S0003-6951(98)00748-7]

Since its invention in the 1980's, photoconductive (PC) sampling has been widely used to measure the terahertz (THz) electric field coherently generated by femtosecond lasers.[1,2] Its high signal to noise ratio has enabled many THz applications including spectroscopy,[3,4] imaging,[5] and ranging.[6] But its speed is limited by the resonant characteristic of the antenna structure and the finite lifetime of the photogenerated carriers in the detector. Recently free-space electro-optic sampling (FS-EOS) of THz radiation was demonstrated to be an alternative to PC-sampling.[7] Due to its high bandwidth and ease of implementation, it is becoming increasingly popular. Despite the wide use of PC-sampling and FS-EOS, the waveforms measured by the two methods have not been compared closely. The comparison has mainly been limited to the speed and the signal to noise ratio.[8,9] In this letter, we quantitatively compare the waveforms measured by these two methods and demonstrate a simple modeling procedure that predicts the PC-sampling waveform directly from the measured FS-EOS waveform.

FS-EOS detects the polarization change of the probe beam induced by THz electric field through the electro-optic (E-O) effect in the sensor crystal. Because the E-O effect is almost instantaneous on the THz time scale, especially in compound semiconductors, FS-EOS gives a signal directly proportional to the THz electric field. Although there are several effects which could distort measured waveforms, including group velocity mismatch (GVM) between copropagating optical probe and THz beams, phonon-polariton coupling and finite probe pulse width, waveform distortion from these effects is minimal for the pulse width, crystal thickness, and THz bandwidth used in our experiments.

On the other hand, measurements with a PC-antenna receiver generate waveforms which depend not only on the actual THz electric field $e(t)$ incident at the receiver, but also on the frequency dependent antenna response $H(\omega)$ and the carrier lifetime τ_R and momentum relaxation time τ_C. The collected charge Q as a function of delay τ of the gating pulse is given by

$$Q(\tau)=\int dt\, v(t) g(t-\tau), \tag{1}$$

where the induced bias voltage across the photoconductive gap $v(t)$ is

$$v(t)\sim\int d\omega H(\omega)E(\omega)\exp(i\omega t), \tag{2}$$

and the time dependent conductance $g(t)$ is

$$g(t)=\int^{t} dt' I(t')\{1-e^{-(t-t')/\tau_C}\}e^{-(t-t')/\tau_R}. \tag{3}$$

Here, $I(t)$ is the temporal intensity profile of the gating pulse and $E(\omega)$ is the Fourier transform of $e(t)$. The finite photocurrent rise time and the current recovery time are represented by τ_C and τ_R, respectively.[10] The response function $H(\omega)$ represents the frequency dependent ratio of voltage induced at the sampling gap to incident electric field $E(\omega)$, where $E(\omega)$ is assumed to approximate a plane wave at the receiver. $H(\omega)$ depends on the coupling of the incident wave onto the antenna as well as the impedance matching conditions between the antenna and the transmission line in which it is embedded; both of these factors may be frequency dependent. As reported in the following, for our experiments on a short dipole antenna without substrate lens, we find a flat frequency response $[H(\omega)=1]$ gives a good fit to our data; i.e., $v(t)$ is directly proportional to the incoming electric field profile. This is in marked contrast to the well-known $j\omega$ frequency dependence of a short dipole transmitting antenna. The flat frequency response can be explained as follows. Because the overall length of the dipole antenna is much shorter than the shortest wavelength of the incoming electric field, the electric field $E(\omega)$ (for any given ω) is spatially uniform across the antenna times a frequency independent constant. Therefore, the induced open circuit voltage, $V_{oc}(\omega)$, is just $E(\omega)$ multiplied by the length of the antenna.[11] The actual voltage across the gap, V_g, when there is a transmission line feed connected to the antenna, can be calculated from the following voltage divider expression $V_g=V_{oc}Z_0/(Z_0+Z_A)$, where Z_0 and Z_A are the impedances of the transmission line and antenna, respectively. The radiation impedance of our short dipole is small in the frequency region of interest between tens of GHz and 2 THz. (At very low frequency the antenna reactance becomes large and this leads to a zero dc response.) When Z_A is small compared to Z_0, V_g can be approximated by V_{oc}. Therefore, if the measurement is limited to the THz range where the wavelength

[a]Electronic mail: sanggyu@ecn.purdue.edu

THz spectroscopy and source characterization by optoelectronic interferometry

Stephen E. Ralph and D. Grischkowsky
IBM Watson Research Center, P.O. Box 218, Yorktown Heights, New York 10598

(Received 4 November 1991; accepted for publication 3 January 1992)

We demonstrate a new type of THz optoelectronic interferometer, by fully characterizing a recently developed THz source to beyond 6 THz, and by measuring the absorption coefficient of high-resistivity GaAs from 1 to 5 THz. The two source THz interferometer is driven with two 4 mW beams of 60 fs dye-laser pulses and produces interferograms with exceptional signal-to-noise ratios.

Recently, many new optoelectronic sources of freely propagating THz radiation have been demonstrated.[1-14] Common to all these sources has been the problem to properly characterize the emitted THz radiation with receivers of limited bandwidths. The broadest bandwidth receivers have used ion-implanted, silicon-on-sapphire (SOS), photoconductive switches. In general, the limiting response of photoconductive receivers will be determined by the rise-time of the photocurrent itself, if they are not constrained to lower frequencies by their THz optical properties or electrical circuitry. For an ultrafast ion-implanted SOS receiver, this limiting photoconductive rise time has been experimentally determined to be 190 fs,[15] giving an ultimate response time of 150 fs.

An alternative method of source characterization, which bypasses the problems of receiver bandwidth, is based on interferometric techniques using a power detector. This approach was first demonstrated for THz radiation sources by Greene *et al.*[16] They measured autocorrelation signals with a full width at half maximum (FWHM) of 230 fs for the THz radiation pulse from laser-created carriers accelerated by the surface field of a photoconductive semiconductor.[11] In their approach, they used a single-THz radiation source, illuminated by 10 Hz repetition rate, amplified, 100 fs pulses from a colliding-pulse, mode-locked (CPM) dye laser, together with a Martin–Puplett interferometer and a liquid-helium-cooled bolometer.

Here, we report an alternative interferometric approach, which uses unamplified, 100 MHz repetition rate, CPM dye-laser pulse excitation of a two-source interferometer. Via this approach, together with fast, scanning-delay-line averaging, we obtain orders-of-magnitude improvements in the signal-to-noise ratio of the measured interferograms. Consequently, we were able to demonstrate the applicability of the technique to spectroscopy by measuring the absorption of GaAs to 5 THz. We used the newly developed THz radiation source,[12] based on the photogeneration of carriers within trap-enhanced electric fields,[17] to produce radiation to beyond 6 THz. With this THz source, we measured a 230 fs FWHM autocorrelation signal and an average power of 30 nW for 4 mW of laser power. These results extend earlier characterizations of this source by broad-band photoconductive receivers.[12,15]

The optoelectronic THz configuration [Fig. 1(a)] is identical for both sources, and has been described earlier;[12] the coplanar transmission-line structure consists of two 10 μm-wide metal lines separated by 80 μm, fabricated on high-resistivity GaAs. Typically, 100 V are applied across the lines. Illuminating the edge of the positively biased line with focused (5 μm diam) ultrafast laser pulses produces synchronous bursts of THz electromagnetic radiation. A CPM dye laser provides the 623 nm, 60 fs excitation pulses in two beams with average powers of 4 mW at the excitation spots.

The optoelectronic interferometer is illustrated in Fig. 1(b), where the two identical THz radiation sources are depicted. It is important to notice that the interferometer is

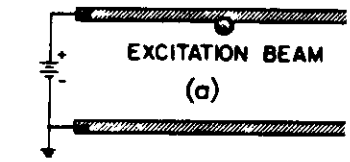

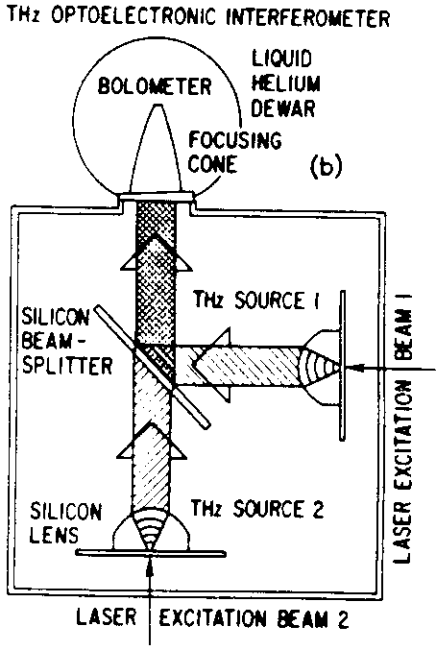

FIG. 1. (a) Configuration used to generate the freely propagating pulses of THz radiation. (b) Two-source THz optoelectronic interferometer shown in the horizontal plane.

 0003-6951/92/091070-03$03.00

High average-power THz radiation from femtosecond laser-irradiated InAs in a magnetic field and its elliptical polarization characteristics

Nobuhiko Sarukura,[a] Hideyuki Ohtake, Shinji Izumida, and Zhenlin Liu
Institute for Molecular Science (IMS), Myodaiji, Okazaki 444-8585, Japan

(Received 10 December 1997; accepted for publication 8 April 1998)

The THz-radiation power from bulk InAs irradiated with femtosecond optical pulses is significantly enhanced and reaches 650 μW in a 1.7-T magnetic field with 1.5-W excitation power. The THz-radiation power is related almost quadratically both to the magnetic field and excitation laser power. We have also found that the power of the THz-radiation from an InAs sample in a magnetic field is over one order of magnitude higher than that from GaAs. Additionally, a dramatic change of ellipticity is observed, and the spectra of the horizontal and vertical polarization components are found to differ. © *1998 American Institute of Physics*. [S0021-8979(98)09313-X]

Various THz-radiation sources have been intensively studied including photoconductive switches irradiated with ultrashort optical pulses,[1–5] two different color cw lasers,[6] or parametric oscillators.[7] The average power of optical short-pulse excited THz-radiation source was at most mW level, mostly limited by the electric breakdown of the photoconductive antennas.[4] For applications to sensing or imaging[8] and time-resolved spectroscopy in the far-infrared region,[9] an intense, compact, and simple light source is required. Zhang *et al.* reported quadratic dependence of the laser induced THz-radiation on the magnetic field.[10] There was also a report of Landau-level contribution.[11] In this communication, we report the significant enhancement of THz-radiation power from semiconductors irradiated with femtosecond optical pulses. The power reaches 650 μW in a 1.7-T magnetic field with 1.5-W excitation power. This is the highest average power ever achieved in THz radiation at around a 100-MHz repetition rate. A 200-μW average power was obtained even using a compact 1-T permanent magnet. Moreover, we found an interesting change of ellipticity of the magnetic field.

The experimental setup for the THz-radiation emitter in a magnetic field is shown in Fig. 1. A mode-locked Ti:sapphire laser delivered 70-fs pulses at 800 nm with an 80-MHz repetition rate using 1.5-W average power for the excitation. The sample was nondoped bulk InAs with a (100) surface. The conduction type of nondoped bulk InAs was slightly n, and the carrier density of this InAs was 3.0×10^{16} cm^{-3}. The InAs sample itself is highly reflective, unlike transparent GaAs. The reflectivity of the THz radiation was measured to be approximately 70% for a 45 degree incidence angle. Therefore, the THz radiation was totally generated in the reflection direction. This highly reflective nature of InAs is preferable for the THz-radiation emitter in two points. First, it eliminates the rear surface reflection of the radiation that normally produces interferometric structures in the spectrum. Second, it enhances THz radiation due to the reflection from the irradiated surface itself. A liquid-helium-cooled InSb bolometer with sub-nW sensitivity (QMC Model QFI/2BI) was provided for detection. The advantage of the bolometer for this measurement is the easiness of the collection of the beam and the lack of timing or optical delay control. The InAs sample was placed 45° to the magnetic field, and the excitation laser was parallel to the magnetic field. The excitation laser irradiated the sample with a 2-mm diameter spot. This sufficiently large excitation area is advantageous for reducing the diffraction effect and decreases the possibility of damaging the emitter even for such high average-power excitation. In this geometry, the THz radiation was detected even without the magnetic field, similar to GaAs in Ref. 12. In this case, the mechanism of the THz radiation was attributed to the carrier motion in the surface depletion electric field.[13,14] The THz-radiation power dependence on the excitation power was measured in a 1.7-T magnetic field as shown in Fig. 2. The radiation power exhibits almost quadratic dependence on the excitation power, and saturation of the THz-radiation power was observed when excitation power exceeded 500 mW. For cw Ti:sapphire laser excitation without mode locking at the same wavelength, the same

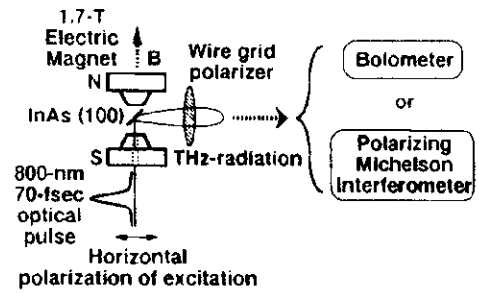

FIG. 1. The experimental setup for THz-radiation emitter in a magnetic field. A mode-locked Ti:sapphire laser delivered 70-fs pulses at 800 nm for excitation. The sample was nondoped bulk InAs with a (100) surface. A liquid-helium-cooled InSb bolometer with calibrated sensitivity was provided for detection. The InAs sample was placed at 45° to the magnetic field, and the excitation laser was parallel to the magnetic field. The maximum field of the electric magnet was 1.7 T, and the magnetic field can also be applied in the opposite direction. For the polarization-resolved spectral measurement, a wire-grid polarizer was inserted into the optical path.

[a]Electronic mail: sarukura@ims.ac.jp

Jpn. J. Appl. Phys. Vol. 37 (1998) pp. L 125–L 127
Part 2, No. 2A, 1 February 1998

THz-radiation Generation from an Intracavity Saturable Bragg Reflector in a Magnetic Field

Nobuhiko SARUKURA, Hideyuki OHTAKE, Zhenlin LIU*, Taro ITATANI[1], Takeyoshi SUGAYA[1], Tadashi NAKAGAWA[1] and Yoshinobu SUGIYAMA[1]

Institute for Molecular Science (IMS), Myodaiji, Okazaki 444, Japan
[1]*Electrotechnical Laboratory (ETL), Umezono 1-1-4, Tsukuba 305, Japan*

(Received October 2, 1997; accepted for publication December 2, 1997)

We have demonstrated a new method to generate intense THz-radiation, up to a sub-microwatt level from a saturable Bragg reflector in a magnetic field. The saturable Bragg reflector is substituted in place of the end mirror in a femtosecond mode-locked Ti:sapphire laser pumped by an all-solid-state green laser.

KEYWORDS: THz-radiation, intracavity, saturable Bragg reflector, magnetic field

The THz radiation emitted from various devices has been studied intensively[1–5] for the time-resolved spectroscopy in the THz-frequency region or various imaging applications.[6] An intense, compact, simple light source is required for all of these applications. There was a breakthrough in mode-locking techniques for solid-state lasers some years ago.[7,8] Among these techniques, the use of semiconductor saturable absorbers is attractive for mode locking because they are inexpensive and compact, and can be designed to operate over a wide spectral range.[9,10] A saturable Bragg reflector (SBR), developed by Tsuda *et al.*,[10] is a nonlinear mirror utilizing a thin-film semiconductor. We previously reported on direct THz-radiation generation from a mode-locked Ti:sapphire laser with an intracavity SBR.[11] THz-radiation from GaAs was reported to have a quadratic dependence on the magnetic field.[12] We also discovered a significant enhancement of THz-radiation from InAs with magnetic field.[13] In this paper, by combining these two ideas together, we describe a further enhancement in THz-radiation generation from an SBR in a mode-locked Ti:sapphire laser on applying a magnetic field.

An SBR should provide other functions besides that of a saturable absorber for mode locking, as demonstrated in our previous paper.[11] The single quantum well is known to emit THz-radiation,[3] and the quantum well in the SBR is located in the field-enhanced position in the Bragg reflector structure. Therefore, the SBR structure has an advantage over the simple quantum well structure for the generation of THz-radiation. If the SBR was introduced into a mode-locked laser cavity, a higher optical peak power inside the cavity will yield higher THz-radiation power. Our SBR was the same sample that we previously used for the 1-GHz mode locking of a Ti:sapphire laser[14] and the intracavity THz-radiation generation.[11]

The mode-locked Ti:sapphire laser containing the SBR, described above as an intracavity THz emitter, is shown in Fig. 1. The SBR is placed in the laser cavity instead of the end mirror, and another high reflection mirror for folding the cavity was also installed for the fine adjustment. A 1-T compact ($10\times10\times20\,cm^3$) permanent magnet placed close to the SBR provides the field parallel to the surface and the horizontal plane. Except for the SBR used as a THz-radiation emitter, the remaining configuration of the laser cavity is essentially the same as in a mode-locked Ti:sapphire laser with a saturable absorber.[8] The saturable absorber dye for self-start mode-locking was 1,1′,3,3.3′,3′-hexamethylindo-tricarbocyanine iodide (HITCI) in ethylene glycol. The Ti:sapphire laser cavity consists of a six-mirror cavity with an additional focus for a dye jet, a 1% output coupler for monitoring femtosecond pulse formation, and a pair of high-dispersion SF6 Brewster prisms with 26 cm separation. A continuous-wave (cw) all-solid-state green laser (spectra-physics millennia X) was operated at 10 W for pumping the mode-locked laser. The autocorrelation trace and the spectrum were monitored with a rapid-scanning autocorrelator and an optical spectrum analyzer. 130 fs pulses, assuming a sech^2 pulse shape as shown in Fig. 2, were obtained with a 6.0 nm spectral width at 800 nm, yielding a nearly transform-limited time and bandwidth product of 0.36. The average and peak output powers inside the cavity were 8 W and 610 kW (103 MHz repetition rate), respectively. The peak power of the optical pulse irradiating the SBR exceeded 25 MW/cm^2, assuming a 1 mm beam diameter. The THz-radiation was emitted in the transmitted direction. Without the magnetic field, no radiation was detected in this geometrical configuration or for the (100) surface of the SBR. The spectrum of the THz-radiation which peaked around 0.8 THz was obtained by Fourier transformation of the autocorrelation of the radiation from a polarizing Michelson interferometer (Graseby Specac) as shown in Fig. 3. The interferometer was evacuated to avoid the possible absorption of water vapor in the air. With the wire-grid polarizer, the THz-radiation was confirmed to be

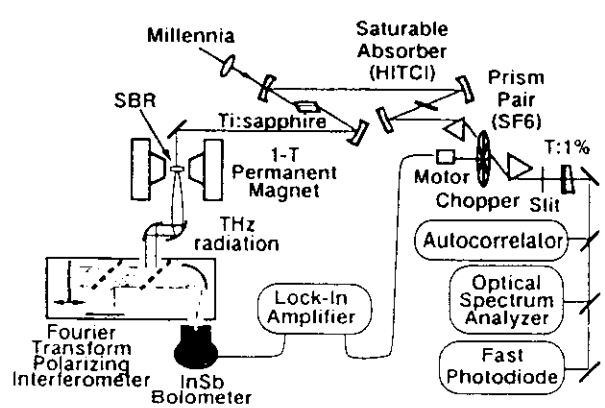

Fig. 1. The experimental setup of a mode-locked laser with an intracavity SBR in a magnetic field as a THz-radiation emitter.

*E-mail address: zliu@ims.ac.jp

Real-time electron cyclotron oscillations observed by terahertz techniques in semiconductor heterostructures

D. Some and A. V. Nurmikko
Division of Engineering and Department of Physics, Brown University, Providence, Rhode Island 02912

(Received 8 March 1994; accepted for publication 2 November 1994)

We demonstrate the application of optoelectronically generated terahertz electromagnetic transients to real-time detection of coherent oscillations by free electrons in modulation doped semiconductor heterostructures, due to the cyclotron resonance. The damping of these oscillations gives a direct measure of the electron dephasing which can be compared with scattering rates obtained from dc transport measurements. © *1994 American Institute of Physics.*

Among the limited repertoire of techniques available to characterize the high-frequency response of mobile electrons in a semiconductor, far-infrared spectroscopy of the cyclotron resonance (CR) has been used to elucidate electronic interactions with the host system and its excitations. The CR lineshape may be analyzed to determine quantum scattering and quasiparticle lifetimes,[1,2] including their dependence on Landau level filling factor in the integer and fractional quantum Hall regime in high mobility GaAs heterostructures.[3,4] Additionally, it is possible to induce coupling of the CR to other available modes of excitation, such as intersubband transitions,[5] resonant longitudinal optical (LO) phonons,[6] polarons,[7] and magneto-plasmons.[8] The conventional approach for performing CR spectroscopy is based on Fourier-transform infrared (FTIR) spectroscopy utilizing a broadband infrared source, or far-infrared molecular gas lasers, which may be cw or pulsed typically on a (sub-) microsecond time scale.

In this letter, we report the application of optoelectronically generated and detected, freely propagating, coherent terahertz (THz) electromagnetic (EM) transients to the study of CR for free electrons in high mobility GaAs quantum wells, in real time with subpicosecond resolution. An initial report showed the feasibility of detecting two-dimensional (2D) electrons in quantum wells (QW) by this technique.[9] We have now been able to fully resolve the electric field oscillations due to coherent cyclotron motion of electrons in our samples, the duration of which may be considerably longer than the exciting THz pulse. The decay of these oscillations, while quite different from, e.g., the free-induction decay of excitons, yields a measure of the electron phase relaxation times which we briefly compare with those obtained from transport experiments. Notably, we are also able to measure the quasiparticle relaxation time at zero magnetic field as a function of the Fermi energy (E_F), which is quite difficult by conventional techniques.

We focus here chiefly on one sample containing a GaAs/(Al,Ga)As single heterojunction (SHJ), modulation doped with $n_s = 6.7\times10^{11}$ cm^{-2} electrons with a mobility $\mu = 2.7\times10^5$ cm^2/V s at $T = 4$ K. A semitransparent NiCr gate was deposited on the sample surfaces and indium dots were alloyed into the epitaxial layers to contact the electron gas ohmically. Application of a reverse bias depletes the electron gas, lowering the Fermi energy (E_F); a full bias of 5 V will completely depopulate the quantum well. As described below, varying the gate bias is useful in the differential technique employed by us. Our experimental apparatus consisted of a THz generation and detection system similar to that described in recent literature[10] employing a Ti:sapphire mode-locked laser and photoconductive coplanar stripline antennas based on GaAs (emitter) and silicon-on-sapphire (receiver). The setup incorporated a 5 T superconducting magnet housing the samples, immersed usually in a superfluid helium bath at $T = 2$ K.[9] The THz radiation is focused onto the sample and recollimated with polyethylene lenses. Free-standing wire grid polarizers ensure that the incident and detected electric fields have the same polarization direction.

The impulse of broadband THz radiation, $E_0(t)$, is incident on the electron gas in the sample (top trace in Fig. 1), which then reradiates an induced field $E_{ind}(t)$. The resulting total field $E_{tot}(t) = E_0(t) + E_{ind}(t)$ is time resolved by the detection system. By alternating the reverse bias on the NiCr gate between values of 0 and 5 V at a rate of 1 kHz, we modulate the electron population between n_s and zero. This modulation is used in conjunction with a lock-in amplifier to detect a differential THz signal which is proportional only to that component of the total transmitted electric field which originates from the two-dimensional electron gas (2DEG) [i.e., $E_{ind}(t)$].

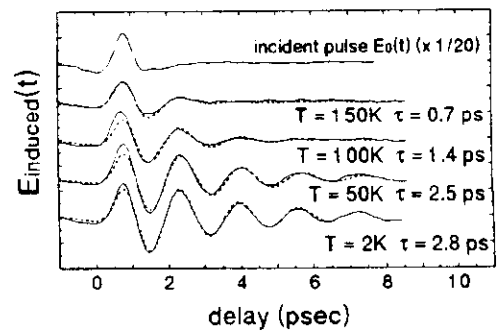

FIG. 1. Temperature dependence of real-time electron cyclotron oscillations in a 2D electron gas at $B = 3.1$ T from $T = 2$ to 150 K. The incident THz pulse is shown for comparison. The dashed lines represent the fitted convolutions of the incident pulse with a dynamic conductivity $e^{-i\omega_c t}\cos(\omega_c t)$, resulting in the estimated dephasing times given. The wave forms are offset vertically for clarity.

 0003-6951/94/65(26)/3377/3/$6.00

Far infrared spectroscopy with subpicosecond electrical pulses on transmission lines

R. Sprik,[a] I. N. Duling, III, C.-C. Chi, and D. Grischkowsky
IBM T. J. Watson Research Center, P. O. Box 218, Yorktown Heights, New York 10598

(Received 30 April 1987; accepted for publication 18 June 1987)

Optically generated and detected electrical pulses on transmission lines in the subpicosecond range have frequencies extending up to 1 THz, thereby covering the far infrared region of the spectrum from 0 to 30 cm^{-1}. We have studied the propagation of these short pulses through a section of the transmission line covered with erbium iron garnet which shows distinct absorption lines in the far infrared at low temperatures (2–30 K). The absorption and dispersion of the garnet modify the shape of the pulse, and the absorption spectrum is obtained by Fourier transforming the propagated pulse shape.

Recently optoelectronic techniques have been used to generate and detect subpicosecond electrical pulses on coplanar transmission lines.[1,2] The frequency bandwidth of these short electrical pulses ranges up to 1 THz and covers an interesting part of the far infrared energy spectrum (0–30 cm^{-1}, $\lambda > 330\,\mu m$) in which can be found the gap frequencies of superconductors, magnetic excitations, and the far infrared modes in lattices and molecules. This situation, plus the fact that the earlier observations showed that the subpicosecond pulses broadened to only 2.6 ps after propagating 8 mm on the transmission line, encouraged us to consider spectroscopic applications of these guided wave electrical pulses.

The recent use of superconducting transmission lines showed that by observing pulse reshaping as a function of propagation distance, the frequency-dependent absorption and dispersion of the line could be obtained. The absorption sharply increased at the frequency associated with the breaking of the Cooper pairs in the superconducting niobium metal lines.[2] In this letter we demonstrate that this time domain optoelectronic technique can be more generally used for far infrared spectroscopy by covering a section of the transmission line with an absorbing material and studying the consequent reshaping of the transmitted pulse. We demonstrate the feasibility of this spectroscopic method by measuring the magnetic resonances in erbium iron garnet (ErIG) and studying the temperature dependence of the frequencies between 2 and 30 K. The particular choice of ErIG was guided by the fact that this system is known to have sharp absorption resonances in the currently accessible spectral range of the technique and was readily available to us.

The optoelectronic generation of short electrical pulses is based on the temporary shorting of the charged transmission line by carriers excited in the photoconductive material (ion-implanted Si on sapphire) underneath the lines with a short laser pulse. The minimum electrical pulse width, which is measured by the same electro-optic technique, appears to be limited by the lifetime of the photoexcited carriers in the photoconductive material.[3] Figure 1 shows the experimental arrangement, the coplanar transmission line, and the focused spots of the laser, where the electrical pulse is generated by focusing the exciting beam between the lines ("sliding contact") and detected after propagation by the sampling beam focused on the gap. By scanning the time delay between the exciting beam and the sampling beam one measures the pulse shape. Both beams are derived from the same laser, a prism-compensated, colliding-pulse, mode-locked, dye laser producing 70-fs pulses at a repetition rate of 100 MHz.[4] The exciting beam is chopped at 2 kHz and the resulting photocurrent signal is detected as a function of time delay with a lock-in amplifier, whose output is stored in a computer for further processing.

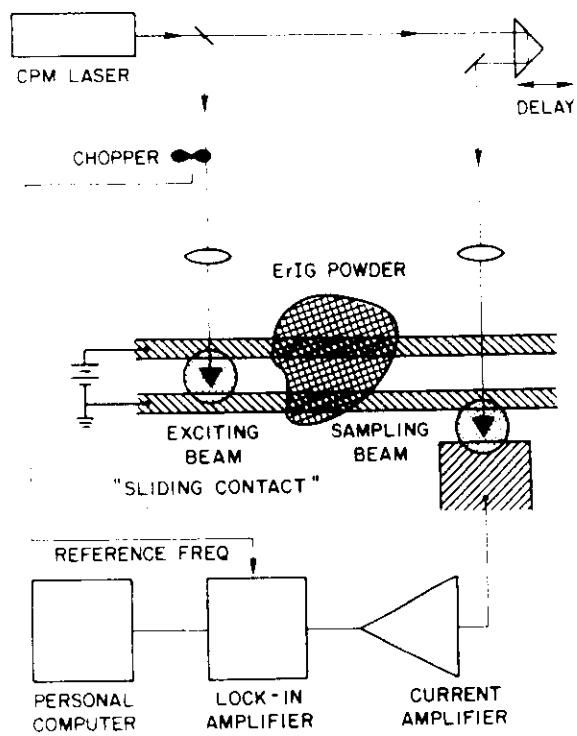

FIG. 1. Schematic diagram of the experimental arrangement together with the coplanar transmission line configuration.

[a] Permanent address: Natuurkundig Laboratorium, Universiteit van Amsterdam, Valckenierstraat 65, 1018 XE Amsterdam, The Netherlands.

 0003-6951/87/330548-03$01.00

Measurement and analysis of terahertz radiation from bulk semiconductors

M. Li, F. G. Sun, G. A. Wagoner, M. Alexander,[a] and X.-C. Zhang[b]
Physics Department, Rensselaer Polytechnic Institute, Troy, New York 12180-3590

(Received 30 January 1995; accepted for publication 18 April 1995)

We report the recent measurement and analysis of the transmitted and pseudoreflected optically induced terahertz (THz) beams emitted from a semiconductor wafer under femtosecond laser illumination, where the static electric field is either parallel or perpendicular to the surface. In general, the amplitude of the transmitted THz field is different from that of pseudoreflected THz field, except at the Brewster angle. © *1995 American Institute of Physics.*

When illuminated by femtosecond laser pulses, where the photon energy lies above the optical absorption band edge, a semiconductor wafer will emit pulsed submillimeter-wave (THz) radiation, via ultrafast photocarrier transport, in both the transmitted and pseudoreflected directions.[1,2] The Maxwell equations can be used to provide a semiclassical theoretical description of the electrodynamics underlying the radiation phenomena.[1,3] Pulsed THz radiation can be used to coherently probe the ultrafast electronic properties of semiconductors.[4,5] However, due to the technical difficulties associated with THz beam measurements, the potential of this technique has not been fully exploited. For example, a detailed comparison of the amplitude and polarity of the transmitted and pseudoreflected THz beams has not yet been reported.

In this letter, we present the results of our recent measurement and analysis of the amplitude and polarity of both the transmitted and pseudoreflected THz beams, generated through the optical injection of carriers into the static electric field associated with a semiconductor surface. We find that the ratio of the peak transmitted THz signal relative to the peak pseudoreflected THz signal is simply given by the following: $1 \pm r$, depending on the direction of the field relative to the surface, where r is angular dependent Fresnel reflection coefficient of the THz field at the semiconductor/air interface. Therefore, the amplitude of the transmitted THz field is different from that of the pseudoreflected THz field, except at the Brewster angle. Based on this straightforward analysis, we are able to explain the anomalous THz emission from metal/semiconductor interfaces.

In an unbiased wafer, the surface depletion field is directed normally, where in a wafer under transverse bias, the surface field is tangential to the surface. In these two cases, the carriers injected into the field region will accelerate along the field direction, thereby emitting a THz pulse. As a result of the particular field alignment, both the polarity and amplitude of the emitted radiation will differ between the biased and unbiased cases. Figure 1(a) schematically illustrates the polarization and propagation of optically induced THz beams from an unbiased semiconductor surface, where photocarrier transport is perpendicular the surface. A generalized Snell's law relates the three angles, with: $\sin(\theta_{op}) = \sin(\theta_{el}^{out}) = n_{el} \sin(\theta_{el}^{in})$. Within the wafer, the optically induced dipole layer near the surface generates radiation in the forward direction along θ_{el}^{in}, and in the backward direction along $(\pi - \theta_{el}^{in})$. Ignoring the surface field contribution, Fig. 1(b) shows the THz beams from a planar biased wafer. In each case, the radiation in either direction satisfies the far-field dipole radiation equation:

$$\vec{E} = \frac{1}{4\pi\epsilon c^2 r^3} \mathbf{r} \times \left(\mathbf{r} \times \frac{\partial \mathbf{j}}{\partial t} \right), \tag{1}$$

where $\mathbf{j}$ is the retarded photocurrent density at surface and it follows the surface static field direction. In the unbiased case, shown in Fig. 1(a), because photocarrier transport is along the surface normal, the forward- and backward-radiated THz pulses have opposite polarities. When photo-

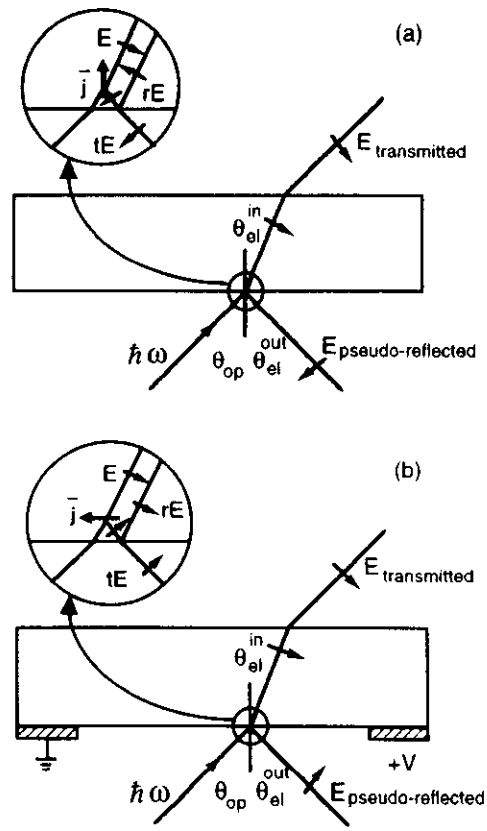

FIG. 1. The polarization of forward-radiated, backward-radiated, reflected backward-radiated, transmitted and pseudoreflected THz radiation with photocarrier transport (a) perpendicular and (b) parallel to the surface.

[a]Rome Laboratory, Hanscom Air Force Base, MA 01731
[b]Electronic mail: zhangx2@rpi.edu

 0003-6951/95/67(1)/25/3/$6.00

Ultrafast electro-optic field sensors

Q. Wu and X.-C. Zhang[a)]
Physics Department, Rensselaer Polytechnic Institute, Troy, New York 12180-3590

(Received 21 November 1995; accepted for publication 15 January 1996)

We report our recent study of ultrafast electro-optic field sensors for the coherent measurement of freely propagating subpicosecond pulsed electromagnetic waves (THz beams). The sensitivity and bandwidth of these electro-optic sensors are comparable with the conventional ultrafast photoconductive dipole antennas. The simplicity of the detection geometry and capability of optical parallel processing make these sensors suitable for real-time 2D subpicosecond far-infrared imaging. © *1996 American Institute of Physics.* [S0003-6951(96)01312-3]

Over the last ten years, generation, propagation, and detection of ultrafast electromagnetic pulses have been the "hot topics" in many research groups in the ultrafast optics and electronics communities.[1] Their pioneering work has made significant contributions to the scientific understanding of ultrafast phenomena and produced a wide variety of applications.[2-14] In particular, the subfield of far-infrared time-domain spectroscopy has seen the development of several new techniques for the generation, propagation, and ultrafast detection of terahertz bandwidth electromagnetic radiation.[15,16] These versatile techniques are essential for characterizing ultrahigh speed electronic materials, devices, and systems, as well as for exploring and understanding fundamental physics in the far-infrared spectral range.

To date, the measurement of terahertz pulse is primarily being carried out using ultrafast photoconductive antennas and far-infrared interferometric techniques. In this letter, we present our recent work on ultrafast electro-optic field sensors for the coherent measurement of freely propagating THz beams. As an extension of our previous work on electro-optic field sensors,[17] the sensitivity of these ultra-wide-band field sensors is improved to be comparable with the ultrafast photoconductive dipole antennas currently used. We also present the results of two detection geometries and the use of several different electro-optic crystals.

The generation and detection of terahertz beam via photocarrier transport and Pockels effect in this pump/probe system is similar to one we used previously,[17] except that the velocity of the optical beam reflected from the right facet of the $LiTaO_3$ crystal in the projection of the THz beam propagation direction matches that of the traveling THz field. Figure 1 schematically illustrates the side view of the sensor head geometry for a counterpropagating detection. When a THz beam illuminates the electro-optic $LiTaO_3$ crystal with its polarization parallel to the crystal c axis, the index of refraction is modulated via the Pockels effect. A fs optical pulse with its polarization 45° to the crystal c axis probes the field-induced change in the index of refraction. To convert the field-induced phase retardation into an intensity modulation, the probe pulse is analyzed by a compensator and a polarizer, then detected by a photodetector.[17] During this experiment, we used a mode-locked Ti:sapphire laser (Spectra-Physics, Tsunami) which provides 130 fs optical pulses at 800 nm with an 82 MHz repetition rate. The average power of the optical pump beam and probe beam is about 1 W and 100 μW, respectively. An unbiased GaAs wafer attached on a metal-coated glass (ITO), triggered by femtosecond pump pulses, radiates the THz pulses.[18] In the $LiTaO_3$ crystal, the angle between the THz beam and interacting optical beam reflected from the window facet is about 71°, so that the velocity of the optical beam projected in the THz beam propagating direction matches that of the traveling THz field. The interaction length of optical probe beam and THz beam in the crystal is about 200 μm. Figure 2 displays a measured transient waveform with the unbiased GaAs emitter 15 cm away from the $LiTaO_3$ sensor. This nearly velocity-matched condition reduces the walkoff effect, and yields a signal-to-noise ratio (SNR) better than 100 from a single scan with a 0.3 s time constant.

The detection configuration in Fig. 1 is similar to that used in the conventional geometry of photoconductive dipole antenna based systems and is widely used in time-resolved far-infrared spectroscopy. However, since the THz beam and optical beam are incident from opposite directions, if an array of optical beams is used instead of one single beam, as in the case of an imaging application, this configuration would not be convenient. To overcome this limitation, we have tested an experimental setup where the optical and THz beams propagate collinearly in the electro-optic crystal. A similar system has been used recently for the measurement of high power THz beams.[19] Figure 3 illustrates this collinear configuration. A 1 in. pellicle beamsplitter which is transparent for the THz beam directs the optical probe beam along the THz beam. A lens (f=1 m) is placed in optical probe beam path, but no lens is used for the pump beam and THz beam. The diameter of the unfocused THz beam and the

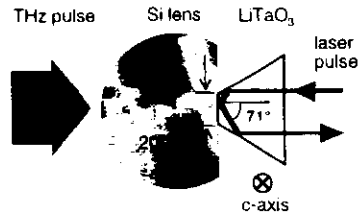

FIG. 1. Electro-optic field sensor with counterpropagating terahertz and optical beams. The electro-optic crystal is attached to the silicon lens.

a)Electronic mail: zhangx2rpi.edu

 0003-6951/96/68(12)/1604/3/$10.00

Electro-optic detection of THz radiation in $LiTaO_3$, $LiNbO_3$ and ZnTe

C. Winnewisser,[a] P. Uhd Jepsen, M. Schall, V. Schyja, and H. Helm
Fakultät für Physik, Albert-Ludwigs-Universität, D-79104 Freiburg, Germany

(Received 6 January 1997; accepted for publication 10 April 1997)

Freely propagating THz pulses are detected in electro-optic (eo) crystals by monitoring the phase retardation (PR) of an infrared femtosecond probe pulse. This technique permits the determination of the temporal shape of the THz pulse in the subpicosecond time domain. We present measurements in $LiTaO_3$, $LiNbO_3$, and ZnTe and compare their signal performance as eo crystals with theoretical calculations for the PR signal. ZnTe shows the best performance for eo detection.
 [S0003-6951(97)01523-4]

A variety of techniques for the detection of freely propagating electro-magnetic pulses in the subpicosecond time domain, so-called terahertz (THz) pulses, have been developed. These include the method of optically gated photoconductive antennas,[1] interferometric techniques with helium cooled bolometers,[2] pyroelectric detectors,[3] and electro-optic (eo) detection.[4–7]

The motivation for eo detection of THz pulses is based on the advantage of a nearly flat frequency response (low dispersion) for certain eo-sensor crystals in the far-infrared region.[8,9] Furthermore the eo detection promises the possibility of spatially resolved THz imaging without the need to spatially scan the object. This technique was proposed recently[5,6] and as a first step Wu *et al.* succeeded in detecting the spatial profile of a THz beam.[7]

Pioneering experiments on eo sampling inside $LiTaO_3$ and $LiNbO_3$ crystals have been carried out by Auston *et al.* and Valdmanis *et al.*[10,11] Work concerning eo detection of freely propagating THz pulses has been reported only recently.[4,5,12] Our previous work[6,12] has been concerned with eo detection using $LiTaO_3$ as a sensor eo crystal and the derivation of a formula for the phase retardation (PR) induced in a copropagating probe pulse. In the present letter we have extended our earlier studies to $LiNbO_3$ and ZnTe as eo-sampling crystals. For experimental details the reader is referred to Ref. 6.

The eo detection of the THz pulses is based on the linear eo effect (Pockels effect). The electric THz field strength modifies the refractive index ellipsoid of the eo crystal. Thus the index of refraction n_i becomes $n_i = n_i(E_{\mathrm{THz}})$, where i represents one of the principal axes x,y,z. If the THz beam propagates along the z direction different phase shifts, ϕ_x and ϕ_y, result for the electric field components of the electric field strength E_x and E_y of an optical probe beam, which also propagates along the z direction. The differential PR experienced by the probe beam due to the THz field over a distance dz is denoted by $\delta\phi = \phi_y - \phi_x$.

Of the three crystals studied here $LiTaO_3$ and $LiNbO_3$ are uniaxial crystals. We also investigated ZnTe ⟨110⟩ which is an isotropic crystal with zinc blende structure.

In Figure 1 the different orientations of the eo crystals relative to the E_{THz} polarisation are illustrated. The actual PR due to the THz field depends on the crystal orientation:

(i) b-cut case: The differential PR is given by[13]:

$$\delta\phi_{\mathrm{THz}}(T) = \frac{1}{2}\frac{\omega}{c}(n_o^3 r_{13} - n_e^3 r_{33}) E_{\mathrm{THz}}(T)\cdot dz = C_b E_{\mathrm{THz}}(T)\cdot dz, \quad (1)$$

where T is the relative time delay betweeen the THz pulse and the probe pulse, r_{13} and r_{33} are components of the electro-optic tensor, C_b is a constant appropriate for the b-cut crystal orientation, and ω is the optical probe beam frequency. There is an additional, static PR term due to the natural birefringence of the b-cut crystal of

$$\delta\phi_{nat} = \frac{\omega}{c}(n_e - n_o)dz, \quad (2)$$

which gives a background signal, which cannot be cancelled by orientation of the crossed polarizers.

(ii) c-cut case: The differential PR may be written as:

$$\delta\phi_{\mathrm{THz}}(T) = \frac{\omega}{c} n_o^3 r_{22} E_{\mathrm{THz}}(T)\cdot dz = C_c E_{\mathrm{THz}}(T)\cdot dz. \quad (3)$$

In the case of a c-cut crystal the probe beam does not suffer a static PR, but has a smaller C-factor and therefore a smaller overall PR magnitude $\delta\phi_{\mathrm{THz}}$.

(iii) ZnTe ⟨110⟩ cut: In this case no intrinsic PR occurs in the crystal and the differential PR due to the THz field strength may be written as

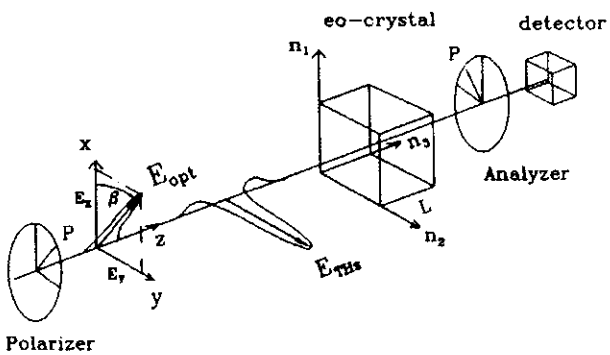

FIG. 1. eo detection setup. The optical probe pulse and the THz pulse propagate along the z axis. The optical probe beam is linearly polarized at $\beta = 45°$ and the THz field strength E_{THz} is parallel to the y axis. For b-cut crystals the following conditions hold: $n_o = n_1 = n_3$ and $n_e = n_2$. For a c-cut crystal: $n_o = n_1 = n_2$ and $n_e = n_3$.

[a]Electronic mail: winnewis@frhe20.physik.uni-freiburg.de

 0003-6951/97/70(23)/3069/3/$10.00

Two-dimensional electro-optic imaging of THz beams

Q. Wu, T. D. Hewitt, and X.-C. Zhang[a)]
Physics Department, Rensselaer Polytechnic Institute, Troy, New York 12180-3590

(Received 1 May 1996; accepted for publication 11 June 1996)

We report on a novel electro-optic sampling system for real-time terahertz (THz) imaging applications. By illuminating a 6×8 mm^2 ZnTe crystal with a 300 μW optical sampling beam and detecting the beam with a digital CCD camera, we achieved time-resolved images of pulsed far-infrared radiation emitted from an unbiased GaAs wafer. At the focal point of the peak far-infrared field, the THz beam diameter is approximately 0.75 mm (full width at half-maximum). The temporal and spatial resolutions of this imaging system are mainly limited by the laser pulse duration and the diffraction limit of the THz beam, respectively. © *1996 American Institute of Physics.* [S0003-6951(96)03834-X]

The use of terahertz (THz) beams for imaging applications was first demonstrate by Hu and Nuss.[1] Far-infrared images (t-ray imaging) of tree leaves, bacon, and semiconductor integrated chips were demonstrated as examples of a variety of applications. Because their imaging system used a single photoconductive dipole antenna as the detector, the samples to be imaged were scanned in two dimensions, relative to the fixed beam, during the measurement. As a result, the acquisition time of an image was typically on the order of minutes, depending on the total number of pixels and the lowest THz frequency components of interest.[2] Although it is highly desirable to further improve the data acquisition rate for real-time imaging through the fabrication of a focal plane antenna array, such a device would be hindered by technical issues such as high optical power consumption and limits on the antenna packing density.

Recently, a free-space electro-optic sampling technique for the coherent characterization of THz beams was developed,[3-5] featuring diffraction-limited spatial resolution, femtosecond temporal resolution, THz frequency bandwidth, mV/cm field sensitivity, and signal-to-noise ratio (SNR) better than 10 000.[3] Advantages intrinsic to electro-optic detection include nonresonant frequency response (dc to THz), large detector area (~cm^2), high scan rate, and linear dynamic range (~160 dB).[6] The excellent performance of the single detector measurements in a collinear geometry has shown great promise for real-time two-dimensional (2D) imaging.[7] Electro-optic detection is capable of mapping a time-resolved THz (far-infrared) image onto an optical beam, for which array detection such as CCDs and digital-signal-processing technologies are well developed.

In this letter, we report the first real-time 2D imaging of a THz beam from a table-top electro-optic sampling module. We demonstrate the conversion of a time-resolved far-infrared image into a time-resolved optical image using a ZnTe sensor and a high performance digital CCD camera. A full frame readout time of 0.133 s for 384×288 pixels makes this a true "real-time" measurement. The average readout optical power is 300 μW, with a temporal resolution of 50 fs, and submillimeter spatial resolution, corresponding to THz wavelengths.

Figure 1 schematically illustrates the experimental arrangement for free-space electro-optic THz imaging. The basic operating principles and experimental details of collinear electro-optic sampling have been described previously.[3] Fundamentally, this system is based on the linear Pockels effect in electro-optic crystals where a pulsed microwave signal acts as a transient bias to induce a transient polarization in the sensor crystal. This polarization induces a birefringence that is then probed by a synchronously pulsed laser beam, and finally converted to an optical amplitude modulation via optical polarization analysis. The laser source is a Ti:sapphire laser with a pulse duration less than 50 fs, and an unbiased GaAs wafer is used to generate pulsed electromagnetic radiation.[8] Parabolic mirrors were used to focus the THz radiation on a 0.9 mm thick, 6×8 mm^2(110) oriented ZnTe crystal. An optical readout beam with a diameter larger than that of the THz beam probes the electric field distribution within the crystal via the Pockels effect. The 2D field distribution in the sensor crystal is converted into a 2D optical intensity distribution after the readout beam passes through a crossed polarizer, and the optical image is then recorded by a digital CCD camera. The imaging area of the CCD camera (8.4×6.3 mm^2) is comparable to the area of the ZnTe sensor (6×8 mm^2), and no focusing optical element was used between the sensor and the camera. There are no

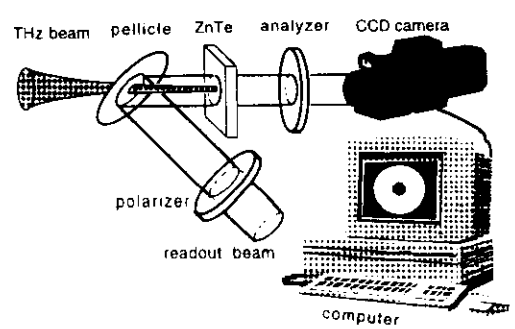

FIG. 1. Experimental setup for the conversion of a far-infrared (THz) image into an optical image as measured by a CCD camera.

a)Electronic mail: zhangx2@rpi.edu

 0003-6951/96/69(8)/1026/3/$10.00

Free-space electro-optics sampling of mid-infrared pulses

Q. Wu and X.-C. Zhang[a)]
Physics Department, Rensselaer Polytechnic Institute, Troy, New York 12180-3590

(Received 16 May 1997; accepted for publication 7 July 1997)

We report on the coherent detection of ultra-broadband mid-infrared electromagnetic pulses using a 30-μm-thick ZnTe electro-optic sensor. The detected frequency spectrum exceeds 37 THz, extending from microwave to the mid-infrared. The frequency response can be further improved by reducing the sensor thickness to 10 μm. © *1997 American Institute of Physics.* [S0003-6951(97)02536-9]

Despite the rapid advance of terahertz optoelectronics in the recent decade, the frequency region above 10 THz has yet been accessible for coherent detection. Whereas Katzenllenbogen *et al.* reported a frequency response of 6 THz from their photoconducting dipole antenna (PDA),[1] the record was recently pushed to 7 THz with a much broader 3-dB bandwidth[2] in a GaP-based free-space electro-optic sampling (FS-EOS) system. However, because of the Reststrahlen region near 11 THz, a GaP sensor is unlikely to reach 10 THz. This is generally the case for most electro-optic (EO) sensor materials since the frequency of the fundamental TO phonon resonance in GaP is one of the highest known of many semiconductor EO crystals.

The possibility of extending FS-EOS into the mid-infrared region is nevertheless favored by the following factors. First, most semiconductor EO materials are transparent in the frequency region between phonon resonance (far-IR) and the electronic resonance (near-IR); Second, it is reasonable to assume an instantaneous nonlinear response and a constant electro-optic coefficient across the mid-infrared region for covalent semiconductor EO crystals, where the dominant nonlinearity is electronic in origin; And the last, 10 fs lasers, which now proliferates rapidly, can readily provide a sampling bandwidth (FWHM) of as high as 44 THz.

The generation of broadband mid-infrared radiation through optical rectification was recently demonstrated by Bonvalet *et al.*[3] In their experiment, an incoherent detector (HgCdTe) and interferometric technique were employed to characterize the mid-infrared pulses. The spectrum of the generated radiation, as they noted, spanned beyond the detection bandwidth of the HgCdTe detector. Furthermore, due to the dispersion of GaAs, which has an index of $n(5\ \mu\text{m}) = 3.2978$ and $n(25\ \mu\text{m}) = 3.058$,[4] the spectral phase of the mid-infrared pulse in fact cannot be assumed constant even for their 100-μm-thick GaAs emitter. Incoherent detector based linear correlation technique was therefore unable to provide an accurate characterization of the ultra-broadband radiation. FS-EOS, as a coherent detection technique, becomes attractive when combined with an ultra-broadband mid-infrared source.

In this letter, we report the use of electro-optic sensors for coherent characterization of mid-infrared terahertz beams with a bandwidth up to 37 THz. This represents a significant improvement over the previous record of 7 THz,[2] and also confirms the broadband nature of the radiation generated by optical rectification.

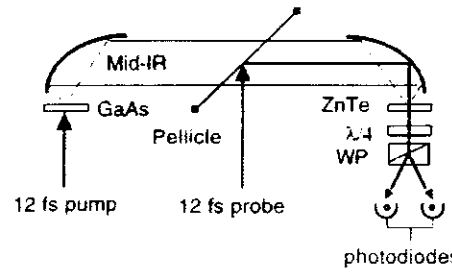

FIG. 1. Schematic of experimental setup. λ/4: achromatic quarter wave plate; WP: Wollaston prism.

Figure 1 schematically illustrates the experimental setup of the FS-EOS detection system. The 12 fs Ti:sapphire laser (Kapteyn-Murnane Labs) delivered an average power of nearly 500 mW at a center wavelength of 800 nm. A 0.45-mm-thick (110)-oriented GaAs was used as an emitter and a 30-μm-thick (110) ZnTe crystal as an EO sensor. 350 mW of the laser power was focused on the GaAs emitter by a gold-coated off-axis parabolic mirror with a 5 cm effective focal length. The broadband THz radiation generated from the GaAs emitter by optical rectification[3] was collimated and then focused on the ZnTe EO sensor by a pair of $f/0.6$ off-axis parabolic mirrors. The laser probe beam was combined to collinearly travel with the THz beam through a 2-μm-thick pellicle, which had a negligible effect on laser pulse width and THz beam. The EO modulation induced by the ultrafast Pockels effect was detected by using a pair of bal-

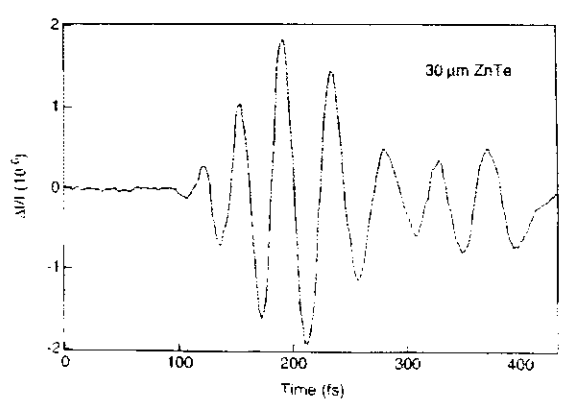

FIG. 2. Temporal waveform of the THz radiation measured by a 30 μm ZnTe sensor. The shortest oscillation period is 31 fs.

a)Electronic mail: zhangx2@rpi.edu

 0003-6951/97/71(10)/1285/2/$10.00

7 terahertz broadband GaP electro-optic sensor

Q. Wu and X.-C. Zhang[a)]
Physics Department, Rensselaer Polytechnic Institute, Troy, New York 12180-3590

(Received 10 December 1996; accepted for publication 31 January 1997)

We report a broadband coherent terahertz detection system using GaP as a free-space electro-optic field sensor with a demonstrated 3 dB bandwidth of 3.6 THz, useful bandwidth of 7 THz, and a pulse width of 185 fs. These figures represent new records in the coherent detection of free-space THz radiation. Sensor response as a function of crystal thickness and copropagation velocity mismatch dispersion in the THz regime is studied. © *1997 American Institute of Physics.* [S0003-6951(97)01714-2]

The spectral region of submillimeter waves have traditionally lacked suitable sources and detectors. Although heterodyne techniques are routinely used to access the microwave regime, and recent advances in Schottky varactors have extended the upper limit of heterodyne detection up to 1 THz,[1] incoherent detection remains common at higher frequencies. Recently, THz time-domain spectroscopy[2] has opened up this important spectroscopic region, and ultrabroadband coherent optoelectronic detection methods continue to see rapid improvement. At present, the highest reported frequency response of a photoconducting dipole antenna has been 6 THz.[3] However, the resonant nature of dipole structure seriously limits the detection bandwidth and spectral response. In contrast, recently developed free-space electro-optic sampling (FS-EOS)[4–6] provides an alternative method for the coherent detection of THz transients which overcomes many of the inherent limitations of antenna based systems. Among the various electro-optic materials we studied, ZnTe has shown the highest field sensitivity near 2 THz (Ref. 7) due to its excellent optical-group-velocity/THz-phase-velocity matching within the tuning range of Ti: sapphire lasers.[8,9] However, because the first transverse optical (TO) phonon resonance of ZnTe lies at 5.3 THz, the dispersion and absorption associated with this resonance limits the high frequency response of ZnTe sensors to 5 THz.[9]

In this letter, we report an all-optical terahertz generation and detection system with a record bandwidth of 7 THz. The ultrabroadband THz radiation is generated via optical rectification from ⟨110⟩ oriented GaAs, and coherently detected via FS-EOS using a ⟨110⟩ GaP sensor.

GaP is an indirect ($E_g = 2.3$ eV) zincblende semiconductor having its first TO phonon resonance near 11 THz.[10] Figure 1 shows the optical group index and THz phase index of GaP. The data (solid lines) were calculated from Ref. 10, and the experimental data (open circles) were measured using 100 fs laser pulses. The slight difference between the calculated and herein experimentally measured optical group indices may be due to different growth conditions leading to different impurity concentration. Because of the optical and THz dispersion, a given optical wavelength will only be velocity matched to a certain THz frequency. As an example, 810 nm is matched to 6 THz. The response function of the sensor is thus entangled by the frequency-dependent velocity mismatching.

To study the frequency response of the EO sensor, we consider a simple case of a monochromatic THz wave, $\exp(i\Omega t)$ and a delta-functionlike optical pulse centered at λ_0. After the pulse and THz wave have copropagated through a sensor of thickness d, the accumulated GVM time is

$$\delta(\Omega) = \frac{n_g(\lambda_0) - n(\Omega)}{c} d, \tag{1}$$

where $n_g(\lambda_0)$ is the optical group index, $n(\Omega)$ the THz phase index, and d the crystal thickness. In this analysis, we explicitly neglect contributions from multiple reflections in both optical and THz beams. The resulting EO modulation of the optical pulse induced by the THz wave is proportional to d as well as the time average of the electric field across the GVM time $\delta(\Omega)$. It has the form as:

$$G(\Omega) = \frac{t(\Omega)}{\delta(\Omega)} \int_0^{\delta(\Omega)} e^{i2\pi\Omega t} dt = t(\Omega) \frac{e^{i2\pi\Omega\delta(\Omega)} - 1}{i2\pi\Omega\delta(\Omega)}, \tag{2}$$

where $t(\Omega) = 2/[n(\Omega) + 1]$ is the Fresnel transmission coefficient. $G(\Omega)$ thus determines the frequency response function of the EO sensor. Although it appears that the EO signal is proportional to the sensor thickness, $|G(\Omega)|$ critically depends on d, as shown in Fig. 2. A trade-off clearly exists between broadband response and long interaction length. If the thickness of GaP is reduced to 50 μm, the frequency response can further extend to beyond 9 THz. Knowing the frequency response $G(\Omega)$, it is straightforward to calculate

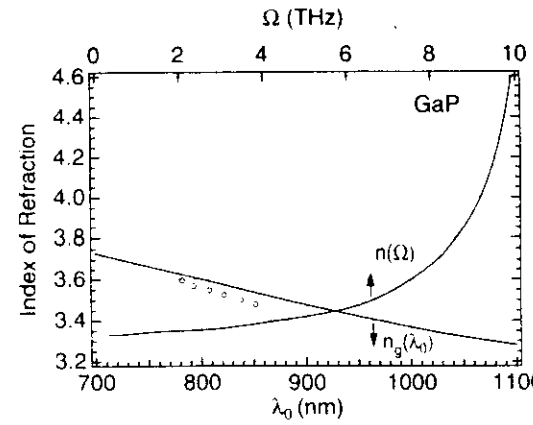

FIG. 1. Optical group index $n_g(\lambda_0)$ and THz $n(\Omega)$ in GaP.

a)Electronic mail: zhangx2@rpi.edu

 0003-6951/97/70(14)/1784/3/$10.00

Broadband detection capability of ZnTe electro-optic field detectors

Q. Wu, M. Litz,[a] and X.-C. Zhang
Physics Department, Rensselaer Polytechnic Institute, Troy, New York 12180-3590

(Received 15 December 1995; accepted for publication 14 March 1996)

We present our measurements of the broadband detection capability of copropagating electro-optic ZnTe field detectors for the characterization of free-space pulsed electromagnetic radiation. To demonstrate ultrawide detection bandwidth, radiation from both gigahertz and terahertz bandwidth pulsed microwave sources has been characterized. The high frequency limitation of the sensor is the first TO phonon resonance (5.31 THz). The ultrashort temporal resolution is demonstrated by the detection of a 177 fs (full width at half-maximum) pulse generated via THz optical rectification in ⟨111⟩ GaAs. © *1996 American Institute of Physics.* [S0003-6951(96)01521-5]

In the ultrafast optoelectronics community, one of the major concerns about the extension of conventional electro-optic sampling techniques from local field measurements to free space applications is the field sensitivity. In general, electro-optic sampling as performed in the characterization of local fields cannot offer a comparable signal-to-noise ratio (S/N) to that achieved via photoconductive sampling, such as through Auston switches. In the past, most of the activities in THz beam detection were conducted using photoconductive dipole antennas,[1–8] while much less effort was directed toward the development of free-space electro-optic sampling applications.

Recently, we reported the use of a counterpropagating electro-optic sampling system[9,10] to measure subpicosecond THz pulses. We used a $LiTaO_3$ crystal tip attached to a silicon lens to measure the freely propagating pulsed microwave radiation. Due to the short microwave–optical interaction length in the crystal tip, the S/N ratio in this geometry was well below that of conventional photoconductive antennas under comparable conditions. However, signal detection was greatly improved when the system was switched to a copropagating geometry.[11] In this configuration, a S/N ratio $>10\,000$ has been achieved even when the microwave beam was unfocused on the detector. A copropagating geometry has also previously been used for the detection of high power THz pulses.[12] The sensitivity, detector area, and stability for the field detectors in the collinear electro-optic sampling technique are comparable or better than the ultrafast photoconductive antennas.

The superior performance capabilities of electro-optic sampling techniques in transient local field measurements result from the ultrawide detection bandwidth of the sensor crystal. Similarly, in free-space electro-optic sampling systems, since there are no conducting elements or wiring associated with the crystal detector, the bandwidth should be limited only by the dielectric response of the electro-optic crystal. In this letter, we report the first experimental investigation of the broadband detection capability of copropagating electro-optic sampling for the characterization of freely propagating pulsed electromagnetic radiation. Specifically we have tested the sampling system using several pulsed microwave emitters where the central emission frequency ranged from tens of gigahertz to several terahertz. Our results demonstrate the ultrawide detection bandwidth capabilities of these systems.

Figure 1 schematically illustrates the experimental setup of a free-space copropagating electro-optic sampling system. This system is similar to the copropagating geometry we used previously.[11] The field detectors are ⟨110⟩ oriented ZnTe crystals of various thickness ranging from 0.25 to 1.5 mm. ZnTe has a comparable electro-optic figure of merit ($n^3 r/\epsilon$) to that of $LiTaO_3$, without the limitations associated with intrinsic birefringence and a reduced sensitivity by thermal fluctuations.

We tested several photoconductively gated pulsed microwave emitters, including cm-size photoconductive tapped antennas (transient current source), unbiased ⟨100⟩ GaAs wafers with Brewster angle incidence (transient photoconductive source), and ⟨111⟩ zinc-blende wafers with normal incidence (optical rectification source). These emitters provide microwave pulses with a pulse duration from approximately 150 fs to 65 ps. The shortest microwave pulses are generated from THz optical rectification (⟨111⟩ zinc-blende crystal) while the longest pulses are from large-end photoconductive tapped antennas.

The first set of emitters we tested were the photoconductive twin-line center-fed antennas. These antennas had two Cu conductors each resembling an Alpine-type horn. A GaAs photoconductor with approximately a 1 mm gap was electrically contacted to a uniform transmission-line section. The length of the open ends of these emitters was on the

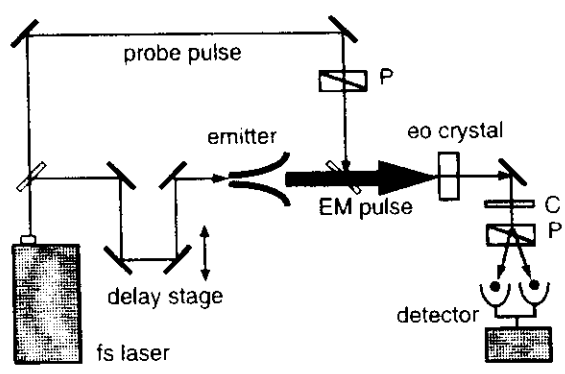

FIG. 1. Experimental setup of the copropagating free-space electro-optic sampling field detector.

[a]Army Research Laboratory, Adelphi, MD 20783-1197.

 0003-6951/96/68(21)/2924/3/$10.00

Electrically pumped tunable terahertz emitter based on intersubband transition

Bin Xu[a] and Qing Hu
Department of Electrical Engineering, Computer Science and Research Laboratory of Electronics, Massachusetts Institute of Technology, Cambridge, Masachusetts 02139

Michael R. Melloch
School of Electrical and Computer Engineering, Purdue University, West Lafayette, Indiana 47907

(Received 10 April 1997; accepted for publication 24 May 1997)

An electrically pumped three-level system was designed and fabricated using an AlGaAs/GaAs multiple quantum well structure. Under appropriate biases, the structure emits terahertz (THz) radiation, as a result of diagonal (or interwell) intersubband transition. The emission spectra were resolved using an external Fourier transform infrared spectrometer. The center frequency of the emission was voltage tunable. The emission spectra and the power-voltage relation showed clear evidence that the middle level was depopulated by fast longitudinal optical-phonon scattering, thus, a population inversion between the two upper levels is feasible. © *1997 American Institute of Physics*. [S0003-6951(97)02530-8]

The terahertz (THz) frequency range (1–10 THz, or 30–300 μm wavelength) is among the most underdeveloped electromagnetic spectra, mainly due to the lack of compact, coherent solid-state sources. Conventional interband laser diodes can only be operated at frequencies above their energy gap, which is >10 THz even for narrow-gap lead salt materials. Long-wavelength lasers based on intersubband transitions were first proposed more than two decades ago,[1] and several more detailed design analyses were reported in the last decade.[2–8] The successful development of intersubband lasers (or quantum-cascade lasers) operating at mid-infrared frequencies (3–5 μm and 8–12 μm wavelengths) was only recently achieved.[9,10] Despite this great success, major obstacles remain for the development of THz intersubband lasers, even though the intersubband emission was first observed in this frequency range.[11] The narrow subband separation corresponding to THz frequencies (4–40 meV) makes selective injection and the removal of electrons difficult. The long wavelength also requires new methods of mode confinement. Optical pumping is highly selective in populating specific subbands,[12,13] but its drawback is low efficiency. In this letter, we report our investigation on an electrically pumped, intersubband three-level THz emitter using multiple quantum wells (MQWs).

The intersubband emission structure was grown using molecular beam epitaxy (MBE) on an n^+ GaAs substrate. The active region is clamped by two 0.4-μm-thick n^+ contact layers ($n=2\times10^{18}$ cm^{-3}), and it consisted of ten nominally identical modules of MQWs made of $Al_{0.3}Ga_{0.7}As$/GaAs heterostructures. Each module contained three quantum wells with widths of 6.8 nm, 6.5 nm, and 8.8 nm; and barrier thicknesses of 2.6 nm, 2.0 nm, and 4.8 nm, respectively, as shown in Fig. 1(a). The 8.8-nm well was δ-doped at the center with a doping level of 0.9×10^{11} cm^{-2}. This doping was used to avoid the space charge effect under injection. Each module is a three-level system, with E_1, E_2, and E_3 levels located in the 8.8-nm, 6.5-nm, and 6.8-nm wells, respectively. Under a proper bias, which is ~60 mV/module, these three-level systems were cascade connected. Figure 1(a) shows the band diagram, subband positions, and squared magnitude of the wavefunctions at this bias (corresponding to $E=18.9$ kV/cm) as a result of self-consistent numerical solution of the Schrödinger and Poisson equations. The ground level E_1' of an earlier stage is aligned with the upper level E_3 of the following stage: Thus, E_3 can be selectively populated through resonant tunneling. Furthermore, the separation between E_2 and E_1 was slightly >36 meV [which corresponds to the longitudinal optical

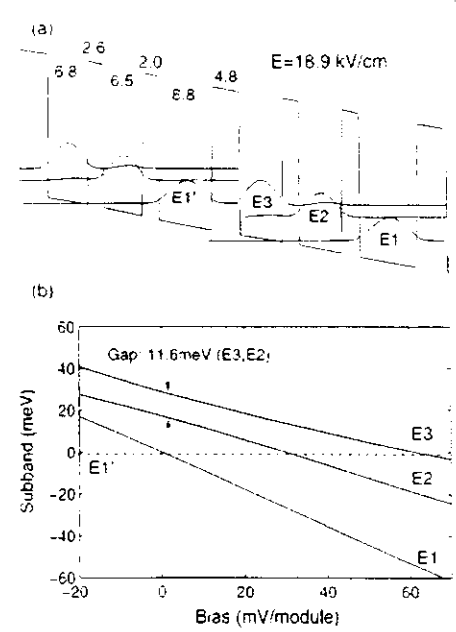

FIG. 1. (a) Numerically calculated band diagram, subband levels, and squared magnitude of wavefunctions of two cascade connected triple-quantum-well modules, under a bias of 60 mV/module. The MQWs are made of GaAs/$Al_{0.3}Ga_{0.7}As$ heterostructures and the well widths and the barrier thicknesses are indicated in nm. (b) Calculated subband positions E_1, E_2, and E_3 as functions of the bias per module. The dashed line indicates the E_1' level of an earlier stage, chosen as the zero-energy reference.

[a]Electronic mail: binx@mit.edu

 0003-6951/97/71(4)/440/3/$10.00

Generation of femtosecond electromagnetic pulses from semiconductor surfaces

X.-C. Zhang, B. B. Hu, J. T. Darrow, and D. H. Auston
Electrical Engineering Department, Microelectronics Sciences Laboratories, and Center for Telecommunications Research, Columbia University, New York, New York 10027

(Received 18 October 1989; accepted for publication 19 December 1989)

We have generated electromagnetic beams from a variety of semiconductors. When a bare semiconductor wafer was illuminated by femtosecond optical pulses, electromagnetic waves radiate from the surface and form collinear diffraction-limited electromagnetic beams in the inward and outward directions. The amplitude and phase of the radiated field depend on carrier mobility, the strength and polarity of the static internal field at the semiconductor surface.

Several novel techniques have been developed recently to generate broadband electromagnetic pulses in free space by ultrafast laser pulses. These techniques include the use of high-speed photoconductors as fast current sources for radiating antennas,[1-5] and rectification of optical pulses in crystals by electro-optic Cherenkov radiation.[6] Newly developed large aperture planar photoconductors radiate a directional electromagnetic pulse which can be steered by varying the angle of incidence of the optical beam.[7] The electro-optic Cherenkov radiation extracted from an electro-optic crystal in free space has a superior pulse duration and bandwidth.[6] These electromagnetic beams have been used in submillimeter wave and far-infrared spectroscopy.[8]

In this letter we report a technique to generate femtosecond electromagnetic pulses from the depletion layers of semiconductor surfaces. The amplitude and phase of the radiated field depend on carrier mobility and the strength and polarity of the static internal field at the semiconductor surface.

Figure 1 shows the sample illuminated by an unfocused optical beam with the outward radiated field $E_1(\theta)$ and transmitted radiated field $E_t(\theta)$. The optical excitation source used here is a balanced colliding pulse mode-locked (CPM) dye laser which produced an output pulse energy of 2 nJ at a repetition rate of 100 MHz and a 70 fs pulse duration at a center wavelength of 620 nm. The optical beam was split into two beams (30%/70%) by a beamsplitter. The stronger beam, used for the optical excitation, was modulated by a mechanical chopper at a 2 kHz rate; the weaker beam passed through a variable time delay stage and was used for the temporal measurement. The semiconductor wafer used as a transmitter was illuminated by the unfocused optical excitation beam. A dipole antenna fitted with a sapphire lens was used to detect the electromagnetic beam. This antenna has been used to characterize electro-optic Cherenkov radiation and its structure has been described previously.[1,6] The time-delayed laser beam was focused on the dipole antenna with a 5× microscope objective, and the measured signal from the antenna was amplified and averaged by a current amplifier and a lock-in amplifier.

Figure 2 schematically illustrates a band diagram of semi-insulating InP with photocarriers near the air/semiconductor interface. The surface state of a semi-insulating InP is near the conduction-band edge. As a result of Fermi level "pinning" at the interface, both the conduction band and valence band bend downward and form a depletion layer of width l_d near the interface. When an ultrafast laser pulse illuminates a bare semiconductor surface with the photon energy greater than the band gap, photons are absorbed, creating electron-hole pairs. The built-in static field drives the two kinds of carriers in opposite directions—the electrons to the surface and the holes to the wafer. The free carriers are swept across the depletion width l_d, the photocurrent flows in, and a dipole layer builds up. The rise time of the photocurrent is on the order of the laser pulse duration, and generally the decay time is the transit time of free carriers crossing the depletion layer (assuming the carrier lifetime is longer than the carrier transit time). The transient current in the depletion layer radiates electromagnetic waves. The estimated bandwidth of radiation is over 1 THz and is independent of the free-carrier lifetime of the semiconductor. The inward and outward directions of the radiation beams are diffraction limited, and they satisfy generalized Fresnel laws. The outward radiation field is collinear with the reflected optical beam, and the inward radiation field emerges from the sample after microwave absorption in the wafer and Fresnel's loss at the boundary.

Figure 3 shows the waveform of the radiated field from a semi-insulating InP, detected by the dipole antenna in the outward direction (45° relative to the normal) with a 4 mm nominal diameter laser beam. A single cycle of 2.4 ps is estimated between two adjacent minima. The measured band-

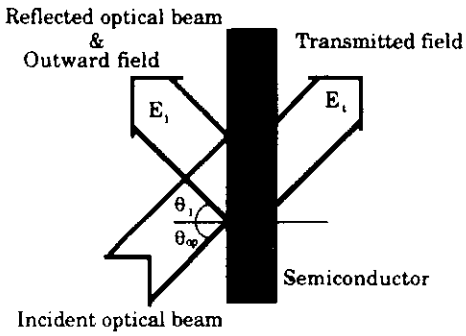

FIG. 1. Electromagnetic beams generated from semiconductor surface. The incident optical beam, the outward radiated field E_1, and inward radiated field satisfy the generalized Fresnel laws.

 0003-6951/90/111011-03$02.00

Here is a list of other groups involved in THz-TDS. Some are directly involved in advanced instrument development and characterization, while others are using it strictly as a source for far-infrared spectroscopy. This is a partial list, in no particular order. It is taken from Dan Mittleman's home page

(http://www.ece.rice.edu/~daniel/Mittleman.html).

There are direct links to the groups listed below on his home page. It is worth while to visit this home page.

Martin Nuss, Bell Labs, Lucent Technologies
Igal Brener, Bell Labs, Lucent Technologies
Xi-Cheng Zhang, RPI
A number of people at the **CUOS, University of Michigan,** including **Phil Bucksbaum, Ted Norris,** and **John Whitaker.**
Jeff Bokor, University of California, Berkeley
Joe Orenstein, University of California, Berkeley
Tony Heinz, Columbia University
Brian Kolner, UC Davis
Frank Hegmann, Univ. of Alberta
Center for Terahertz Science and Technology, UCSB
Dan Grischkowsky, Oklahoma State University has an interactive THz lab tour!
John Federici, NJIT
Andy Weiner, Purdue University
Norbert Scherer, University of Chicago
Robin Hochstrasser, University of Pennsylvania
Stephen Ralph, Georgia Tech (nascent web page)
Dan van der Weide, Delaware
Beth Parks, Colgate University
Ultrafast Optoelectronics Lab, Univ. of Maryland
Picometrix, Inc.
Molecular Optoelectronics Corporation
Toni Taylor, Los Alamos
Ted Heilweil, NIST Gaithersburg
Charles Schmuttenmaer, Yale University
Shun Lien Chuang, U. of Illinois, Urbana
Bob Guenther, Duke University
Elliot Brown, DARPA Electronics Technology Office
S. R. Andrews, Bath University, UK
Dan Some, Weizmann Institute
Frank De Lucia, Microwave Laboratory, Ohio State University
Hermann Harde, Hamburg
Jochen Feldmann, Munich
Martin Koch, Braunschweig
Martin Wegener, Karlsruhe
Rene Beigang, Kaiserslautern, in German
Heinrich Kurz and Peter Haring Bolivar, Aachen
Karl Unterrainer, University of Innsbruck
Hartmut Roskos, Frankfurt
Søren Keiding, Aarhus, Denmark
Jurgen Kuhl, Max-Planck Institute, Stuttgart
Ingrid Wilke, University of Hamburg
Hanspeter Helm, University of Freiburg
Klaas Wynne, Femtosecond Research Ctr., Strathclyde UK, as well as
GODOT, a European consortium of THz groups.
ENSTA, Palaiseau, France (does the English version work yet?)
M. Tani, Kansai Research Center, Kobe, Japan
Institute of Solid State Electronics, Technical University of Vienna
Jean-Louis Coutaz, University of Savoy, France
Joungho Kim, Korea Advanced Institute of Science and Technology

Characterization of an Optoelectronic Terahertz Beam System

MARTIN VAN EXTER AND DANIEL R. GRISCHKOWSKY, SENIOR MEMBER, IEEE

Abstract—**We describe the performance of an optoelectronic THz beam system. The transmitter operation is based on the repetitive, subpicosecond laser excitation of a Hertzian dipole antenna embedded in a charged coplanar line. With this transmitter electromagnetic beams of 1/2 cycle THz pulses at a repetition rate of 100 MHz are produced. The associated optoelectronic receiver is gated in synchronism with the excitation of the transmitter by subpicosecond pulses from the same laser source. With this receiver, the 10 nW beams of THz pulses were observed with a signal-to-noise ratio greater than 10000:1. Several sources contributing to the noise of the receiver are discussed, together with ways to reduce them. With an integration time of 125 ms, a signal-to-noise ratio of 1 is obtained for a THz beam with an average power of 10^{-16} W. The receiver operates in the sampling mode and has a time resolution of 0.5 ps.**

I. INTRODUCTION

IN A SERIES of recent papers, the features and applications of a new high-brightness pulsed THz beam system have been reported [1]–[4]. The highest performance version of the system is based on repetitive, subpicosecond optical excitation of a Hertzian dipole antenna [3]–[5] embedded in a charged coplanar transmission line structure. The burst of radiation emitted by the resulting transient dipole is collimated by a THz optical system into a diffraction-limited beam and focused onto a similar receiver structure, where it induces a transient voltage and is detected. The THz optical system gives exceptionally tight coupling between the transmitter and receiver, while the excellent focusing properties preserve the subpicosecond time dependence of the source.

As mentioned previously [2]–[4], the combination of THz optics with the synchronously gated, optoelectronic detection process has exceptional sensitivity for repetitively pulsed beams of THz radiation. With lenses and mirrors it is possible to direct a large fraction of the radiation, emitted during the excitation of an optoelectronic device, onto a distant device. The transmitted waveforms have been measured with subpicosecond resolution and with signal-to-noise ratios of more than 10000:1. This result was obtained with a repetition rate of 100 MHz, an integration time of 125 ms, and ar average power of 10 nW in the THz beam.

In this paper we present measurements and analysis o the total emitted power, the beam collection efficiency and the limiting noise properties of the THz receiver. Ir particular, we show how the combination of THz optic with the optoelectronic, subpicosecond, synchronous gat ing of the receiver allows for the measurement of inciden THz beams with peak powers far less than the inciden room-temperature thermal radiation in the same fre quency range. Methods to further improve the perfor mance of the receiver are also discussed.

The exceptional sensitivity is due in part to the higl performance of the THz optics. Via two stages of collima tion a THz beam with a frequency-independent diver gence of 25 mrad is obtained from the THz transmitter The THz receiver with identical optical properties collect essentially all of this beam. The resulting tightly couple system of the THz transmitter and receiver gives stron reception of the transmitted pulses of THz radiation afte many meters of propagation.

Another reason for the exceptional sensitivity is tha the optoelectronic gating changes the effective resistanc of the receiving antenna from 22 MΩ in the off state t 550 Ω in the on state. The gating window of the on stat lasts for approximately 0.6 ps. The duty cycle of $0.6 \times 10^{-}$ is given by the ratio of the 0.6 ps gating time to the perio of the 100 MHz sampling rate. Consequently, the averag resistance seen by a current amplifier directly connecte to the receiving antenna is about 7 MΩ. Therefore, wit respect to the current amplifier, the receiver has a hig impedance together with a subpicosecond response.

A final important feature of the detection method that it is a coherent process; the electric field of a repet tive pulse of THz radiation is directly measured. Becau we synchronously detect a repetitive signal, the tot charge (current) from the signal increases linearly wi the number of sampling pulses, while the charge (currer from noise increases only as the square root of the nur ber of pulses.

II. EXPERIMENTAL SETUP

The setup used to generate and detect beams of sh pulses of THz radiation is presented in Fig. 1. The tra mitting and receiving antennas are identical, each consi ing of the metallic pattern shown in Fig. 1(a) [3], wh

Manuscript received October 18, 1989; revised June 25, 1990. This work was supported in part by the U.S. Office of Naval Research.

M. van Exter was with the IBM Watson Research Center, P.O. Box 218, Yorktown Heights, NY 10598. He is now with the Huygens Laboratories, Postbus 9504, 2300 RA Leiden, the Netherlands.

D. R. Grischkowsky is with the IBM Watson Research Center, P.O. Box 218, Yorktown Heights, NY 10598.

IEEE Log Number 9038470.

0018-9480/90/1100-1684$01.00 ©1990 IEEE

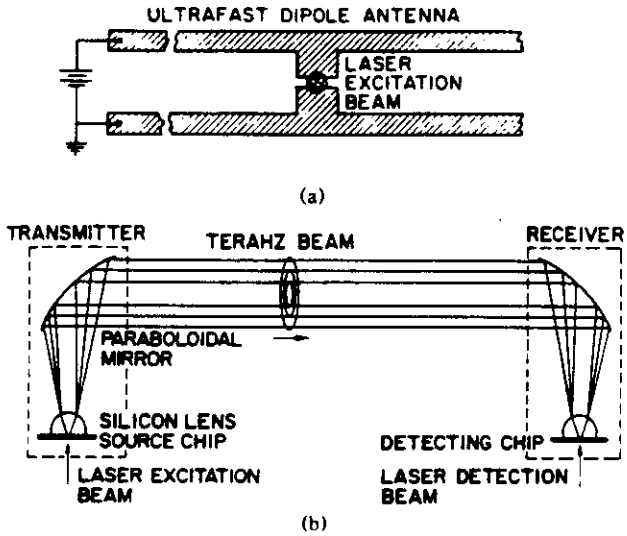

Fig. 1. (a) Ultrafast dipolar antenna. (b) Schematic diagrams of the THz transmitter and receiver.

has been fabricated on an ion-implanted silicon-on-sapphire (SOS) wafer. The 20-μm-wide antenna structure is located in the middle of a 20-mm-long coplanar transmission line consisting of two parallel 10-μm-wide, 1-μm-thick, 5 Ω/mm aluminum lines separated from each other by 30 μm. A colliding-pulse mode-locked (CPM) dye laser produces 623 nm, 70 fs pulses which are focused onto the 5-μm-wide photoconductive silicon gap between the two antenna arms. This 100 MHz periodic excitation causes pulsed, subpicosecond changes in the conductivity of the antenna gap. When a dc bias voltage of typically 10 V is applied to the transmitting antenna, these changes in conductivity result in pulses of electrical current through the antenna, and consequently bursts of electromagnetic radiation are produced. A large fraction of this radiation is emitted into the sapphire substrate in a cone normal to the interface [2] and is then collected and collimated by a dielectric lens attached to the back side (sapphire side) of the SOS wafer [1]–[4].

For the work reported here, the dielectric lenses were made of high-resistivity (10 kΩ·cm) crystalline silicon with a measured absorption of less than 0.05 cm^{-1} in our frequency range. The use of silicon gave significant improvement over the sapphire lenses previously used [1]–[3], although the 10% mismatch in dielectric constant between the silicon lens and the sapphire wafer causes a slight reflection. The center of the truncated 9.5-mm-diameter silicon sphere (lens) is 2.0 mm above the ultrafast antenna located at the focus of the lens.

After collimation by the silicon lens, the beam propagates and diffracts to a paraboloidal mirror, where the THz radiation is recollimated into a highly directional beam. Although the 70 mm aperture paraboloidal mirrors have a 12 cm focal length, a 16 cm distance was used between the silicon lenses and the mirrors to optimize the response of the system at the peak of the measured spectrum. While the high-frequency components of the THz pulses remain reasonably well collimated, the very low frequency components quickly diffract and illuminate the entire paraboloidal mirror, which presents a solid angle of 0.15 steradians to collect radiation from the source. After recollimation by the paraboloidal mirror, beam diameters (10–70 mm) proportional to the wavelength were obtained; thereafter, all of the frequencies propagated with the same 25 mrad divergence. The combination of the paraboloidal mirror and silicon lens (THz optics) and the antenna chip constitute the transmitter, the source of a highly directional, freely propagating beam of (sub)picosecond THz pulses. After a 50 cm propagation distance this THz beam is detected by an identical combination, the THz receiver, where the paraboloidal mirror focuses the beam onto a silicon lens, which focuses it onto a SOS antenna chip, similar to the one used in the emission process. The electric field of the focused THz radiation induces a transient bias voltage across the receiving antenna, directly connected to a low-noise current amplifier. The amplitude and time dependence of this transient voltage are obtained by measuring the collected charge (current) versus the time delay between the THz pulses and the CPM laser pulses that periodically gate the sensitivity of the receiver. The detection process with gated integration can be interpreted as a subpicosecond boxcar integrator.

III. Measurements

A typical time-resolved measurement is shown in Fig. 2(a). The clean pulse shape is a result of the fast action of the photoconductive switch at the antenna gap, the broad-band response of the ultrafast antennas, the broad-band THz optical transfer function of the lenses and paraboloidal mirrors, and the very low absorption and dispersion of the silicon lenses. The measured pulse width of only 0.5 ps (FWHM) is only an upper limit to the true pulse width, because no deconvolution has been applied to the measurement to take out the response time of the antenna gap. The value of 14 mV was established as a lower limit for the peak transient voltage across the gap; this was done by determining the required dc voltage for a photocurrent in the receiving antenna equal to the measured average current at optimum delay. The words *lower limit* indicate that the measured current results from a convolution of the transient voltage with the transient conductivity of the gate. In this regard, notice that the FWHM of the central spike is only 0.5 ps wide, compared with the 0.6 ps pulse width of the integrating gate. A deconvolution results in a peak transient voltage of 35 mV, which is about 2.5 times larger than the simple estimate mentioned above. The associated electrical pulse generated on the coplanar line by the excitation of the transmitting antenna is typically measured to be 1.0 ps in duration and close to 1 V in amplitude. Taking into account the response time of the measurement, the pulse on the line is considered to have a pulse width of about 0.7 ps with a rise time of the order of 0.3 ps and a longer

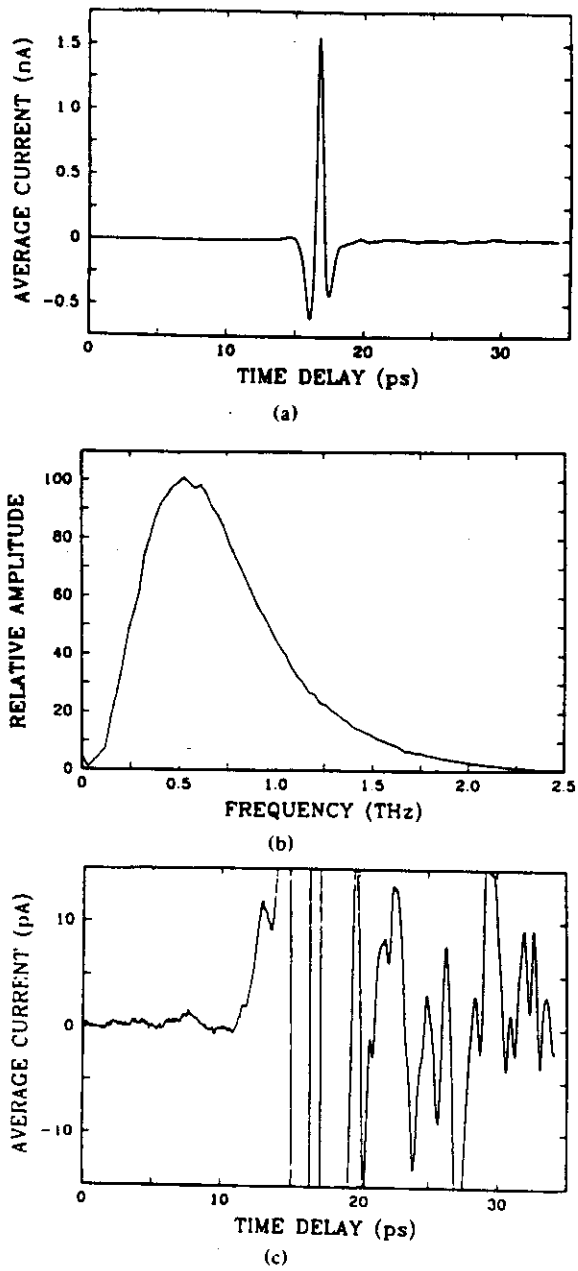

Fig. 2. (a) THz pulse measured by scanning the time delay between the optical gating pulses and the incident THz pulses, while monitoring the current induced in the THz receiver. (b) Amplitude spectrum of the measured pulse shape. (c) THz pulse on a 100 times expanded vertical scale.

fall time determined by the 0.6 ps carrier lifetime in implanted silicon [7].

In Fig. 2(b), the Fourier transform of the measured signal (Fig. 2(a)) is shown to stretch from about 0.1 to 2.0 THz. This represents only a lower limit to the true extent of the emitted radiation as it contains the frequency response of the receiver. At the low-frequency end, the efficiency of both emitter and receiver has been shown to be proportional to the length of the antenna, i.e., proportional to the separation between the two lines of the coplanar transmission line. For extremely low frequencies

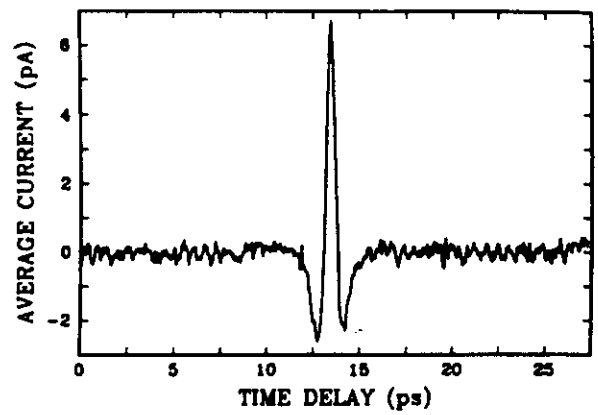

Fig. 3. Measured THz pulse with a 10^5 times reduction (compared with Fig. 2(a)) of the THz beam power.

the size of the paraboloidal mirrors will also limit the efficiency. For the high-frequency limit the efficiency of the antenna is strongly reduced when 1/2 the wavelength (in the dielectric) of the emitted radiation is no longer large compared with the antenna length. This frequency for our 30 μm antenna is 1.5 THz, so that the observed signal and corresponding spectrum are somewhat limited by the antenna response, which has dropped by 50% at this frequency. The high-frequency part of the spectrum is also limited by the finite rise time of the current transient and the nonideal imaging properties of the THz optics.

In Fig. 2(c), the time-resolved signal is shown on a vertical scale that has been expanded by a factor of 100. The structure observable after the main pulse is reproducible and is due to reflections of the electrical pulse on the transmission line, reflections of the THz pulse from the various dielectric interfaces, and absorption and dispersion of water vapor [4] in the 1 cm path outside the vaportight box placed around most of the setup. The observed noise in front of the main pulse is about 1.3×10^{-13} A rms for an integration time of 125 ms, corresponding to an integration bandwidth of 1 Hz determined by a 12 dB/octave filter. An identical noise value is obtained when the far-infrared beam is completely blocked. The signal-to-noise ratio in this 4 minute scan is more than 10000:1. Another 4 minute scan is shown in Fig. 3, for which the intensity of the pump laser beam was reduced from the 6 mW normally used to only 15 μW. This 400-fold reduction in laser power led to a reduction in the transient photocurrent of 320, instead of the expected 400. The discrepancy indicates a slight nonlinearity due to the onset of saturation, related to the fact that the electrical pulses generated on the transmission line are quite strong (almost 1 V in either direction). This 320-fold reduction in photocurrent led to a reduction in the power of the THz beam by the factor 1.0×10^{-5}. However, despite this enormous reduction in power, the peak amplitude is still more than 30 times larger than the rms noise. Based on calculations presented in the next section we believe that the average power in the THz beam during this measurement was about 10^{-13} W. If the

agreement with the previously derived value of 11 nW from the point of view of the transmitter.

An alternative analysis makes use of the concept of antenna impedance, defined as the ratio of the emitted power over the mean square of the current. In this respect it is important to notice that the current is constant along the antenna structure, which makes it a more efficient emitter than the related center-fed antenna [11]. The interface increases the antenna impedance and we find a value of 12 Ω at 0.6 THz for our situation. From the transmitter point of view, a peak current of about 1.8×10^{-2} A is pulsed through the antenna. If we assume that the current and emitted power were concentrated in a narrow band around 0.6 THz, then the emitted peak power would simply be I^2R, and the average emitted power would be about 17 nW, a number that includes the aforementioned 15% coupling efficiency into the THz beam and the 0.6×10^{-4} duty cycle. From the 35 mV induced voltage at the receiving antenna, one can derive an average incident power of 4.5 nW in a similar way. It was only a rough approximation to assume that all radiation was concentrated around the 0.6 THz peak of the spectrum. When we take the proper frequency integrations into account together with the corrections mentioned above, we arrive at 11 nW for the emitted power and 3.5 nW for the received power at the receiving antenna. Taking into account the 30% reflection at the silicon lens, the value obtained from calculations at the receiving antenna gives 5 nW incident on the silicon lens.

Another useful parameter is the ratio of the voltage induced in the receiving antenna to the current in the transmitting antenna. This frequency-dependent ratio is called the mutual impedance [11], [12]. For perfect coupling the mutual impedance should equal the impedance of the (identical) antennas [12]. From our measurements we extract a mutual impedance of about 3 Ω at 0.6 THz, corresponding to 25% amplitude coupling between the transmitter and the receiver for this frequency.

By reasoning from both the transmitter and the receiver point of view, we calculated the average power in the far-infrared beam to be about 11 nW and 5 nW or 7 nW, respectively. For the purposes of the discussion to follow, we consider the average transmitted power in the THz beam to be 10 nW, and we believe that this value is within a factor 2 of the actual value. This average power is comparable to that of conventional thermal sources [13], but the peak power of our source is orders of magnitude larger.

V. Noise in the Receiver

In this section we will present an analysis of the noise of the THz receiver. The following noise analysis is generally applicable to any type of photoconductive switch, although the actual numbers will depend on the type of device. If we were to destroy the directionality of the receiver by removing the paraboloidal mirror and the add-on silicon lens, the noise characteristics of the antenna/switch would in fact be unchanged. However, the sensitivity of the receiver for the THz beam would be drastically reduced.

Experimentally, we measured the receiver noise with a frequency analyzer (Hewlett Packard 3585B) connected to the output of a low-noise current amplifier (Ithaco 1211). The amplifier was in turn connected to the receiving antenna via the terminating coplanar transmission line. This arrangement allowed the investigated noise to be separated from the small pickup of harmonics of the line current. An alternative approach was to measure the fluctuations on the output of the lock-in amplifier that was also connected to the current amplifier (CA). These fluctuations were then converted to an rms current at the input terminals of the current amplifier and could thus be compared with the noise floor (in dBm) measured with the spectrum analyzer.

In the absence of the CPM laser beam, the noise of the first receiving antenna chip investigated was 1.5×10^{-13} A rms for a 125 ms integration time on the lock-in (−73 dBm, with the CA at a setting of 10^{-8} V/A and a bandwidth of 10 Hz). That this value was due to the thermal Johnson noise, also called Nyquist noise, could be demonstrated by replacing the antenna chip by an ordinary resistor of identical value (0.7 MΩ). The easiest way to reduce this noise is to strip the silicon from the areas of the chip that are not illuminated by the laser during normal operation. Such an antenna chip with stripped silicon showed a much increased resistance of 22 MΩ in the off state. For this antenna the noise measurement gave about 3.9×10^{-14} A rms (125 ms), being only slightly affected by the much lower, open-ended current noise of the CA of 1.5×10^{-14} A rms.

When a 6 mW laser beam was focused on the antenna gap, the noise increased to 2.2×10^{-13} A rms (125 ms) for the first antenna chip and to 1.3×10^{-13} A rms for the second stripped antenna chip. For the second chip we could show that the amplitude of the additional noise was proportional to the square root of the laser power. A likely candidate for this additional noise is the Johnson noise arising from the thermally driven random motion of electrons. Each laser pulse temporarily reduces the resistance between the two lines of the terminating coplanar transmission line. During the 0.6 ps switching time the resistance is typically about 550 Ω. The integrated thermal noise power scales with the average conductivity, which in our situation is reduced from 22 MΩ to about 7 MΩ. Thus, we would expect this noise to be 4.8×10^{-14} A rms (125 ms, 1 Hz). However, at 6 mW the measured noise power was equal to the Johnson noise of a 1 MΩ resistor and not that of the measured average resistance of 7 MΩ. Consequently there must be additional noise sources, some of which are described below. The measured antenna noise can also be interpreted as a random effective voltage and charge transfer at each shot of the laser. The 1.3×10^{-13} A rms (125 ms) noise level corresponds to a shot-to-shot effective voltage of 4.2 mV. This value seems to be very large, but results only in a charge transfer of 4.6×10^{-18} C or roughly 30 electrons per shot,

Inst. Phys. Conf. Ser. No 126: Section III
Paper presented at Int. Symp. on Ultrafast Processes in Spectroscopy, Bayreuth, 1991

Time-domain spectroscopy of molecular vapors with subpicosecond pulses of THz radiation

H. Harde*, D. Grischkowsky

IBM Watson Research Center, P.O. Box 218, Yorktown Heights, New York 10598

A newly developed optoelectronic beam system generating subpicosecond pulses of THz radiation was used for time-domain studies of N_2O vapor. After the excitation the molecules were observed to radiate coherent transients on the free-induction decay originating from the periodic rephasing of coherently excited rotational absorption lines. Numerical simulations of the terahertz pulse propagation through the sample, based on the linear dispersion theory, exactly reproduce the measured pulse structures. Additional calculations of terahertz pulses interacting with OCS and HCN vapor are presented.

1. INTRODUCTION

While in recent years spectroscopy with ultrashort pulses was restricted to optical and infrared frequencies, with the newly developed terahertz beam sources, producing subpicosecond pulses of terahertz radiation (van Exter *et al* 1989a, Zhang *et al* 1990), a new frequency range is becoming accessible for time domain spectroscopy and the studies of fast transients. At IBM an optoelectronic terahertz transmission and detection system has been developed and used for measurements of dielectrics and semiconductors (Grischkowsky *et al* 1990a) as well as high T_c substrates (Grischkowsky *et al* 1990b). Also molecular vapors of H_2O (van Exter *et al* 1989b) and N_2O (Harde *et al* 1991a, Harde and Grischkowsky 1991b) have been investigated with this setup. The teraHz pulses are unique in terms of their pulse duration and corresponding bandwidth. They essentially consist of a single oscillation and are characterized by a transform-limited white spectrum extending to beyond 2 THz. The radiation is well collimated into a low-divergence beam and can be detected with a signal-to-noise ratio of better than 20.000.

In this paper we report an experimental and theoretical study of time-resolved terahertz spectroscopy of N_2O vapor, where we refer to some of the results presented in an earlier publication (Harde and Grischkowsky 1991b), and we add numerical simulations of the pulse propagation through OCS and HCN vapor. These molecules with a similar structure to N_2O but with larger electric dipole moment are interesting candidates for studies of propagation effects through optically dense media. Terahertz pulses passing through one of these vapors excite a multitude of pure rotational transitions in the impact approximation and cause the molecules to reradiate a free-induction-decay (FID) signal that consists of a series of well defined ultrashort pulses (for similar observations in the infrared see, Forster *et al* 1974, Heritage *et al* 1975, Woerner *et al* 1989, and Bratengeier *et al* 1989). These pulses have their origin in a periodic rephasing of the equally spaced rotational lines. For N_2O vapor we have measured trains of coherent transients extending to beyond 600 ps which are compared with theoretical simulations that we derived from calculations based on the linear dispersion theory. Owing to the exceptionally

* Permanent address: Universität der Bundeswehr, Holstenhofweg 85, 2 Hamburg 70, Germany

high time resolution of the measurements, a reshaping of the individual pulses in the train can be observed which in the case of N_2O and OCS originates from the anharmonicity in the line spacing. For HCN vapor a strong reshaping and even new formation of the emitted pulse train is calculated which is due to dispersive propagation effects.

2. EXPERIMENTAL SETUP

The optoelectronic terahertz radiation source and detection system is shown in Figure 1 and has been already described by van Exter *et al* (1989a). For the case here, a transmitting antenna with bow-tie geometry was used, fabricated on an intrinsic, high-resistivity gallium arsenide wafer. The antenna is driven by photoconductive shorting the biased 5μm wide antenna gap with 70 fs pulses coming at a rate of 100 MHz in an excitation beam from a colliding-pulse mode-locked dye laser. The generated THz radiation is collimated by a silicon lens and paraboloidal mirror and directed towards the receiver, where it is focused onto an ultrafast receiving antenna, which uses a micron-sized dipole structure on an ion-implanted, silicon-on-sapphire wafer. The electric field of the teraHz pulses across the receiving antenna gap is sampled by shorting the gap with the 70 fs optical pulses of a detection beam and monitoring the current versus the time delay between the optical excitation and detection beam. For the measurement with N_2O vapor a gas cell of 38.7 cm length with high resistivity silicon windows is placed into the beam.

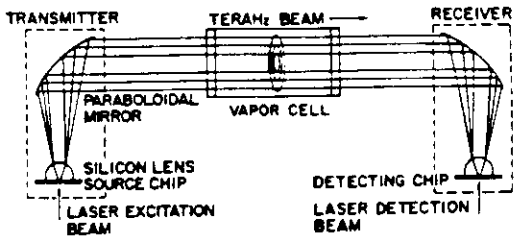

Fig.1. Experimental setup of the terahertz beam system.

3. N_2O-MEASUREMENTS

When the terahertz pulses propagate through the vapor they will be reshaped due to the absorption and dispersion in the sample. These changes can be directly observed by comparing a transmitted pulse with a reference scan, taken without vapor in the cell. Such a measurement is displayed in Figure 2a. The pulses are detected with a time resolution of better than 0.2 ps and a signal-to-noise ratio of more than 20,000. They consist only of a single oscillation and their numerical Fourier transform corresponds to a smooth amplitude spectrum extending up to 1.5 THz (see also dashed curve in Figure 5a).

When the cell is filled with 800 hPa of N_2O vapor, the output changes to that shown in Figure 2b. Within the broad spectral range covered by the terahertz pulses the N_2O molecule has a multitude of equally spaced rotational lines which can be excited simultaneously in the impact approximation. Consequently, a periodic rephasing and dephasing of the entire ensemble of more than 50 transitions occurs during the

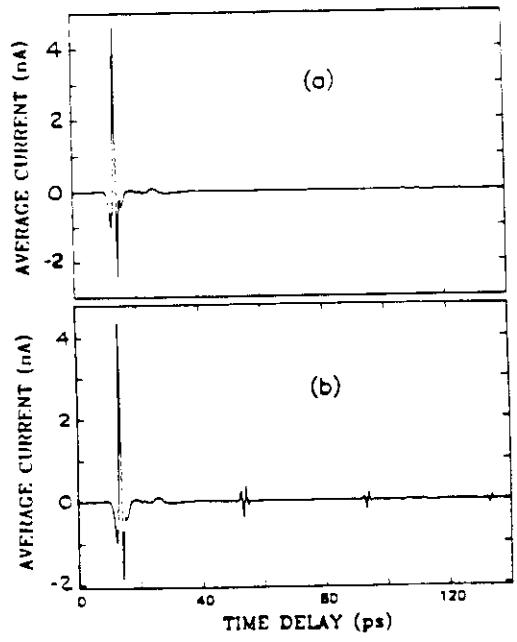

Fig.2. (a) Measured terahertz pulse without vapor in the cell, and (b) with 800 hPa of N_2O vapor.

4. THEORY

An accurate theoretical description and simulation of the measurements requires the solution of the coupled Maxwell-Bloch equations, which under certain conditions can be solved by introducing the pulse area concept. As the terahertz pulses are characterized by a bandwidth comparable with the frequencies of the spectral distribution, it is not appropriate to describe them by a carrier and a time-dependent envelope as is usually done in the infrared and visible regions. This precludes the use of the pulse area concept for pulse propagation effects, and also the slowly varying envelope approximation cannot be applied for pulses essentially consisting only of a single cycle.

However, under our experimental conditions we can assume a linear response of the sample to the exciting pulses. Then the Maxwell-Bloch equations reduce to that of linear dispersion theory (see, e.g., Allen and Eberly 1975). The interaction of the electric field with the medium then is best described in the frequency domain by means of the dispersion $\Delta k(\omega)\,L$ and amplitude absorption $\alpha(\omega)\,L/2$ over the sample length L. A pulse $E(z,t)$ propagating in z-direction through the medium can then be calculated by

$$E(z,t) = \int_{-\infty}^{\infty} E(\omega)\, e^{-i(\omega t - k_0 z)} e^{i\Delta k(\omega) z} e^{-\frac{1}{2}\alpha(\omega) z} d\omega \tag{1}$$

where $E(\omega)$ is the spectral distribution of the input pulse. The absorption coefficient of three-atomic linear molecules on a single rotational transition from $J \rightarrow J+1$ and with Lorentzian lineshape is given by

$$\alpha_J(\omega) = \frac{p\, f_0\, \mu^2\, h\, B_V\, \omega^2}{6\, n\, c\, \epsilon_0\, (kT)^3} (J+1)\, e^{-hB_V J(J+1)/kT} \frac{\Delta\omega_J}{(\omega_J - \omega)^2 + (\Delta\omega_J/2)^2} \tag{2}$$

with the transition frequency $\omega_J/2\pi = 2\,B_V\,(J+1) - 4\,D_V\,(J+1)^3$. Here, $\Delta\omega_J$ is the linewidth, B_V the rotational constant of the vibrational state and D_V the centrifugal stretching constant. k_0 and n represent the wave vector and refractive index in the sample far from any material resonance and p is the gas pressure, f_0 the fraction of molecules in the lowest vibrational state, μ the electric dipole moment, kT the thermal energy, h Planck's constant, and c the speed of light. For the change of the wave vector it is found:

$$\Delta k_J(\omega) = \frac{p\, f_0\, \mu^2\, h\, B_V\, \omega^2}{6\, n\, c\, \epsilon_0\, (kT)^3} (J+1)\, e^{-hB_V J(J+1)/kT} \frac{\omega_J - \omega}{(\omega_J - \omega)^2 + (\Delta\omega_J/2)^2} \tag{3}$$

The absorption and dispersion over the whole spectral range of the teraHz pulse is obtained by summing Eqs.(2) and (3) over all transitions within this spectral width.

5. NUMERICAL SIMULATIONS OF THE PULSE PROPAGATION

Our numerical calculations of pulse propagation were performed as follows. The measured reference pulse, shown in Figure 2a, was chosen to be the input pulse to the vapor. Its numerical Fourier transform $E(\omega)$ was multiplied by the amplitude absorption and dispersion which were calculated from Eqs.(2) and (3) using the known molecular constants. The inverse numerical Fourier transform then gives the predicted output pulses. If such a calculated pulse is fitted to the measurement in Figure 2b, where the spectral linewidth, here assumed to be identical for all transitions, is used as the only free parameter, on a double plot the different curves cannot be further distinguished. From the fit the self-pressure broadening of N_2O vapor can be accurately determined (Harde and Grischkowsky 1991b). The calculation reproduces the measurement in pulseshape and absolute amplitude, for the exciting pulse as well as the commensurate echoes remarkably well. This is demonstrated by the comparison in Figure 4 between theory (- - -)

and experiment (--). Here, the change of the echo-shape is well simulated with a stretching constant of $D_V = 5.3\ kHz$, as known from the literature. The background oscillations on the measurement result from the residual water.

Due to the excellent agreement between measurements and calculations for the N_2O we can also expect to obtain reliable results for the simulations of the pulse propagation through OCS and HCN vapor. The OCS molecule is distinguished by a frequency spacing between adjacent lines of $2B_V = 12.2\ GHz$ with an anharmonicity of only $D_V = 1.3\ kHz$, while HCN has a spacing of 88.6 GHz and a stretching constant of about 80 kHz. The calculated absorption spectra for 133 hPa of OCS and HCN are displayed in Figure 5a and 5b respectively. A terahertz pulse propagating through OCS vapor excites the entire manifold of absorption lines with rotational quantum numbers of up to $J = 100$. The Fourier transform spectrum of the input pulses is shown as the dashed curve in Figure 5a. Because the anharmonicity is related to the third order of J, even with the small stretching constant of OCS a significant reshaping of the echoes which is only due to centrifugal dephasing can be calculated. This is illustrated by Figure 6 showing the seventh echo of the emitted train, while the first echo appearing at 82 ps after the excitation pulse has the same shape as displayed in Figure 4a. For this calculation a pressure of 13.3 hPa and a self-pressure broadening of 8.7 MHz/hPa was assumed.

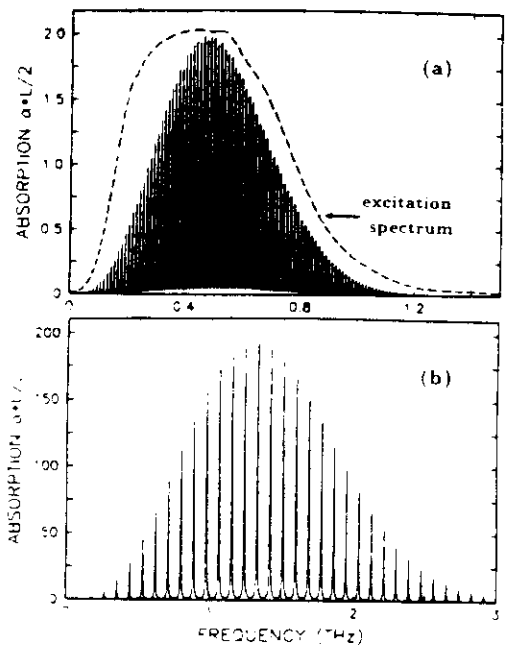

Fig.5. Calculated absorption spectra for 133 hPa of (a) OCS, and (b) HCN vapor.

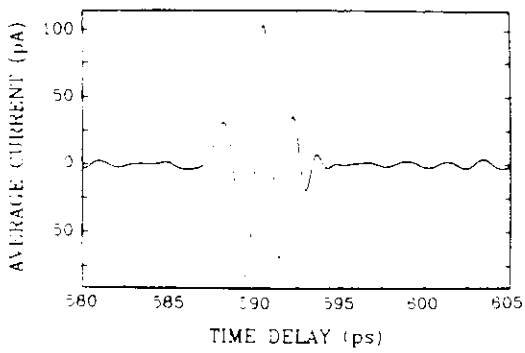

Fig.6. Calculated shape of the 7th echo for 13.3 hPa of OCS vapor.

The rotational spectrum of HCN extends to larger frequencies than the spectrum of the input pulses used in our simulations. In this case only the lowest 16 transitions are excited by the terahertz radiation and contribute to the radiated pulse train with a pulse separation of 11.3 ps. Since the width of a spectral line is proportional to the pressure, the absorption on line-center is independent of the pressure. This peak absorption (see Figure 5) is for HCN more than two orders of magnitude larger that of OCS and N_2O ($\alpha_{max}L/2 = 0.6$), assuming the same propagation length of 38.7 cm through the cell. Therefore, already at low pressures strong echoes can be observed, as this is demonstrated in Figure 7a for a propagating pulse through 1.33 hPa vapor of HCN.

For a peak absorption greater than unity the vapor behaves as an optically thick sample and propagation effects become noticible. So, at the line center the absorption is already saturated and causes an additional spectral broadening which in the time domain is manifest as a faster decay of the measured pulse train than expected from the coherence relaxation time. In Figure 7a the observed damping is only attributed to this absorptive effect, while that contribution due to collisional dephasing with $T_2 = 2/\Delta\omega = 6.2\ ns$, cannot be observed on this time scale.

T-Ray Imaging

Daniel M. Mittleman, Rune H. Jacobsen, and Martin C. Nuss, *Member, IEEE*

(Invited Paper)

***Abstract*—The use of terahertz pulses for imaging has opened new possibilities for scientific and industrial applications in the terahertz frequency range. In this article, we describe the technology necessary to perform terahertz "T-ray" imaging, novel imaging techniques, and commercial applications of T-ray imaging.**

I. Introduction

THE TERAHERTZ, or far-infrared, region of the electromagnetic spectrum is of critical importance in the spectroscopy of condensed matter systems, gas phase analysis, and vibronic spectroscopy of polar liquids. In the past, terahertz spectroscopy has been hindered by the low brightness of incoherent far-infrared sources and poor sensitivity of bolometric detectors. But with the advent of terahertz time-domain spectroscopy (THz-TDS) [1], [2], [3], these difficulties are overcome in a radical way. THz-TDS is based on electromagnetic transients generated opto-electronically with the help of femtosecond laser pulses. These terahertz transients are single-cycle bursts of electromagnetic radiation of typically less than 1-ps duration. Their spectral density spans the range from below 100 GHz to more than 5 THz. Furthermore, the brightness of the THz transients exceeds that of conventional thermal sources, and the gated detection is orders of magnitude more sensitive than bolometric detection.

The many advantages of the terahertz time-domain technique have resulted in rapid proliferation among researchers interested in studying properties and physical phenomena of materials in the far-infrared frequency range. On the other hand, prospects for commercial applications of this technology have been unclear so far, mostly due to the sophisticated femtosecond laser equipment needed. Within the last two years, the availability of semiconductor-diode-pumped solid-state lasers is transforming femtosecond lasers into compact, wall-plug efficient and highly practical light sources that are often not larger than an electrical power supply.

On another front, advances in the efficiency of terahertz transmitters and receivers and improved optical designs have led to the extension of terahertz time-domain techniques to real-time imaging [4], [5], [6]. This terahertz "T-ray" technology combines imaging, real-time acquisition of terahertz waveforms and advanced signal processing techniques to obtain far-infrared images of objects and materials. In many cases, T-Ray images can also distinguish chemical compositions of the object. These features of T-ray imaging have generated interest in commercial applications in diverse areas as moisture analysis, quality control of plastic parts, packaging inspection, and trace gas analysis and monitoring. Now, with practical and cost-effective femtosecond lasers arriving on the market, vT-ray applications have the potential to become cost effective in the commercial arena.

This paper attempts an overview of the features and capabilities of T-ray imaging, and the many potential applications that this new technology has in science, industry, and manufacturing. We will also discuss novel imaging techniques such as the terahertz Hall effect and T-ray tomography, which extends T-ray technology to three-dimensional imaging.

II. Characteristics of T-Rays for Chemical Imaging

The potential for imaging applications using Terahertz "T-ray" pulses results from a number of characteristics. Terahertz waves penetrate most dry, nonmetallic and nonpolar objects like plastics, paper, cardboard and nonpolar organic substances. In the case of dielectrics, the absorption is governed by optical phonons and depends on the polarity and the optical phonon resonances of the material [7]. On the other hand, metals are completely opaque to T-rays, and polar liquids such as water strongly absorb in this frequency region [8], [9]. In the gas phase, most polar molecules have very sharp and strong absorption lines in this frequency range, which reflect the unique rotational or ro-vibrational spectra of the absorbing species [10], [11].

Terahertz pulses cover a broad frequency range from under 100 GHz to several terahertz. Because the terahertz time-domain technique measures these pulses in both amplitude and phase, the complex dielectric function (both amplitude and phase) can be obtained for the material under investigation when comparing input and output waveforms. A particularly useful feature of the THz-TDS technique is that this spectroscopic information manifests itself directly in the time-domain. Fig. 1 shows how different materials modify the terahertz waveforms in characteristic ways. On the top [Fig. 1(a)], the terahertz waveform after propagation through a 10-mm-thick piece of stycast is shown, together with the input pulse (dotted). The transmitted waveform shows significant "chirp," indicative of the strong frequency-dependent refractive index of stycast. Fig. 1(b) shows the same waveform after propaga-

Manuscript received October 18, 1996; revised November 21, 1996.

D. M. Mittleman was with Bell Laboratories, Lucent Technologies, Holmdel, NJ 07733 USA. He is now with the Electrical and Computer Engineering Department, Rice University, Houston, TX 77005 USA.

R. H. Jacobsen is with the Department of Chemistry, Aarhus University, DK-8000 Aarhus C, Denmark.

M. C. Nuss is with Bell Laboratories, Lucent Technologies, Holmdel, NJ 07733 USA.

Publisher Item Identifier S 1077-260X(96)09584-6.

the terahertz beam. In fact, a collimated beam with frequency-independent beam diameter and without wavefront curvature cannot be obtained using this substrate lens design [22].

These problems can be avoided by modifying the substrate lens design. Use of hemispherical substrate lenses, for which the antenna is located at the center of radius of the lens, completely eliminates all diffraction and total internal reflection effects as no refraction occurs at the lens-air interface. However, the cone angle of the terahertz emission can be quite large, so that optics with very large numerical aperture is required to subsequently collimate the beam. An excellent compromise is the aplanatic hyperhemishperical substrate lens. In this design, the dipole is located at a distance h from the tip of the lens given by

$$h = R\left(1 + \frac{1}{n}\right)$$

where R is the radius of the lens and n is its refractive index. Like the hemispherical lens, this lens design has no spherical aberration or coma and, when using silicon as a substrate lens material, no chromatic aberration throughout the terahertz range [23]. Using this lens design, we obtain collimated terahertz beams with essentially no frequency-dependent beam diameter, and achieve diffraction-limited focusing to a 300-μm focal spot at a center frequency of 1 THz.

D. Signal Acquisition

The traditional method for acquiring terahertz waveforms has relied on a photoconductive sampling technique, in which the delay of one of the gating pulses is swept relative to that of the other, and the average photocurrent generated in the receiver is measured as a function of the delay. The resulting signal is the convolution of the terahertz waveform with the temporal shape of the photoconductive sampling gate. Most of the time, the signal is acquired with a lock-in amplifier, and one of the gating beams (or the terahertz beam) is modulated with a chopper wheel. Since this requires a lock-in time constant in the range of tens to hundreds of milliseconds, the sweep time of the delay is quite slow, on the order of hundreds of milliseconds per data point. At this rate, it takes several minutes to acquire a single 1024-point terahertz waveform.

In order to obtain images, where the entire waveform is measured and analyzed at each pixel, this acquisition time must be reduced dramatically. To accomplish this, the slow stepper motor that provides the optical delay is replaced with a scanning optical delay line (ODL). The ODL (Clark-MXR) used in our experiments, a retro-reflecting mirror mounted on a galvanometric shaker, provides roughly 3 cm of optical path delay on each sweep, and can sweep at up to 100 Hz. With this device, the lock-in amplifier and the chopper wheel are no longer necessary. Dispensing with the noise filtering provided by the lock-in detection does degrade the signal-to-noise somewhat, but allows for much faster acquistion times. As a result, the noise is larger by a factor of between 20 and 100 compared to the slow scan using lock-in techniques. But this is more than compensated by the various transmitter, receiver, and optics improvements described above. Fig. 4 shows a waveform measured with a single sweep of the ODL; in Fig. 4(b), the amplitude spectrum of this waveform is shown on a semi-log scale. Each of the 1024 points in this waveform was acquired in roughly 25 microseconds, and the result has a signal-to-noise of approximately 1000, as seen by the noise baseline above ~3 THz. Much of the residual noise in this data arises from power fluctuations in the femtosecond laser, which in turn can be traced to plasma instabilities in the argon-ion pump laser [24]. By moving to an all-solid-state laser system like a Cr:LiSAF laser, this noise source can be effectively eliminated. Thus, it should be possible to measure up to 100-THz waveforms in a second, with a signal-to-noise in each that approaches the one that has been previously reported using slow scanning methods.

IV. T-Ray Imaging

The above descriptions of various aspects of the THz-TDS apparatus, when taken together, represent significant improvements in the portability, reliability, and cost of the system, as well as the overall quality of the terahertz signals. For these reasons, it is now feasible to consider "real-world" applications of terahertz imaging. As described below, a number of applications, in an extremely diverse array of fields, may benefit significantly. For some problems, THz-TDS may be the only technology available to address the issue, while in other cases, it may be that alternative technologies are simply too expensive, inefficient, or impractical. Although the following discussion explores a number of potential uses of terahertz imaging and touches on examples in each of these areas, it is by no means an exhaustive list.

As mentioned in Section I, the industries and applications areas discussed here are quite wide ranging; they are dictated by the characteristics of the terahertz radiation. Many of the applications under consideration rely on either the extreme sensitivity to water or the ability to propagate through common packaging materials, or both. All of these abilities can be combined with the imaging capabilities. In many applications, a reflection geometry will be of substantial advantage, or may even be required. Although much of the work reported so far relies on transmission imaging, it should be emphasized that imaging in reflection is quite feasible, and even affords some additional advantages, as discussed below.

Also important is the ability to detect and identify most polar molecules in the gas phase. This application relies on the broad bandwidth of the radiation, and the fact that, as in the mid-infrared, many molecules have characteristic "fingerprint" absorption spectra in the terahertz region. This has been exploited in the development of an automated real-time gas monitoring system [25]. This system may be a powerful complement to the established gas monitoring devices which are based on FTIR technology, and which rely on the mid-infrared "fingerprint" absorption spectra of such gases as CO, CO_2 and methane. These gases are not highly polar, and therefore do not show significant absorption in the terahertz region. Conversely, polar molecules such as ammonia and HCl absorb quite strongly, with characteristic features within the

bandwidth of the terahertz pulse, but are more difficult to detect using other optical means.

In the following paragraphs, we will discuss a number of applications of T-ray imaging to illustrate these classes of applications.

A. Terahertz Imaging of Moisture

The simplest type of image one can generate in a transmission imaging setup is one in which the transmitted power determines the nature of the image. In our system, this is accomplished using the digital signal processor, which performs a fast Fourier transform of the waveform in real time, and integrates the magnitude of the resulting power spectrum over a certain spectral range. Because of the diffraction-limited focus at the sample, integration over only the high-frequency part of the terahertz spectrum will improve the spatial resolution; conversely, integrating exclusively over the low-frequency portion minimizes the effects of scattering losses, which rise as the fourth power of the frequency [26].

A good example of this is shown in Fig. 5, which shows a terahertz transmission image of a leaf from a common houseplant. The color scale is determined by the amplitude of the transmitted terahertz power, which in turn is related to the amount of moisture present at each point on the leaf. (The dashed box across the figure refers to the measurements of Fig. 6, discussed below.) This image illustrates the extreme sensitivity of this technique to water content. In this frequency range, water absorbs quite strongly. Recently, Keiding and co-workers [8] measured the absorption coefficient of liquid water, using THz-TDS in a reflection geometry. Their value of $\alpha \sim 230\ \mathrm{cm}^{-1}$ at $\nu \sim 1$ THz has been confirmed by transmission measurements, and is in reasonable agreement with molecular dynamics simulations [9]. This value has direct implications for the ultimate sensitivity of terahertz imaging to changes in water content. With a signal-to-noise of 100:1 in the measured electric field, the minimum detectable water concentration is given by $n \cdot x \sim 10^{16}\ \mathrm{cm}^{-2}$, where n is the density of water molecules and x is the length of the path traversed by the terahertz beam in the material. In a material with a thickness of 1 mm, this implies a detection limit of less than 10^{-5} of liquid density.

This extreme sensitivity to water content can be exploited in measurements such as those illustrated by Fig. 5. Indeed, this is of great interest as a method of measuring the water content of leaves on *living* plants. Currently, there is no accepted, nondestructive procedure for measuring the leaf water status of a transpiring plant. Research in the field of plant water relations has been limited to point-in-time observations that provide average values across the tissue being studied [27]. Multiple spatial and repeated temporal observations have been required to account for the dynamic movement of water through the plant and for spatial variation in water status in individual leaves. Using terahertz imaging, it is possible to account for inhomogeneities in the sample by performing a spatially resolved measurement. Because these measurements are inherently nondestructive, repeated measurements may be made on the same tissue, thereby providing for the study of water flow dynamics. A demonstration of this application is shown in Fig. 6, in which the amplitude of the transmitted terahertz radiation is shown as a function of horizontal position across a leaf, at various delay times after the plant was watered. The approximate location on the leaf of these line scans is shown by the dashed box in Fig. 5. In Fig. 6, the variations observed as a function of position on the leaf, which are repeated at each delay time, reflect the different transmission coefficients through different parts of the sample. These result primarily from the stem structure; as seen in Fig. 5, the region of the line scans intersects the primary or central stem, as well as a number of subsidiary stems on either side. As a function of time after watering, the transmission decreases by several percent, indicating that water is absorbed into the leaf on a time scale of hours. Experiments such as this can be used to further understand the early warning signs of plant water stress, and may be valuable aids in irrigation management for a wide range of crops.

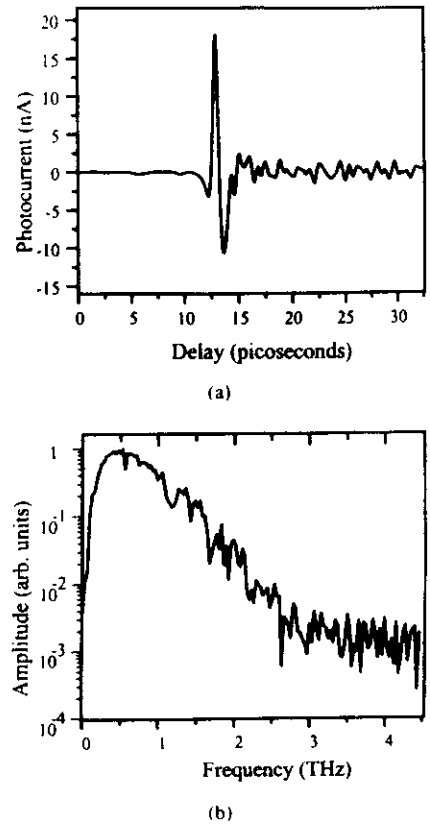

Fig. 4. (a) Terahertz waveform measured in a single scan of the ODL; (b) Magnitude of the Fourier transform of the waveform in (a), on a semi-log scale. The noise baseline is roughly 1000 times lower than the peak signal. The oscillations which follow the main pulse, and which appear as modulations on the spectrum, are a result of water vapor in the beam path, and do not significantly affect the signal-to-noise estimates in the text.

B. Terahertz Imaging for Quality Control

Spatially resolved measurements of the terahertz transmission coefficient may also be used in package inspection or quality control applications. Evidently, since many packaging materials such as plastic and cardboard are transparent to

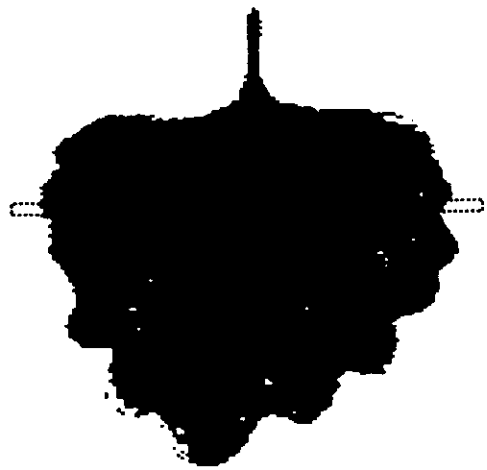

Fig. 5. Terahertz image of a leaf from a common houseplant, Coleus. The false color scale is correlated with water content, with darker green indicating more water. The dashed box indicates the approximate position of the line scans of Fig. 6, as described in the text.

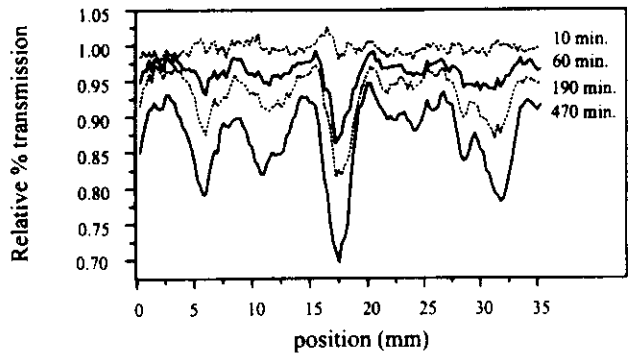

Fig. 6. Terahertz line scans along a line that transects the center of the leaf, as shown by the dashed box in Fig. 5. The modulation in each line scan results from the stem structure of the leaf. Each scan is labeled according to the time (in minutes) after the plant was watered. Decreasing terahertz transmission results from water intake into the leaf tissue.

terahertz radiation, it is quite simple to image through these materials and detect the contents. In many industries, X-ray imaging is currently used for such tasks. T-ray imaging may be a desirable alternative simply because of the health and safety issues involved with ionizing radiation. Because of the low energies of the photons involved and the extremely low intensities generated, T-rays present virtually no safety concerns, particularly if the femtosecond laser pulses are delivered to the terahertz switches via optical fiber. The extreme sensitivity to water content proves important in these types of applications as well. Although numerous methods exist for measuring the water content of moisture-sensitive products, essentially no method exists if the measurement must be performed through a cardboard or thin plastic package. Preliminary tests on samples such as shrink-wrapped food products indicate that the amplitude of the reflected terahertz pulse is a good measure of the moisture content of the surface layer of the product.

Fig. 7 illustrates another use of terahertz imaging as a quality control monitor. This figure shows the terahertz image of a manufactured part, representative of innumerable mold-

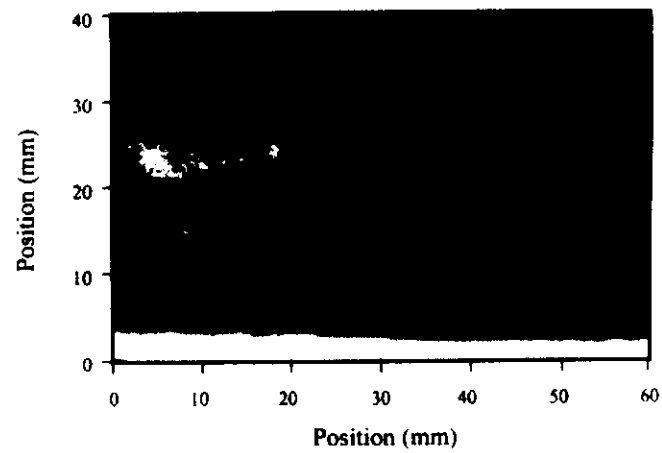

Fig. 7. Terahertz image of a molded composite plastic piece, as described in the text. The image clearly shows the presence of a roughly circular ~2-cm void in the internal foam-filled region.

fabricated plastic piece-parts. This part consists of two parallel black plastic sheets, with a rubberized foam padding between them. In the manufacturing process, the foam is sprayed between the plastic sheets, holding them together when it dries. However, occasionally bubbles or voids develop in the foam, sometimes as large as an inch in diameter or more. Detection of these voids is a significant quality control issue, and no simple method currently exists. X-ray transmission does not provide a high contrast between the plastic-rubber foam and the air; in addition, health and safety issues preclude the use of X-ray diagnostics here. Ultrasound analysis is effective only with the use of an index-matching fluid, while other probing techniques such as magnetic resonance imaging are too expensive and cumbersome. Probing the parts with microwaves would work quite nicely, except that it would be difficult to detect voids significantly smaller than the wavelength of the radiation used. Since, in this case, it is desirable to detect voids smaller than one centimeter in diameter, this effectively eliminates conventional microwave analysis from consideration.

The terahertz imaging technique exploits the fact that the rubber foam filling has many tiny air pockets, which act as good scattering sites for radiation in the 0.5-mm wavelength range. Of course, the solid plastic surfaces on the front and rear of the sample are fairly transparent to the terahertz radiation. As shown in Fig. 7, the terahertz image clearly locates the void, simply by observing an increase in the transmission through the sample wherever a smaller length of foam is traversed. Terahertz imaging is extremely sensitive to small voids or other morphological variations which may occur inside solid plastic or plastic composite parts. It may seem somewhat fortuitous that the foam rubber in this particular example consists of scattering sites ideally suited for the wavelength range spanned by the terahertz pulses. It should be emphasized that one could detect voids of this sort without relying on such a coincidence by observing the *transit time* of the terahertz pulse through the material, rather than the transmitted *amplitude*. The combination of the amplitude and phase information measured in THz-TDS make for a very powerful tool for quality control measurements.

C. T-Ray Tomography

Because the technique of THz-TDS relies on a coherent detection scheme, in which the electric field of the terahertz pulse is measured explicitly, the detected waveforms typically contain far more information than simply the power transmission coefficient of the sample under study. Changes in the phase of the measured waveform also can frequently be correlated with important properties of the sample. As a crude measure of phase changes, one may simply monitor the change in the arrival time of the peak (or first zero crossing) of the terahertz waveform. Changes in this arrival time as a function of position on the sample indicate changes in the optical path length of the terahertz beam, relative to the femtosecond beam. This may result from either changes in the thickness of the sample as it is scanned transversely across the terahertz beam, or changes in the refractive index, or both. The change in arrival time Δt is given by $\Delta t = \frac{1}{c}\int n(z)dz$, where $n(z)$ is the refractive index seen by the terahertz beam along its optical path, and where the integral is along the path. An illustration of this technique is shown in Fig. 8, in which a small gas flame has been imaged in transmission. In this experiment, the ionized molecules which make up the flame may have a significant absorption at certain frequencies within the spectrum of the pulse [28], but the gas density is so low that this effect cannot be observed. However, the flame heats the air locally, which changes the refractive index along the terahertz optical path $n(z)$. A crude estimate of the magnitude of this effect would assume that the refractivity of air varies inversely with temperature. If the flame has a thickness of roughly 5 mm, this would lead to a shift in the transit time of the terahertz pulse by ~3 fs for a flame of 1000 °C [29]. Each contour in Fig. 8 represents a shift of 5 fs in transit time.

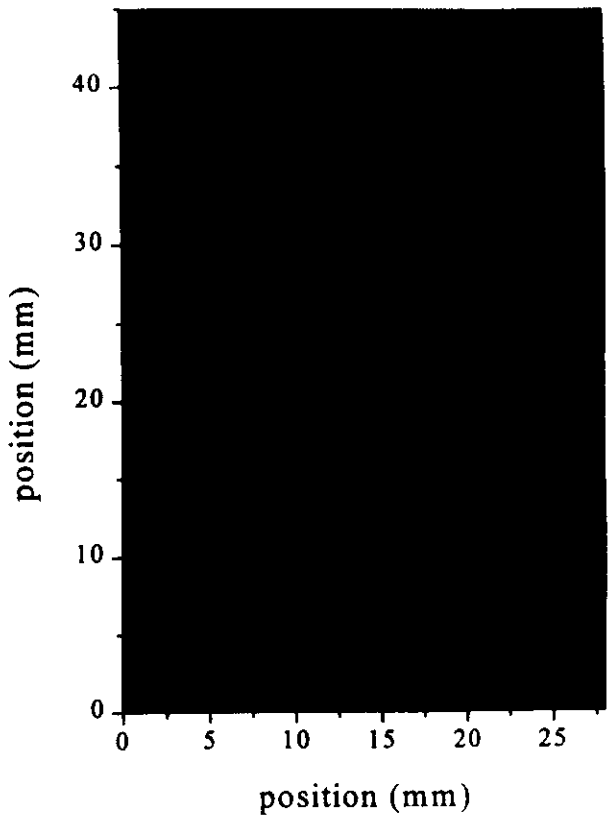

Fig. 8. Terahertz image of a small gas flame. This image is formed by measuring the transit time of the terahertz pulse through the flame, and encoding shifts in this time in false color. Each contour corresponds to a 5-fs shift in the time delay, which results from local heating of the air, as described in the text. The gas nozzle is visible in black at the bottom center of the figure.

One can imagine performing time-of-flight measurements in a reflection geometry similar to those described in the transmission experiment above [30]. Fig. 9 shows the modified beam path for reflection geometry, in which the terahertz beam focuses at the sample, and is reflected at near normal incidence. This presents a situation which is quite analogous to optical coherence tomography (OCT), a technique which has achieved considerable success in recent years in such fields as opthamology and developmental biology. In an OCT device, a short coherence length light source is split into two beams; one is reflected off of the sample and the other off of a reference. The two are then correlated to provide information about the reflectivity of the sample [31], [32]. Distance measurements are possible because a correlation signal is only measured when the path length of the reference arm is equal to that of the sample arm, within the coherence length of the light source. As a result, the ultimate spatial resolution achieved in depth (i.e., the propagation direction of the reflected beam) is limited by the coherence length of the source. As illustrated above, the terahertz tomographic measurement is not limited in the same way. The coherence length of a terahertz pulse is determined by the pulse duration, which is on the order of several hundred femtoseconds. However, the measurement of the flame presented above is sensitive to temporal shifts as small as 5 fs. This sensitivity stems from the phase-sensitive nature of the measurement, and from the fact that each terahertz pulse is a single cycle of the electromagnetic field. It is possible to measure the zero-crossing of an electric field much more accurately than the peak of an intensity autocorrelation. Using this simple idea, it is possible to measure changes in either refractive index or thickness with extremely high accuracy. For example, one can detect, in transmission, a single sheet of paper added to a stack; in reflection, it is possible to achieve a depth resolution of approximately 1 μm. The limitation in this measurement is simply the accuracy with which the optical scanning delay line repeats its position on each scan.

The idea of T-ray tomography is illustrated in Fig. 10, which is a T-ray image, taken in reflection, of a ball-point pen. A pen is an ideal sample for demonstration of this technique, because it consists of a number of smooth, well-separated dielectric interfaces. The vertical axis is parallel to the long (cylinder) axis of the pen, while the horizontal axis of the figure corresponds to depth inside the pen. Fig. 11 shows the input and output waveforms. The output waveform Fig. 11(b) consists of a series of reflected replicas of the input waveform. Each reflection originates from one of the eight dielectric interfaces, either from air to plastic or from plastic to air, formed by the two concentric plastic cylinders which form the pen. These eight surfaces are observed, tomographically, in Fig. 10. This technique is particularly interesting because,

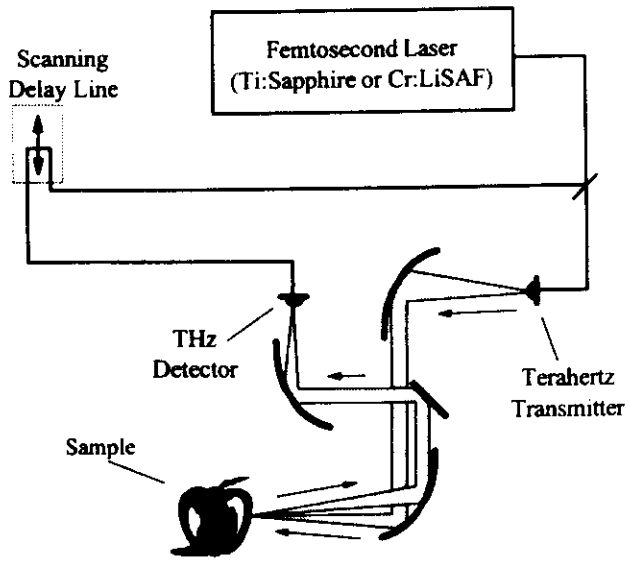

Fig. 9. Schematic of the setup used for terahertz reflection images. The terahertz beam is incident on the sample at near normal incidence, and is focused onto it with a confocal parameter of ~1 cm.

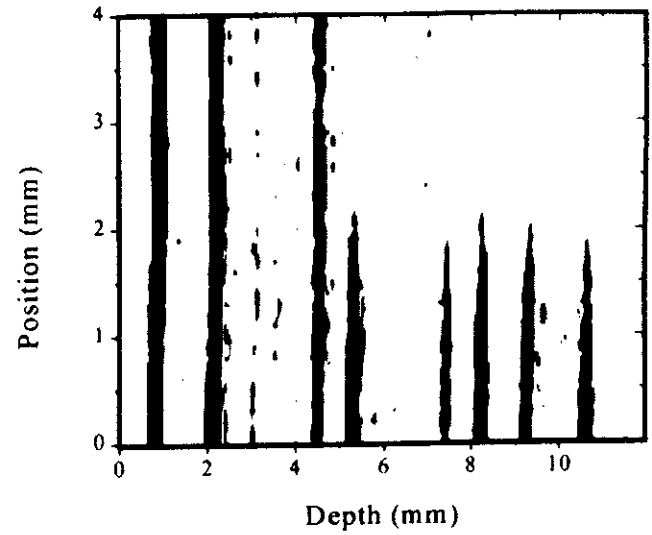

Fig. 10. Terahertz tomographic image of a bic pen. The vertical axis of the figure is parallel to the long (cylinder) axis of the pen, while the horizontal axis of the figure corresponds to depth into the pen. The terahertz pulse is incident from the left. The eight dark lines correspond to the eight dielectric interfaces (either from plastic-to-air or air-to-plastic) encountered by the pulse as it propagates through the pen. The upper right portion of the image is obscured, because these surfaces were shadowed by ink inside the inner plastic cylinder.

in a case such as this where the reflecting surfaces are reasonably well separated in space, each reflected pulse may be isolated in time, and analyzed for spectral information. In other words, each successive reflection contains chemical or spectral information about the additional layers traversed. This idea is illustrated in a rudimentary way in this example; from simply noticing the alternating polarity of the eight reflected pulses Fig. 11(b), one can immediately determine the sign of the refractive index change at each interface. One can also note in Fig. 10 that the rear plastic walls in the upper portion of the figure are not visible; this results from the shadow cast by the ink, an excellent absorber of terahertz radiation, inside the inner cylinder.

D. Terahertz Tomography for Burn Diagnostics

A technique such as terahertz tomography may be of great interest in a wide range of applications. One example, which presents somewhat more of a challenge in interpretation than the example illustrated above, is in the area of burn diagnostics. While the strong water absorption precludes the use of terahertz radiation in most biomedical research areas, those which are particularly concerned with surface (e.g., dermatological, corneal, etc.) issues may find the unique properties of these submillimeter waves to be of interest. In particular, it may be possible to obtain quantitative and highly sensitive measurements of burn depth using terahertz tomography.

The noncontact measurement of burn depths and severities using photonics is a topic of considerable interest [33], [34]. In this field, it is not uncommon to use uncooked chicken breasts as a model for tissue, in order to gain some rudimentary understanding of the tissue–radiation interaction. A chicken breast is burned in several spots with a soldering iron: the severity of the tissue damage is varied simply by controlling the duration of the burn. The entire sample is then covered with a thin (~1 mm) slab of polystyrene, which serves two purposes. First, it keeps the sample flat and stationary during the measurement. Second, the terahertz pulse reflected off of the outer surface of the polystyrene (i.e., the air-plastic interface) serves as a reference pulse, both in amplitude and in delay time, for the subsequent reflections from the tissue underneath. Fig. 12 shows the reflected pulse trains measured at four different points on the sample. The upper pulse train [Fig. 12(a)] corresponds to a measurement of healthy tissue. Here, it is observed that a second pulse, reflected from the interface between the polystyrene and the healthy tissue, follows the reference pulse and closely resembles it. The remaining three pulse trains correspond to measurements of areas with increasing burn severities. Evidently, the pulse reflected from the plastic-tissue interface no longer resembles the reference pulse. Indeed, it appears that, in the case of the most severely damaged tissue, there may be a third reflection a few picoseconds after the second. This may arise from a reflection at a (buried) interface between tissue with no water and tissue with some substantial water content. Clearly, these reflected pulses contain a great deal of information about the dielectric properties of the damaged tissue. Disentangling the details of this information and correlating it with physiological variables will require a good deal of effort, and many more experiments. Nonetheless, this data demonstrates a powerful new technique and a potentially valuable diagnostic tool in biomedical optics.

E. The Terahertz Hall Effect

An example of an application of terahertz imaging in which both the amplitude and phase of the transmitted wave are used to form an image, is found in the field of semiconductor wafer characterization [35]. A powerful tool in the characterization

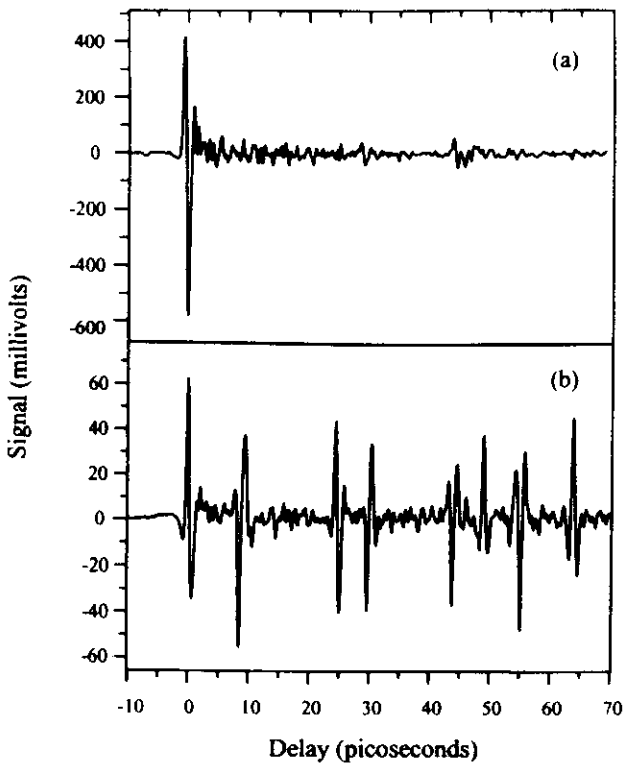

Fig. 11. Terahertz waveforms (a) incident on, and (b) reflected from the bic pen shown in. The small oscillations which follow the main pulse in (a) are a result of residual water vapor in the beam path, and do not significantly affect the measurement. A reflected pulse from each of the eight dielectric interfaces can be observed in (b). The polarity of the reflected pulse immediately allows one to determine the sign of the change in refractive index at each interface.

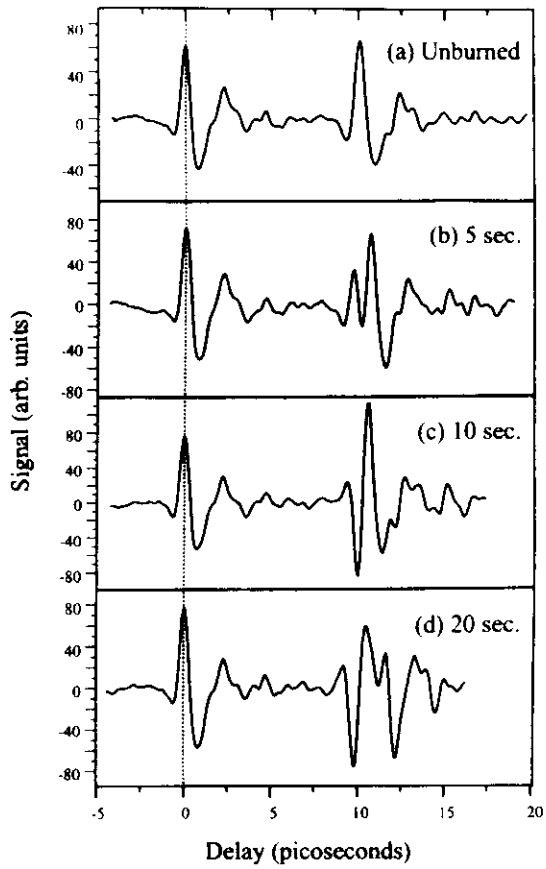

Fig. 12. Terahertz waveforms reflected from various spots on a piece of raw chicken breast: (a) reflection from healthy tissue, (b) tissue which had been burned for 5 s, (c) 10 s, and (d) 20 s. The initial pulse is reflected from a thin plastic overlayer, and can be used as a reference for both delay time and amplitude, as described in the text. The distortions o the reflections from the burned areas could be used to extract quantitative information about the dielectric properties of the damaged tissue.

of doped wafers is the Hall effect. This effect, in which an applied voltage induces a transverse voltage in the presence of a large dc magnetic field, is commonly used to measure material properties of any conducting sample. Indeed, it is the method of choice for measurements of dc properties in thin doped epitaxial layers of semiconductors. A measurement of the Hall parameters is equivalent to measuring the full complex conductivity tensor of the sample. From this measurement, both the mean carrier density and the carrier mobility can be determined. However, it is necessary to contact the sample at four points. The results must be considered as a spatial average over the region contained within the four point contacts. As always in such experiments, contact resistance must be carefully controlled, and can easily lead to spurious results.

It is possible to extract the same information using the terahertz field as the applied electric field in the Hall experiment. A schematic of the experiment is shown in Fig. 13. The samples consist of a 1-μm-thick layer of either n- or p-doped GaAs, epitaxially grown on a ~0.5 mm undoped GaAs substrate. In the presence of a magnetic field pointing parallel to the beam propagation direction ($\hat{z}$), the applied terahertz field (along $\hat{x}$) induces a current (also along $\hat{x}$) which in turn induces a Hall field, oriented in the transverse direction (along $\hat{y}$). This Hall field radiates a terahertz field which is coherent relative to the input terahertz beam, but which is polarized orthogonally to it. A measurement of the amplitude and phase of this radiated beam can be used to determine the conductivity tensor of the sample. In practice, the incident field is polarized at 45°to the vertical axis, and both the vertical ($\hat{y}$) and horizontal ($\hat{x}$) fields are measured simultaneously, with two orthogonally oriented detectors. This phenomenon is related to the early work of Chambers and Jones [36], although in somewhat different physical limits. More recently, a technique using millimeter-wave near-field imaging with similar capabilities has been reported [37].

In the absence of a magnetic field (or in the absence of a sample), the polarizing beamsplitter can be adjusted so that these two measured fields are approximately equal. Then, when the magnetic field is applied to the sample, the two waveforms should be quite different, as the Hall effect transfers energy between the two orthogonal waves. Fig. 14 shows the spectra of $\hat{x}$- and $\hat{y}$-polarized terahertz waveforms without a magnetic field, with a magnetic field of ~1.3 T, and with the same magnetic field in the opposite direction. This serves as a clear demonstration of the terahertz Hall effect. These two terahertz waveforms can be used to calculate both the carrier density and carrier mobility directly, using the semiclassical Drude theory.

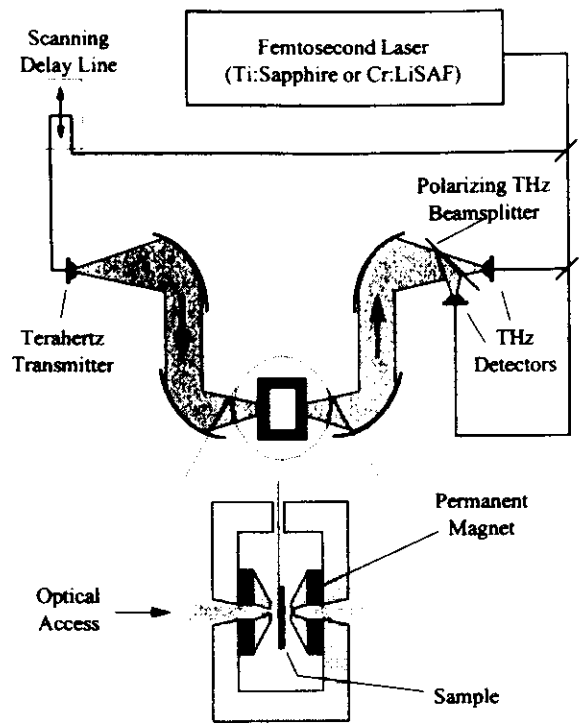

Fig. 13. Schematic of the setup used for terahertz Hall effect measurements, showing permanent 1.3-T magnet, free-standing wire grid polarizing beam splitter, and two receivers operating in parallel for simultaneous detection of two orthogonal polarizations.

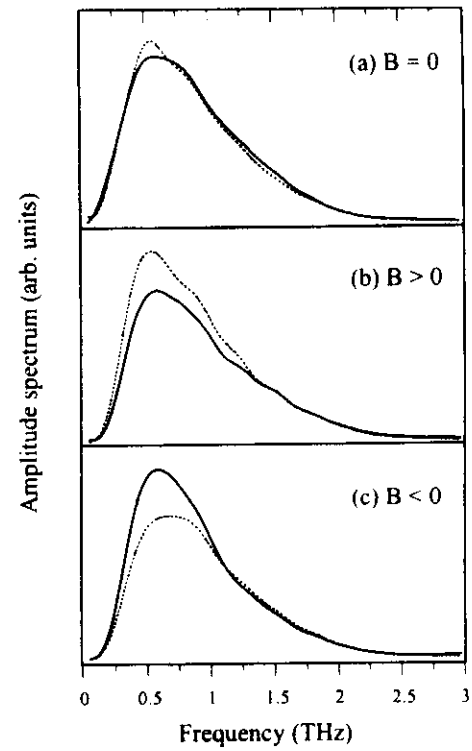

Fig. 14. Terahertz waveforms transmitted through a n-doped sample, of the type described in the text. The nominal doping density for this sample was $1.9 \times 10^{17}\,\mathrm{cm}^{-3}$. The input terahertz field is polarized at 45°; the two curves correspond to the horizontal (solid) and vertical (dashed) components. In (a), no magnetic field is applied, and the two measured components are approximately equal, while in (b) a field of ~1.3 Tesla is applied to the sample in a direction parallel to the terahertz beam propagation. In (c), the same field is applied in the opposite direction. The transfer of energy between the orthogonal components of the field is evidence of the terahertz Hall effect.

The Drude model describes fairly accurately the behavior of the carriers in moderately doped semiconductors [38], [39]. Within this formalism, the magnetoconductivity tensor has two independent values, the diagonal (σ_{xx}) and off-diagonal (σ_{xy}) element. These are related to fundamental parameters by the relations

$$\sigma_{xx} = \sigma_0 \cdot \left(\frac{1 - i\omega\tau}{(1 - i\omega\tau)^2 + (\omega_c\tau)^2} \right) \quad (1)$$

$$\sigma_{xx} = \sigma_0 \cdot \left(\frac{\omega_c\tau}{(1 - i\omega\tau)^2 + (\omega_c\tau)^2} \right) \quad (2)$$

where ω_c is the cyclotron frequency, proportional to the magnetic field, σ_0 is the dc conductivity, $\sigma_0 = Ne\mu$, and τ is the Drude scattering time. Here, N is the carrier density, and μ is the mobility, given by $\mu = e\tau/m^*$. Of course, the off-diagonal element vanishes as $B \to 0$, since the magnetic field provides the transverse coupling in the Hall effect. In this experiment, the doped layer is much thinner than one wavelength, so for the purposes of the propagation this is a surface charge layer. Thus, the experiment measures the *sheet* conductivity, and the carrier density which appears in σ_0 is the *sheet* carrier density [40]. The quantities in (1) and (2) can be related to the input terahertz fields, measured with no sample in the beam, by taking into account the reflection losses at both ends of the sample and the (small) absorption and dispersion effects in the thick undoped substrate, and by using the tabulated values of $n(\omega)$ and $\alpha(\omega)$ for intrinsic GaAs [7]. By so doing, the two terahertz fields can be used to independently determine absolute numerical values for the carrier density N and the mobility μ. This entire calculation can be performed rapidly enough that it can be incorporated into the imaging software, thus permitting real-time imaging of these two important material parameters. Inhomogeneities in both N and μ can be imaged with a spatial resolution of ~250 μm, roughly an order of magnitude better than the best four-point probe measurements. Fig. 15 shows two such images, one for each of N and μ, generated with an n-GaAs sample with a nominal doping density of $1.9 \times 10^{17}\ \mathrm{cm}^{-3}$, as determined by growth conditions. With these techniques, *in situ* noncontact characterization of the uniformity of semiconductor wafers should be possible.

F. Time-Domain Waveform Analysis

The implementation of fast scanning and real-time data acquisition in THz-TDS has focused attention on new ways of analyzing and processing waveforms. In particular, fast and efficient algorithms are important for chemical recognition systems [25], where spectroscopic information is processed in real-time with the aim of determining the chemical compositions of an object. For real-time recognition systems, such as in speech recognition [12], a common stragegy is to perform a signal compression, i.e., to parameterize the characteristic response, and to use these parameters in a subsequent pattern

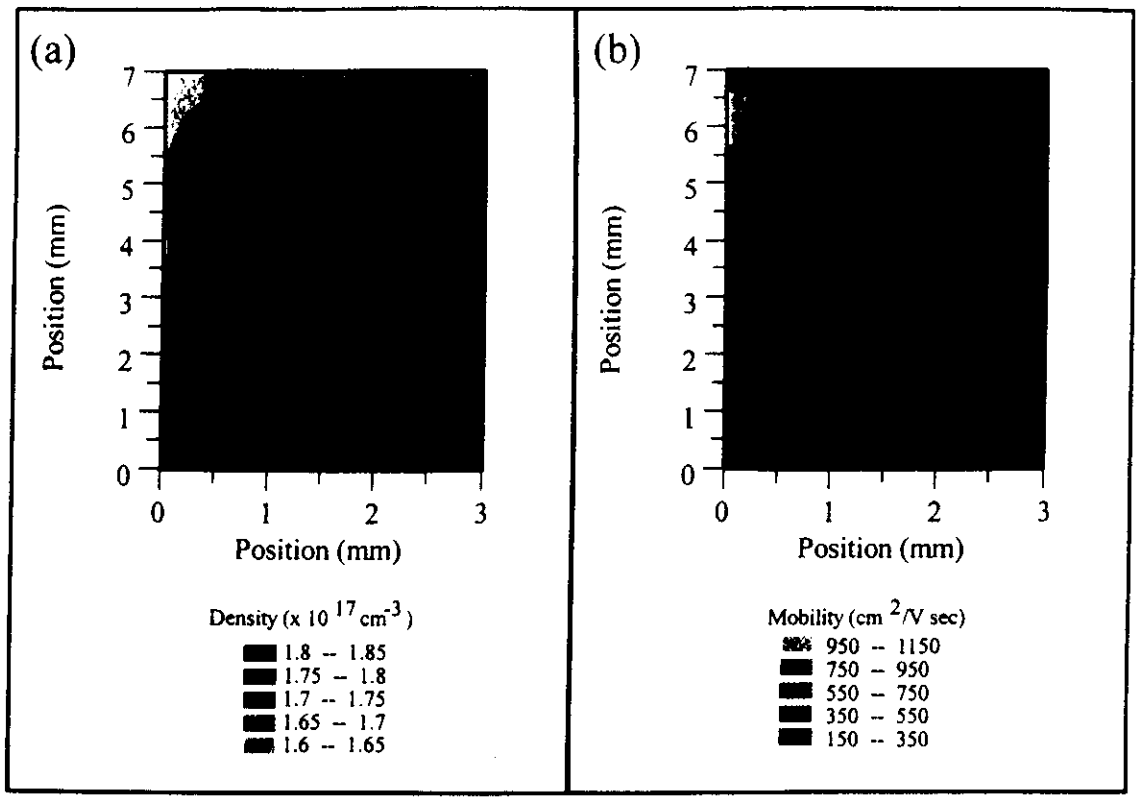

Fig. 15. Terahertz images of the sample from Fig. 14, generated as described in the text. Variations in the doping density are shown in (a), while (b) shows inhomogeneities in the carrier mobility. In each case, the legends show the relation between the color scale and the calculated parameter values.

classification scheme for the recognition of spoken words. Along the same vein, we will in the following discuss some recent approaches in real-time waveform analysis based on signal compression.

The application of digital signal processing techniques [41] in linear spectroscopy involves the modeling of the sample response by linear time-invariant digital filters. In this approach the characteristics of the sample's response is transferred to the digital filter. The most general linear filter takes an input waveform, $x(t)$, and produces an output waveform, $y(t)$, by the formula

$$y(t) = \sum_{j=0}^{N} b_j x(t - j\Delta) + \sum_{k=0}^{M} a_k y(t - k\Delta) \qquad (3)$$

where a_k and b_j are constant filter coefficients, and Δ is the sampling interval. To get some physical insight of the filtering processes we derive the frequency response of the transfer function, $H(z)$, corresponding to the time-domain filter described by (3)

$$H(z) = \frac{\sum_{j=0}^{N} b_j z^{-j}}{1 - \sum_{k=1}^{M} a_k z^{-k}} \qquad (4)$$

where $z = \exp\{i2\pi f\Delta\}$, and f is the frequency. The numerator represents a finite impulse response filter (FIR), and describes a polynomial filtering in z^{-1}, and hence contains the *zeros* of the filter. The denominator corresponds to an infinite impulse response filtering (IIR), and describes the *poles* of the filter. In order to reduce the complexity of an analysis we will often restrict to use either a pure FIR ($a_k = 0$) or a pure IIR filter ($b_j = 0$) depending on the characteristic response exhibited by the sample. In case of sharp resonances, the IIR filter has proven useful [25], whereas samples that exhibit a smooth frequency response is more appropriately modeled by the FIR filter.

The optimum values of the filter coefficients can be determined directly from the time-domain signal using a correlation type of analysis. The time-domain analysis is based on *least-square* principles. In this approach, one must minimize the squared sum of the difference between the measured signal and the signal generated from the filtering process. The analysis yields a system of linear equations [41] that relates the filter coefficients to values of the cross- and autocorrelation of the sampled waveforms. The system of equations can be solved using matrix inversion. For the pure FIR filtering this type of analysis resembles the memory function analysis that has been recently introduced to THz-TDS [42], [43]. In case of pure IIR filtering, the analysis involves only the autocorrelation of the measured signal, and consequently all phase information is lost. Hence, the IIR filter is only capable of estimation the power absorption spectrum. The use of a pure IIR filtering for parameterization of a digital signal is often referred to as *linear predictive coding* [44].

The IIR filter is efficient for predicting sharp spectral features, which makes it particularly well suited for the analysis of THz-TDS waveforms which have interacted with polar gases.